NASA CONTRACTOR REPORT

NASA CR-1144

A METHOD OF CALCULATING COMPRESSIBLE TURBULENT BOUNDARY LAYERS

by H. James Herring and George L. Mellor

Prepared by
PRINCETON UNIVERSITY
Princeton, N. J.
for Lewis Research Center

NATIONAL AERONAUTICS AND SPACE ADMINISTRATION • WASHINGTON, D. C. • SEPTEMBER 1968

NASA CR-1144

A METHOD OF CALCULATING COMPRESSIBLE TURBULENT BOUNDARY LAYERS

By H. James Herring and George L. Mellor

Prepared under Grant No. NGR 31-001-074 by
PRINCETON UNIVERSITY
Princeton, N.J.

for Lewis Research Center

NATIONAL AERONAUTICS AND SPACE ADMINISTRATION

For sale by the Clearinghouse for Federal Scientific and Technical Information
Springfield, Virginia 22151 – CFSTI price $3.00

FOREWORD

The research described herein originally appeared as a Doctoral thesis by the principal author. Initial support was supplied by a Ford Foundation Fellowship, with partial computer facility support under National Science Foundation Grant, NSF-6P579. The work was completed under National Aeronautics and Space Administration Grant NGR 31-001-074. Technical coordination was provided by Mr. S. Lieblein and Mr. A. V. Saule of the Air-breathing Engines Division, NASA-Lewis Research Center.

ABSTRACT

The essential unknown quantity in a compressible turbulent boundary layer is shown to be the kinematic Reynolds stress, as in incompressible flow, and does not explicitly involve density fluctuations. Based on this, the incompressible turbulent viscosity proposed by Mellor is extended to include compressible flows. The same values of the three empirical constants, which were obtained solely from constant-property, constant-pressure experiments, are also used. Without making any further assumptions beyond those related to the usual time averaged boundary layer equations, this system of equations has been programmed for numerical solution. Solutions have been compared to a considerable amount of constant-pressure data in the range from subsonic flows to flows with Mach numbers around 5.0 and the comparisons are quite favorable. Much less pressure gradient data are available but comparison was made to some axisymetric flow data taken in a positive pressure gradient which indicated fairly good prediction of the boundary layer growth, while at the same time pointing up a systematic error in the detailed profile shape prediction in regions of finite longitudinal curvature. This effect has been identified on physical grounds but has yet to be incorperated in the turbulent viscosity model. Unfortunately high speed data taken on a flat wall in an adverse pressure gradient and with a well defined separation point does not seem to be readily available.

Heat transfer data in incompressible flows with variable pressure gradients have been checked against calculations and the comparisons are generally favorable.

TABLE OF CONTENTS

NOTATION

A	constant used in Equation (36) for initialization of profiles.
A_f, A_g	constants used in satisfying outer boundary condition.
B	exponent used in Equation (35) for external velocity distribution.
C_i	coefficients in pseudo-linear forms of momentum and energy equations.
C_f	$= \dfrac{\tau_w}{\frac{1}{2}\rho_e U^2}$, coefficient of skin friction.
C_{f_i}	coefficient of skin friction for an incompressible flow at the same value of R_θ as C_f .
D	$= (R_{LAT.})_x \delta^*/R_{LAT.}$
f'	$= (\rho_e U - \bar{\rho}\,\bar{u})/\rho_e U$.
g'	$= (h_e^o - \bar{h}^o)/(h_e^o - h_r)$.
h	enthalpy
h_r	arbitrary reference enthalpy.
h^o	total enthalpy.
H	$= (h_e^o - h_r)/h_e^o$.
k	molecular thermal conductivity.
K	Clauser constant used in the effective viscosity function (taken here to be 0.016).
K^+	empirical constant.
ℓ	representative scale in x direction.

L reference length used for x in Equation (35).

M Mach number.

M_∞ Mach number used to identify data of Winter, Smith and Rotta [23].

p pressure

P $= (\rho_e U)_x \delta^* / \rho_e U$.

Pr molecular Prandtl number defined by Equation (14).

Pr_t turbulent Prandtl number defined by Equation (15).

q heat flux.

Q $= (\rho_e U \delta^*)_x / \rho_e U$.

$R_{LAT.}$ lateral radius of wall curvature.

$R_{LONG.}$ longitudinal radius of wall curvature.

$\underset{\sim}{R}$ $= \delta_k^* U / \tilde{\nu}$.

$\underset{\sim}{R}_s$ $= \delta_k^* U / \bar{\nu}_s$.

R_x $= xU / \nu_\infty$.

R_{δ^*} $= U\delta^* / \nu_\infty$, displacement thickness Reynolds number.

R_θ $= \theta U / \nu_\infty$, momentum thickness Reynolds number.

R,S defined by Equation (D5).

r,s given by Equation (D8).

S_t $= \dfrac{q_w}{\rho_e U (h_e - h_w)}$, Stanton number.

t temperature.

u,v,w velocities in the directions x, y, and z respectively.

u_τ $= \sqrt{\tau_w/\rho_e}$, friction velocity.

U velocity at the outer edge of the boundary layer.

V $= U_x \delta^*/U$.

x,y,z spatial coordinates defined in Figure 1.

y_1^+ empirical constant.

α molecular diffusivity.

α_e $= \alpha_t + \alpha$, effective diffusivity.

α_t turbulent diffusivity.

γ $= C_p/C_v$, ratio of specific heats.

δ approximate boundary layer thickness.

δ^* $= \int_o^\infty (\rho_e U - \bar{\rho}\,\bar{u})/\rho_e U \, dy$, displacement thickness.

δ_k^* $= \int_o^\infty (U - \bar{u})/U \, dy$, kinematic displacement thickness.

Δ difference between value of variable in mainstream and at wall

ε $= \delta/\ell$, small parameter used in order of magnitude analysis.

η $= y/\delta^*$.

η_1 asymptotic matching point.

θ $= \rho_e/\bar{\rho}$, also used for $\int_o^\infty \bar{\rho}\,\bar{u}(1 - \bar{u}/U)/\rho_e U \, dy$, the momentum thickness.

κ von Karman constant in the effective viscosity function (taken here to be 0.41).

λ $= \delta^*/R_{LAT.}$

Λ $= r/R_{LAT.}$

μ molecular viscosity.

ν molecular kinematic viscosity.

ν_e $= \nu + \nu_t$, effective kinematic viscosity.

ν_s molecular kinematic viscosity at the edge of the viscous sublayer.

ν_t turbulent kinematic viscosity.

ν_∞ molecular kinematic viscosity at the edge of the boundary layer.

ρ density.

σ constant in the effective viscosity function (taken here to be 6.9).

τ shear stress.

T, T_h effective viscosity and diffusivity functions in defect form.

ϕ, Φ wall and defect effective kinematic viscosity functions.

X, X wall and defect layer variables for the effective kinematic viscosity function.

Subscripts

b previous x station.

e outer edge of boundary layer.

h	homogenous solution.
m	intermediate x station.
o	initial x station.
p	particular solution.
w	wall.
x	differentiation with respect to x.

Superscripts

$(\bar{\ })$	time average part of dependent variable.
$(\ )'$	fluctuating part of dependent variable, also used later with f, g and θ to denote partial derivative with respect to η.
$(\ )^+$	non-dimensional variables defined by Equation (A1).

I. INTRODUCTION

It is probable that a quantitative theory of the turbulent transport mechanism which, for example, gives rise to the Reynolds stress in turbulent boundary layers, will not be available in the near future. One is therefore forced to model this mechanism empirically. Most of the previous methods in the literature inject further empirical content in an attempt to side-step the analytical complexities of the time averaged equations of motion. However, with the availability of high speed computers the full equations can now be solved numerically, thus providing a predictive tool which spans a large parametric range. The parametric variables which can in principle be included in the formulation are, Reynolds number, Mach number, pressure gradient, transpiration or aspiration, heat transfer and wall roughness for either planar or axisymmetric flow. Furthermore the same numerical program can be used to calculate the laminar portions of the boundary layer development. Besides serving as an effective tool for the prediction of boundary layer development, the numerical solution of the boundary layer equations is free from analytical approximation and therefore underscores the results of the turbulent transport model.

The seed of the present work was Clauser's suggestion [1,2] that the outermost part of an equilibrium boundary layer (one for which $(U-u)/u_\tau$ represent similar profiles when $(\delta^* \, dp/dx)/\tau_w$ is held constant) could be described with a constant effective viscosity. Recently Mellor [3,4] hypothesized an effective viscosity function for the entire boundary layer. This effective viscosity hypothesis successfully predicted the whole range $(-0.5 < (\delta^* \, dp/dx)/\tau_w < \infty)$ of equilibrium boundary layers which represented a considerable gain since it allowed the detailed development of such layers to be calculated from a function containing only three empirical numbers. Mellor then demonstrated that the effective viscosity hypothesis gave good results for a variety of decelerating non-equilibrium flows in reference [5]. There the profiles, skin friction coefficient and boundary layer growth were all predicted well and, where it occurred, the separation point was correctly predicted. The limitations on the hypothesis are that it has a definite lower Reynolds number limit of $R_{\delta^*} = 700$, with a practical lower limit somewhat higher, and it is in error for boundary layers on walls with curvature in the streamwise direction. The latter does not represent an inadequacy in the basic approach. Experiments are still in progress to find the best way of incorporating the curvature effect into the hypothesis.

The next logical step in the development is taken here - the extension of the incompressible effective viscosity to include compressible flows with heat transfer. The restrictions on the hypothesis for incompressible flow also apply in compressible flow. Here the Reynolds number restriction must be made more specific; $U\delta_k^*/\bar{\nu}_s$ must be greater than 700,

where $\delta_k^* = \int_o^\infty (U-u)/U dy$, and $\bar{\nu}_s$ is the kinematic viscosity at the edge of the viscous sublayer. For large Mach number $\bar{\nu}_s$ can be substantially larger than the freestream value. The density variation in compressible flow also makes the effect of curvature even more significant. Both of these limitations will be discussed later in detail. In addition, a restriction to moderate heat transfer rate becomes necessary. This condition can probably be written

$$1 - \frac{h_e^o / h_w}{1 + \frac{\gamma-1}{2} M_e^2} = O(1) \qquad (1)$$

which if satisfied implies that only the mean density need enter into the determination of the Reynolds stress, and the previously established effective viscosity hypothesis may be adopted.

By assuming constant turbulent and molecular Prandtl numbers, the same effective viscosity function is used in the energy equation. Because the energy equation is actually solved, instead of simply assuming, for instance, constant total enthalpy across the layer, compressible boundary layers with heat transfer can be calculated.

Although the predictive scope of the calculation is much broader, this report restricts attention to a large amount of high speed adiabatic flow data with zero pressure gradient, a series of axisymmetric flow data with pressure gradients and some incompressible flow data with heat transfer.

II. ANALYSIS OF THE PROBLEM

Equations of Motion

Solutions of the complete, time dependent equations of motion for a compressible turbulent boundary layer are beyond the capability of available numerical methods. A number of simplifications are therefore necessary. First, using the familiar method of Reynolds averaging, the equations may be averaged in time so that the effects of the time dependent turbulent fluctuations are expressed as turbulent correlations. In a steady turbulent flow these correlations are then independent of time. Temporarily it will simplify matters to restrict the derivation to include only that region away from the wall where turbulent effects dominate and the direct effects of molecular viscosity and molecular conductivity are negligible. Using the notation shown in Figure 1, these equations may be written

$$\frac{\partial}{\partial x}\left(\bar{\rho}\,\bar{u} + \overline{\rho' u'}\right) + \frac{\partial}{\partial y}\left(\bar{\rho}\,\bar{v} + \overline{\rho' v'}\right) = 0 \quad , \tag{2a}$$

$$\frac{\partial}{\partial x}\left(\bar{\rho}\,\bar{u}^2 + \bar{\rho}\,\overline{u'^2} + 2\bar{u}\,\overline{\rho' u'}\right) + \frac{\partial}{\partial y}\left(\bar{\rho}\bar{v}\bar{u} + \bar{\rho}\,\overline{u'v'} + \bar{u}\,\overline{\rho' v'} + \bar{v}\,\overline{\rho' u'}\right) = -\frac{\partial \bar{p}}{\partial x} \quad , \tag{2b}$$

$$\frac{\partial}{\partial x}\left(\bar{\rho}\bar{u}\bar{v} + \bar{\rho}\,\overline{u'v'} + \bar{v}\,\overline{\rho' u'} + \bar{u}\,\overline{\rho' v'}\right) + \frac{\partial}{\partial y}\left(\bar{\rho}\,\bar{v}^2 + \bar{\rho}\,\overline{v'^2} + 2\bar{v}\,\overline{\rho' v'}\right) = -\frac{\partial \bar{p}}{\partial y} \quad , \tag{2c}$$

$$\frac{\partial}{\partial x}\left(\bar{\rho}\,\bar{u}\bar{h}^{o} + \bar{\rho}\,\overline{u'h^{o\prime}} + \bar{h}^{o}\,\overline{\rho' u'} + \bar{u}\,\overline{\rho' h^{o\prime}}\right) + \frac{\partial}{\partial y}\left(\bar{\rho}\,\bar{v}\bar{h}^{o} + \bar{\rho}\,\overline{h^{o\prime}v'} + \bar{v}\,\overline{\rho' h^{o\prime}} + \bar{h}^{o}\,\overline{\rho' v'}\right) = 0 \quad , \tag{2d}$$

$$\bar{h}^{o} = \bar{h} + \tfrac{1}{2}\left(\bar{u}^2 + \overline{u'^2} + \overline{v'^2} + \overline{w'^2}\right) \quad , \tag{2e}$$

$$\bar{p} = \frac{\gamma - 1}{\gamma}\left(\bar{\rho}\,\bar{h} + \overline{\rho' h'}\right) \quad . \tag{2f}$$

Since these turbulent correlation terms are not known a priori, it is desirable to estimate their importance to determine which are negligible. For a boundary layer this may be done with a standard order of magnitude analysis. If it is assumed that

$$\overline{\rho' v'} \approx \overline{u' v'}\left(\frac{\partial \bar{\rho}}{\partial y}\Big/\frac{\partial \bar{u}}{\partial y}\right) \tag{3a}$$

and

$$\overline{\rho' u'} \approx \overline{\rho' v'} \tag{3b}$$

(which is consistent with equations (7) and (13) discussed below) it is shown in Appendix A that

$$\frac{\overline{\rho' v'}}{U\Delta\bar{\rho}} \quad , \quad \frac{\overline{\rho' u'}}{U\Delta\bar{\rho}} = O(\delta/\ell) \tag{4}$$

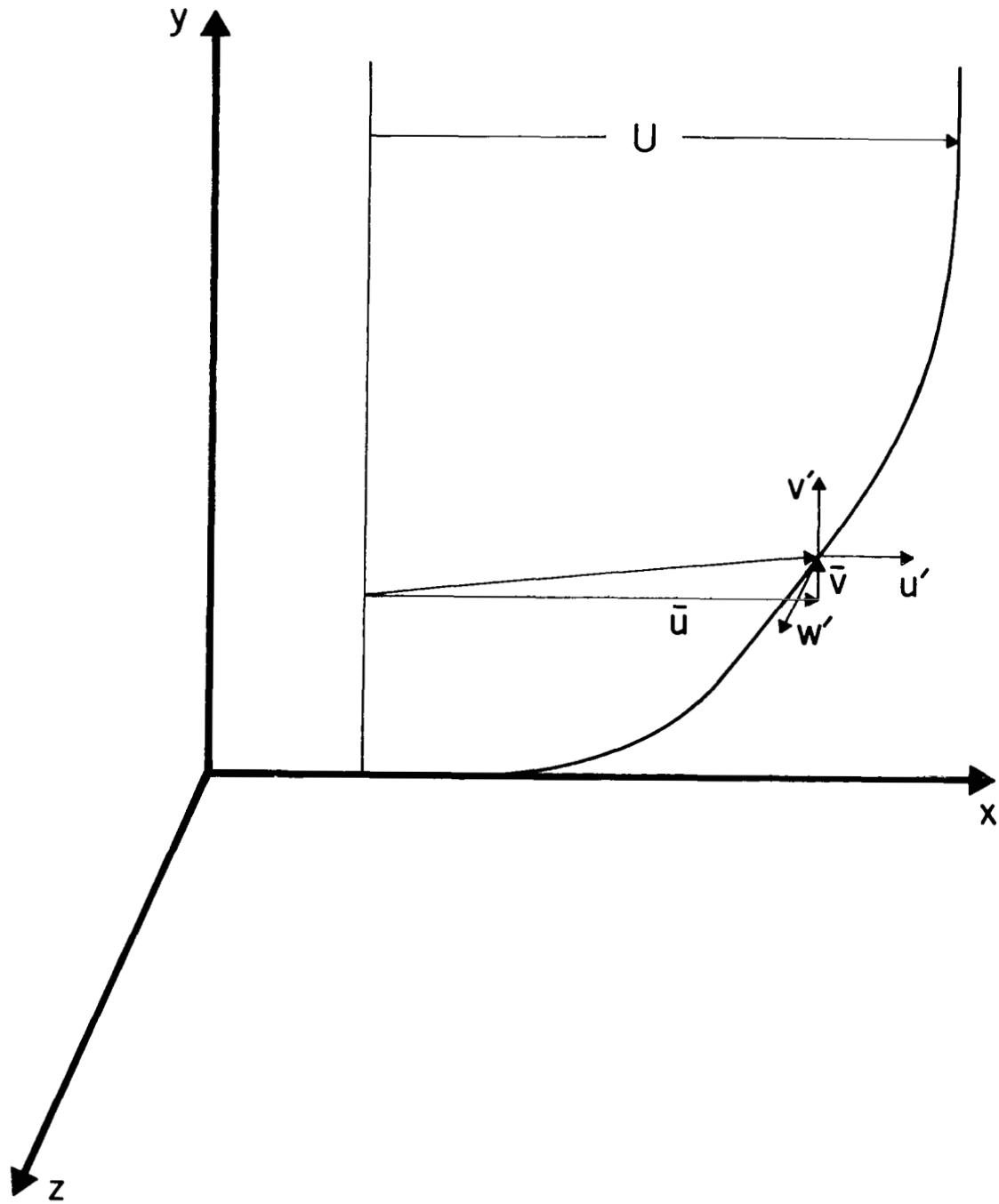

FIGURE 1. Illustration of coordinate system.

(where $\Delta\bar{\rho}$ is the variation of $\bar{\rho}$ across the boundary layer and δ is the thickness of layer which is small with respect to the scale in the x direction, ℓ) so long as

$$\frac{\Delta\bar{\rho}}{\rho_e} = 1 - \frac{h_e^o / h_w}{1 + \frac{\gamma-1}{2} M_e^2} = O(1) \tag{5}$$

Presumably at some high heat transfer rate the condition will be violated. However, in flow regimes where (5) is valid, many of the correlation terms in equation (2) are shown to be negligible. The resulting equations can then be written in the form

$$\frac{\partial \bar{\rho}\,\bar{u}}{\partial x} + \frac{\partial}{\partial y}\left(\bar{\rho}\,\bar{v} + \overline{\rho' v'}\right) = 0 \quad , \tag{6a}$$

$$\bar{\rho}\,\bar{u}\,\frac{\partial \bar{u}}{\partial x} + \left(\bar{\rho}\,\bar{v} + \overline{\rho' v'}\right)\frac{\partial \bar{u}}{\partial y} = -\frac{d\bar{p}}{dx} + \frac{\partial \bar{\tau}}{\partial y} \quad , \tag{6b}$$

$$\bar{\rho}\,\bar{u}\,\frac{\partial \overline{h^o}}{\partial x} + \left(\bar{\rho}\,\bar{v} + \overline{\rho' v'}\right)\frac{\partial \overline{h^o}}{\partial y} = \frac{\partial}{\partial y}\left(\bar{q} + \bar{u}\,\bar{\tau}\right) \quad , \tag{6c}$$

$$\overline{h^o} = \bar{h} + \frac{\overline{u^2}}{2} \quad , \tag{6d}$$

$$\overline{p_e} = \frac{\gamma - 1}{\gamma}\,\bar{\rho}\,\bar{h} \quad , \tag{6e}$$

where

$$\bar{\tau} = \bar{\mu}\,\frac{\partial \bar{u}}{\partial y} - \bar{\rho}\,\overline{u'v'} \quad , \tag{6f}$$

and

$$\bar{q} = \bar{k}\,\frac{\partial \bar{h}}{\partial y} - \bar{\rho}\,\overline{v'h'} \quad . \tag{6g}$$

Molecular viscous stresses and heat flux terms have been added to the equations above to make them valid to the wall. In doing so the terms $\left(\overline{\mu'(\partial u'/\partial y)}\right)$,

$(\overline{\kappa' \partial h'/\partial y})$ have been neglected relative to $\bar{\mu}(\partial\bar{u}/\partial y)$, $\bar{\kappa}(\partial\bar{h}/\partial y)$ which are themselves small everywhere but near the wall.

Effective Viscosity Hypothesis

The influence of turbulence appears in the boundary layer equations (6a),(6b)&(6c) through the terms $\overline{\rho' v'}$, $\overline{u' v'}$ and $\overline{v' h'}$. However, only $\overline{u' v'}$ and $\overline{v' h'}$ need be considered since $\rho' v'$ always occurs in the combined form, $\bar{\rho}\bar{v} + \overline{\rho' v'}$, which may be eliminated from (6b)and(6c) with the continuity equation. Therefore, in order to complete equations(6b) and(6c) the quantities $\overline{u' v'}$ and $\overline{v' h'}$ must be related to the mean flow variables. Since the necessary understanding of the turbulent mechanism which gives rise to these terms is not likely to be available soon, a single concise empirical assumption is the next best alternative. Following the line of argument used by Mellor [3,4,5] for incompressible flow, an empirical relation will be proposed for the terms $\overline{u' v'}$ and $\overline{v' h'}$ in compressible flow with heat transfer.

The empirical relation for $\overline{u' v'}$ is couched in the form

$$\frac{\bar{\tau}}{\bar{\rho}} = \bar{\nu}\frac{\partial\bar{u}}{\partial y} - \overline{u' v'} = \nu_e \frac{\partial\bar{u}}{\partial y} \quad , \tag{7}$$

where ν_e is an effective kinematic viscosity of the type first proposed by Boussinesq. A kinematic viscosity is chosen because of the essentially kinematic nature of the velocity correlation, $\overline{u' v'}$. The hypothesis for the form of ν_e rests on three assumptions which are supposed to be universally valid: 1) in the outer, or defect layer, ν_e depends on only three quantities, $\delta_k^* U$, y and $\frac{\partial\bar{u}}{\partial y}$, where $\delta_k^* U (= \int_0^\infty (U - \bar{u}) dy)$ is the scale suggested by Clauser [2] ; 2) in the inner, or wall layer, ν_e also depends on only three quantities, $\bar{\nu}$, y and $\frac{\partial\bar{u}}{\partial y}$, where $\bar{\nu}$ is the local molecular viscosity; and 3) in this two layer model there is a region where the layers overlap and both expressions for ν_e apply simultaneously. It follows from the first two assumptions that in the defect layer, ν_e must be of the form

$$\frac{\nu_e}{\delta_k^* U} = \Phi\left(\frac{\kappa^2 y^2}{\delta_k^* U}\frac{\partial\bar{u}}{\partial y}\right) \quad , \tag{8a}$$

and in the wall layer, ν_e must be of the form

$$\frac{\nu_e}{\bar{\nu}} = \phi\left(\frac{\kappa^2 y^2}{\bar{\nu}} \frac{\partial \bar{u}}{\partial y}\right) \quad , \tag{8b}$$

where κ is an empirical constant. Thus the hypothesis consists of two forms each individually independent of the Reynolds number, Mach number and pressure gradient. Now, as a consequence of the third assumption, it follows that the form of the effective viscosity in the overlap region must be,

$$\nu_e = \bar{\nu}\,\phi = \delta_k^* U\,\Phi \quad . \tag{9}$$

Thus in the overlap region ϕ and Φ must be linear functions so that

$$\nu_e = \kappa^2 y^2 \frac{\partial \bar{u}}{\partial y} \quad . \tag{10}$$

This is a result identical to that obtained heuristically by Prandtl [6]. Here, however, it evolves as a consequence of the independence of the functional forms for the wall layer and the defect layer. Lastly, for the hypothesis to predict correctly a viscous sublayer it is clear that very close to the wall, $\phi \to 1$.

An alternative functional form, completely equivalent to (8) but offering some computational advantage was later offered by Mellor [5]; it may be written

$$\frac{\nu_e}{U\delta_k^*} = \Phi(X) \quad , \quad X = \frac{\kappa y}{U\delta_k^*}\sqrt{\frac{\bar{\tau}}{\bar{\rho}}} \quad ; \text{ in the defect layer} \tag{11a}$$

$$\frac{\nu_e}{\bar{\nu}} = \phi(X) \quad , \quad X = \frac{\kappa y}{\bar{\nu}}\sqrt{\frac{\bar{\tau}}{\bar{\rho}}} \quad ; \text{ in the wall layer} \tag{11b}$$

Any function in the form of (8a,b) may be transformed to (11a,b) with help of the relation $\partial\bar{u}/\partial y = (\bar{\tau}/\bar{\rho})/\nu_e$.

As before, in the overlap layer, we must have $\nu_e = \overline{\nu}\phi = U\delta_k^*\Phi = \kappa y(\overline{\tau}/\overline{\rho})^{1/2}$ or equivalently $\phi = X$ and $\Phi = X$. Specific functions may be determined by comparison of calculated profiles with constant pressure, incompressible velocity profiles and are shown in Figure 2a,b. The specific curve fit for $\phi(X)$ given in Figure 2b is simpler in form to that previously cited in [5] but is operationally equivalent. The value $\kappa = .41$ is the von Karman constant and is chosen to predict correctly the experimentally observed logarithmic law of the wall (when $\overline{\tau} \simeq \tau_w$). The constant $\sigma = 6.9$ is chosen to give a best fit to Laufer's data [7] in the viscous sublayer in the manner demonstrated in [4]. The outer profile $\Phi(X)$ was specified so as to conform to Clauser's suggestion that Φ = constant = K in the outer layer. Obviously this representation is not correct near the outer edge of the profile and could be replaced by another function $\Phi(X)$ which decreases for large y. However, experience indicates that this would only slightly alter the predicted profile shape.

Finally, it is clear now that relations (11a,b) are a proposal of empirical inner and outer functions for ν_e even though knowledge of a differential equation for ν_e is absent. Therefore a composite function can be constructed using a prescription offered by Van Dyke [8] for combining inner and outer functions (the prescription can be expressed as the sum of the inner and outer functions minus their common asymptote). Thus ν_e can be written for the whole layer as

$$\frac{\nu_e}{\overline{\nu}} = \phi(X) + \underset{\sim}{R}\Phi\left(\frac{X}{\underset{\sim}{R}}\right) - X \quad , \tag{12a}$$

or

$$\frac{\nu_e}{\delta_k^* U} = \frac{1}{\underset{\sim}{R}}\,\phi(\underset{\sim}{R}X) + \Phi(X) - X \quad , \tag{12b}$$

where $\underset{\sim}{R} \equiv \dfrac{U\delta_k^*}{\overline{\nu}}$. Some illustrative examples of (12a,b) in incompressible flow for several values of $\underset{\sim}{R}$, are shown in Fig. 3. For compressible flow, the results are conceptually the same but are complicated by the molecular viscosity variation in $\underset{\sim}{R}$ and X.

It is evident that (12a) or (12b) can only be valid for large Reynolds number. In fact, for $\underset{\sim}{R}_s < 700$ the overlap layer disappears. Here the notation

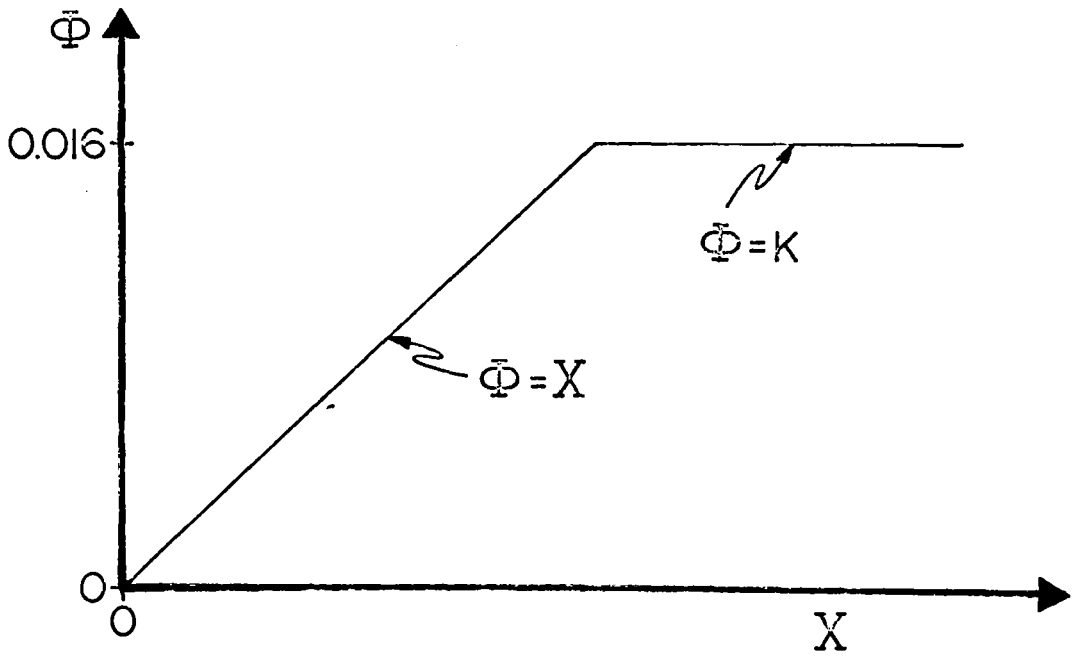

a) outer layer

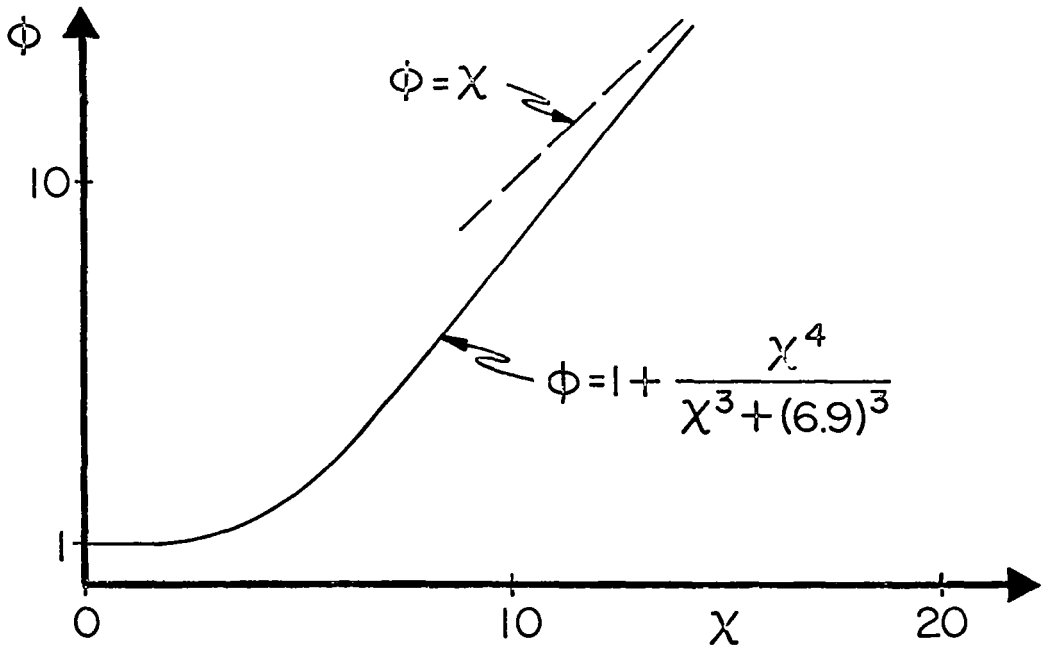

b) inner layer

FIGURE 2. Effective viscosity hypothesis.

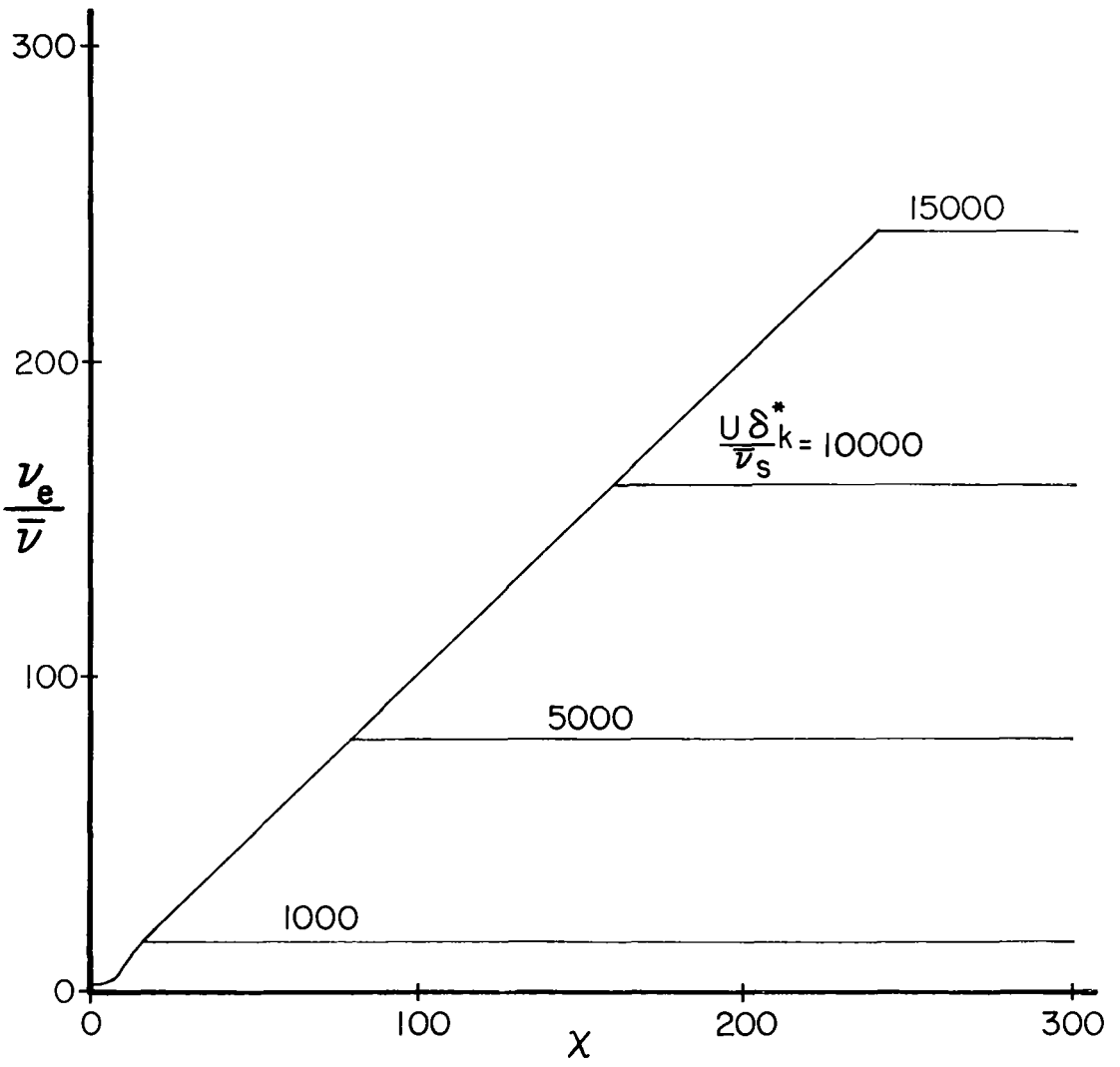

FIGURE 3. Illustrations of the composite effective viscosity function for an incompressible flow.

$\underset{\sim}{R}_s$ is used to designate the value of $\underset{\sim}{R}$ at the edge of the laminar sublayer. From experience it is apparent that, so long as $\underset{\sim}{R}_s > 2500$, very little error due to low Reynolds number effects is evident.

The additional complication in compressible form of the hypothesis compared to the incompressible form is that $\bar{\nu}$, as it appears in (12a) and in the definition of $\underset{\sim}{R}$ and X, is not a constant. Therefore $\bar{\nu}$ will be evaluated according to the thermodynamic property relations between $\bar{\nu} = \frac{\bar{\mu}}{\bar{\rho}}$ and the local mean temperature and pressure. The importance of this consideration is restricted to the viscous sublayer but is nevertheless necessary to accurate predictions in the case of high Mach numbers where $\bar{\nu}$ in the viscous sublayer may be much larger than ν_∞. One effect is that a large $R_\delta^* (= \frac{U\delta^*}{\nu_\infty})$ may correspond to a much smaller $\underset{\sim}{R}_s (= \frac{U\delta_k^*}{\bar{\nu}_s})$ as determined locally in the viscous sublayer. It seems that, for the data to be considered here, the difficulty is frequently encountered in high Mach number flow and some consideration will be given to a tentative correction.

The underlying assumption that has been made both in this and most other effective viscosity hypotheses is that the Reynolds stress, $\overline{u'v'}$, is completely determined by the local mean flow variables. Undoubtedly this is not always the case. The history of the turbulence will probably be important in boundary layers which change rapidly over short distances. In view of this Bradshaw, Ferriss and Atwell [9] have proposed to calculate $\overline{u'v'}$ from the equation governing turbulent energy transport using several empirical functions relating the quantities in the equation. Although it is an interesting approach, we have difficulty in understanding the conceptual basis of some of their assumptions. Furthermore, the nature of the calculation restricts prediction to regions outside of the viscous sublayer, and the numerical scheme can not be applied to laminar flows.

The other assumptions which have been made all apply to the formulation itself. First, there is the assumption of a two layer model. In this, each layer, represented by the effective viscosities (11a) and (11b), has its own scale, $\delta_k^* U$ and $\bar{\nu}$ respectively. Although there have been attempts to formulate the effective viscosity according to a one layer model, (van Driest, [10]), it has been generally acknowledged (Townsend, [11]) that two scales are necessary. The assumption of an overlap layer where both formulations apply has received strong experimental support. This fact was used by Millikan [12] to infer the velocity profile in that region.

Appendix B compares the present hypothesis with others that have appeared in the literature.

The other quantity which must be specified is $\overline{v'h'}$. In order to do this, the assumption is made, following Reynolds, that the heat flux can be written as

$$\bar{q} = \bar{\rho}\,\alpha_e \frac{\partial \bar{h}}{\partial y} \quad , \tag{13}$$

where α_e is the effective heat diffusivity. A relation between α_e and ν_e can be established with the usual assumption of a turbulent Prandtl number, Pr_t. Since $(\nu_e - \bar{\nu})$ and $(\alpha_e - \bar{\alpha})$ are the turbulent (or eddy) viscosity and diffusivity respectively, then a turbulent Prandtl number Pr_t may be defined by analogy to a molecular Prandtl number Pr. Thus

$$Pr = \frac{\bar{\nu}}{\bar{\alpha}} \tag{14}$$

and

$$Pr_t = \frac{\nu_e - \bar{\nu}}{\alpha_e - \bar{\alpha}} \tag{15}$$

so that the effective diffusivity can be written as

$$\alpha_e = \frac{\bar{\nu}}{Pr} + \frac{1}{Pr_t}(\nu_e - \bar{\nu}) \tag{16}$$

In the most general case the turbulent Prandtl number could be a function of local variables. However, in the calculations described in Section IV, the usual assumption of constant turbulent Prandtl number was made.

III. SOLUTION OF THE EQUATIONS OF MOTION

The steady two-dimensional flow in a boundary layer on a plane surface at moderate Mach number and heat transfer rate, from the preceding analysis, is characterized by the equations

$$\frac{\partial \bar{\rho}\bar{u}}{\partial x} + \frac{\partial}{\partial y}\left(\bar{\rho}\,\bar{v} + \overline{\rho' v'}\right) = 0 \quad , \tag{17a}$$

$$\bar{\rho}\,\bar{u}\frac{\partial \bar{u}}{\partial x} + \left(\bar{\rho}\,\bar{v} + \overline{\rho' v'}\right)\frac{\partial \bar{u}}{\partial y} = -\frac{d\bar{p}}{dx} + \frac{\partial \bar{\tau}}{\partial y} \quad , \tag{17b}$$

$$\bar{\rho}\,\bar{u}\frac{\partial \overline{h^o}}{\partial x} + \left(\bar{\rho}\,\bar{v} + \overline{\rho' v'}\right)\frac{\partial \overline{h^o}}{\partial y} = \frac{\partial}{\partial y}\left(\bar{q} + \bar{u}\,\bar{\tau}\right) \quad , \tag{17c}$$

$$\bar{p} = \frac{\gamma - 1}{\gamma}\,\bar{\rho}\,\bar{h} \quad , \tag{17d}$$

$$\overline{h^o} = \bar{h} + \frac{\bar{u}^2}{2} \quad . \tag{17e}$$

From equations (7) and (13) the effective shear stress and heat flux are

$$\bar{\tau} = \bar{\rho}\,\nu_e \frac{\partial \bar{u}}{\partial y} \quad , \tag{17f}$$

and

$$\bar{q} = \bar{\rho}\,\alpha_e \frac{\partial \bar{h}}{\partial y} \quad . \tag{17g}$$

The effective viscosity, from equations (11) and (12), is

$$\nu_e = \bar{\nu}\,\phi(X\ \underset{\sim}{R}) + U\delta_k^*\left[\Phi(X) - X\right] \tag{18a}$$

$$X = \frac{\kappa y}{U\delta_k^*}\sqrt{\frac{\bar{\tau}}{\rho}} \tag{18b}$$

and

$$\underset{\sim}{R} = U\delta_k^*/\bar{\nu} \tag{18c}$$

and from equation (16) the effective conductivity is

$$\alpha_e = \frac{\bar{\nu}}{Pr} + \frac{1}{Pr_t}(\nu_e - \bar{\nu}) \quad . \tag{18d}$$

The Sutherland molecular viscosity relation,

$$\frac{\bar{\nu}}{\nu_\infty} = \left(\frac{\bar{h}}{h_e}\right)^{5/2} \frac{(h_e/c_p) + 110^\circ}{(\bar{h}/c_p) + 110^\circ} \quad (h_e/c_p \text{ in } ^\circ\text{Kelvin}) \ , \tag{19}$$

is used to evaluate $\bar{\nu}$ in equations (18a) and (18d). Finally the appropriate boundary conditions are

$$\bar{u}(y,x_o) = u_o(y) \quad , \tag{20a}$$

$$\bar{u}(o,x) = 0 \quad , \tag{20b}$$

$$\bar{v}(o,x) = 0 \quad , \tag{20c}$$

$$\lim_{y\to\infty} \int_o^y \left[\rho_e U - \bar{\rho}\,\bar{u}(y')\right] dy' = \rho_e U \delta^* \quad , \tag{20d}$$

$$\overline{h^o}(y,x_o) = \overline{h_o^o}(y) \quad , \tag{20e}$$

$$\bar{h}(o,x) = h_w(x) \quad , \quad \text{or} \quad \bar{q}(o,x) = q_w(x) \quad , \tag{20f}$$

$$\lim_{y\to\infty} \int_o^y \bar{\rho}\,\bar{u}\left[\bar{h}_e^o - \overline{h^o}(y')\right] dy' \quad \text{is bounded.} \tag{20g}$$

The integral boundary conditions on $\bar{u}$ and $\overline{h^o}$ are more restrictive than the usual,

$$\lim_{y\to\infty} \bar{u}(y,x) = U \quad , \tag{21a}$$

and

$$\lim_{y\to\infty} \overline{h^o}(y,x) = h_e^o \quad . \tag{21b}$$

As noted by Hartree, the conditions, (21), admit two types of solution for large y

$$U(x) - \bar{u}(y,x) \quad \text{and} \quad h_e^o - \overline{h^o}(y,x) \sim e^{-y^2} \quad , \tag{22a}$$

and

$$U(x) - \bar{u}(y,x) \quad \text{and} \quad h_e^o - \overline{h^o}(y,x) \sim y^{-a} \quad , \quad (0 < a) \quad . \tag{22b}$$

The second of these forms predicts infinite displacement, momentum and enthalpy thicknesses and therefore is not a valid solution. The integral boundary condition specifically avoids this and allows only the form (22a) .

It is convenient to introduce the following definitions:

$$f'(\eta,x) = \frac{\rho_e U - \bar{\rho}\,\bar{u}}{\rho_e U} \tag{23a}$$

$$\theta(\eta,x) = \frac{\rho_e}{\bar{\rho}} \tag{23b}$$

$$g'(\eta,x) = \frac{h_e^o - \overline{h^o}}{h_e^o - h_r} \quad , \tag{23c}$$

$$\eta = y/\delta^* \quad . \tag{23d}$$

Although frequently it would be more useful to have f' be a function of velocity only, the strea function-like form of f' above makes incorporation of the continuity equation much simpler. An arbitrary reference enthalpy, h_r, is used, and can be defined in any way which is convenient to a particular problem. For example, we could set $h_r = 0$ or in the case of low Mach number it is often convenient to set $h_r = h_w$ at some reference wall location. Finally, the use of the normalized variable η largely divorces the change in thickness of the boundary layer, represented by δ^*_x, from the change in shape, represented by $f'_x(\eta)$ and $g'_x(\eta)$. It is therefore possible to use a fixed distribution of η grid points in the numerical calculation rather than one in which the spacing grows with the thickness of the boundary layer.

Substitution of these parameters into equations (17b) and (17c) yields

$$\left\{\frac{\delta^*_k}{\delta^*}\frac{T}{\theta}\left[\theta\left(1-f'\right)\right]'\right\}' = \left\{Q\theta\left(\eta - f\right) - \delta^*\theta f_x\right\}f'' + \left\{\left(V\theta + \delta^*\theta_x\right)\left(f'-2\right) + \delta^*\left(\theta f'_x - \theta' f_x\right) + Q\theta'\left(\eta - f\right)\right\}f' + \left\{Q\theta'\right\}f + \left\{V\left(\theta - 1\right) + \delta^*\left(c_x - \theta f'_x + \theta' f'_x\right) - Q\theta'\eta\right\} \tag{24a}$$

$$\left[\frac{\delta^*_k}{\delta^*}\frac{T_h}{\theta}\left\{-g'' + \frac{\frac{\gamma-1}{2}M_e^2}{H\left(1+\frac{\gamma-1}{2}M_e^2\right)}\left[\frac{T}{T_h} - 1\right]\left[\theta^2\left(1-f'\right)^2\right]'\right\}\right]' = \left\{Q\left(\eta - f\right) - \delta^* f_x\right\}g'' - \delta^*\left(1-f'\right)g'_x \quad . \tag{24b}$$

The density ratio is found from equations (17d) and (17e),

$$\theta = \frac{2\left(1 + \frac{\gamma-1}{2} M_e^2\right)\left(1 - Hg'\right)}{1 + \sqrt{1 + \frac{\gamma-1}{2} M_e^2 (1 - f')^2 \left(1 + \frac{\gamma-1}{2} M_e^2\right)(1 - Hg')}} \tag{25}$$

Primes indicate differentation with respect to η and,

$$Q = \frac{(\rho_e U \delta^*)_x}{\rho_e U} \quad , \tag{26a}$$

$$V = \frac{U_x \delta^*}{U} \quad , \tag{26b}$$

$$H = \frac{h_e^o - h_r}{h_e^o} \tag{26c}$$

From (12b) and (16) the effective viscosity and conductivity are

$$T = \frac{\nu_e}{\delta_k^* U} = \frac{1}{\underset{\sim}{R}} \phi(\underset{\sim}{R} X) + \Phi(X) - X \quad , \tag{27a}$$

$$T_h = \frac{\alpha_e}{\delta_k^* U} = \frac{1}{\underset{\sim}{R}\, Pr} + \frac{1}{Pr_t}\left(T - \frac{1}{\underset{\sim}{R}}\right) \quad . \tag{27b}$$

Here, since the effective viscosity and conductivity have been expressed in terms of the defect variables throughout the layer, $\underset{\sim}{R}$ must appear explicitly in the wall layer parts of both formulations. The boundary conditions are

$$f'(\eta,x_o) = f'_o(\eta) \quad , \tag{28a}$$

$$f(o,x) = 0 \quad , \tag{28b}$$

$$f'(o,x) = 1 \quad , \tag{28c}$$

$$\lim_{y\to\infty} f(\eta,x) = 1 \quad , \tag{28d}$$

$$g'(\eta,x_o) = g'_o(\eta) \quad , \tag{28e}$$

$$g'(o,x) = \frac{h_e^o - h_w(x)}{h_e^o - h_r} \quad \text{or} \quad g''(o,x) = -\frac{\delta^* q_w(x)}{\rho_w \nu_w (h_e^o - h_r)} \quad , \tag{28f}$$

$$\lim_{y\to\infty} g(\eta,x) \quad \text{is bounded.} \tag{28g}$$

These partial differential equations are parabolic in the x direction and are therefore well suited to conversion to ordinary differential equations in η by replacement of the x derivatives with finite differences. This is done according to a scheme used successfully by Mellor [5] . The x derivatives of the functions, f' , g' and δ^* are written as

$$f'_x = \frac{f' - f'_b}{\Delta x} \quad , \tag{29a}$$

$$g'_x = \frac{h' - h'_b}{\Delta x} \quad , \tag{29b}$$

$$\delta^*_x = \frac{\delta^* - \delta^*_b}{\Delta x} \quad , \tag{29c}$$

$$\Delta x = x - x_b \quad , \tag{29d}$$

where f'_b , g'_b , etc. are the known profiles and f' , g' , etc. are the profiles to be calculated. f'_x and g'_x clearly best approximate the derivative of f' and g' at x_m , the midpoint between x_b and x . This can be used to advantage by defining the average values of the variables between x_b and x as

$$f'_m = \tfrac{1}{2}(f'_b + f') \quad , \tag{30a}$$

$$g'_m = \tfrac{1}{2}(g'_b + g') \quad , \tag{30b}$$

$$\delta^*_m = \tfrac{1}{2}(\delta^*_b + \delta^*) \quad , \tag{30c}$$

$$M_{e_m} = \tfrac{1}{2}(M_{e_b} + M_e) \quad , \text{ etc.} \tag{30d}$$

and then rewriting equations (24a), (24b) and (25) in terms of them. These equations are

$$\left\{ \frac{\delta_k^*}{\delta^*} \frac{T_m}{\theta_m} \left[\theta_m \left(1 - f_m' \right) \right]^{-'} \right\}' = \left\{ Q\, \theta_m \left(\eta - f_m \right) \right\} f_m''$$

$$+ \left\{ \left(V\, \theta_m + \delta_m^* \theta_x \right) \left(f_m' - 2 \right) + Q\, \theta_m' \left(\eta - f_m \right) - \frac{\delta_m^*}{\Delta x} \theta_m \left(1 - f_m' \right) \right\} f_m'$$

$$+ \left\{ Q\, \theta_m' + \frac{\delta_m^*}{\Delta x} \left[\theta_m \left(1 - f_m' \right) \right]' \right\} f_m$$

$$+ \left\{ V \left(\theta_m - 1 \right) + \delta_m^* \theta_x - Q\, \eta\, \theta_m' + \frac{\delta_m^*}{\Delta x} \left[\theta_m \left(1 - f_m' \right) f_b' - \left(\theta_m (1 - f_m') \right)' f_b \right] \right\} \tag{31a}$$

$$\left[\frac{\delta_k^*}{\delta^*} \frac{T_{hm}}{\theta_m} \left\{ - g_m'' + \frac{\frac{\gamma-1}{2} M_{em}^2}{H \left(1 + \frac{\gamma-1}{2} M_{em}^2 \right)} \left[\frac{T_m}{T_{hm}} - 1 \right] \left[\theta_m^2 \left(1 - f_m' \right)^2 \right]' \right\} \right]'$$

$$= \left\{ Q \left(\eta - f_m \right) - 2 \frac{\delta_m^*}{\Delta x} \left(f_m - f_b \right) \right\} g_m''$$

$$- \left\{ \frac{\delta_m^*}{\Delta x} \left(1 - f_m' \right) \right\} g_m' + \left\{ \frac{\delta_m^*}{\Delta x} \left(1 - f_m' \right) g_b' \right\} \quad , \tag{31b}$$

$$\theta_m = \frac{2\left(1 + \frac{\gamma-1}{2} M_{e_m}^2\right)\left(1 - Hg_m'\right)}{1 + \sqrt{1 + \frac{\gamma-1}{2} M_{e_m}^2 \left(1 - f_m'\right)^2 \left(1 + \frac{\gamma-1}{2} M_{e_m}^2\right)\left(1 - Hg_m'\right)}} \qquad (31c)$$

$$\theta_x = 2\,\frac{\left(\theta_m - \theta_b\right)}{\Delta x} \quad , \qquad (31d)$$

$$Q_m = \frac{\rho_e U\delta^* - \left(\rho_e U\delta^*\right)_b}{\rho_{em} U_m \Delta x} \quad , \qquad (31e)$$

$$V_m = \frac{\left(U - U_b\right)\delta^*}{U_m \Delta x} \quad , \qquad (31f)$$

$$\eta_m = \frac{y}{\delta_m^*} \quad . \qquad (31g)$$

The equations above are a set of ordinary differential equations involving only the variables f_m', g_m', etc. to be calculated and the known profiles, f_b', g_b', etc. Once f_m' and g_m' have been obtained, the profiles at x, the position of interest, are simply

$$f'(\eta) = 2\, f_m'(\eta) - f_b'(\eta) \quad , \qquad (32a)$$

$$g'(\eta) = 2\, g_m'(\eta) - g_b'(\eta) \quad , \qquad (32b)$$

$$\delta^* = 2\,\delta_m^* - \delta_b^* \quad , \text{ etc.} \qquad (32c)$$

A problem is encountered when using the finite difference method described above. If, for some reason, the known profile at x_b is not accurate, this inaccuracy is passed on with small attenuation to succeeding profiles. This situation results from the fact that near the wall the profiles adjust very quickly to local conditions. Therefore instead of approaching the correct profile more slowly as the outer layer does, the layer near the wall will immediately assume the correct values for the midpoint at each step in x. If the profile at x_b is incorrect, it will be projected through the correct midpoint profile with equation (32a) to an equally incorrect profile at position x. Besides producing profiles which are incorrect near the wall, this overshoot causes oscillating skin friction and heat transfer coefficients. An alternative to the method above is the backward difference method which, although the x derivatives are less accurate, is free of this overshoot. There the equations would be solved in the form (24a) and (24b) and the x derivatives would be approximated by

$$f_x' = \frac{f' - f_b'}{\Delta x} \quad , \tag{33a}$$

$$g_x' = \frac{g' - g_b'}{\Delta x} \quad , \text{ etc.} \tag{33b}$$

However, by combining the two difference methods, the overshoot, when it occurs, can be greatly reduced and yet sufficient accuracy can be maintained. This is accomplished by calculating the intermediate profile somewhere between $(x - x_b)/2$ and x according to the relation

$$f_m' = f_b' + \left(f' - f_b'\right)\left(\frac{x_m - x_b}{x - x_b}\right) \quad , \tag{34a}$$

$$g_m' = g_b' + \left(g' - g_b'\right)\left(\frac{x_m - x_b}{x - x_b}\right) \quad , \text{ etc.} \tag{34b}$$

In places where the boundary conditions change rapidly and overshoot is

likely, x_m can be made closer to x ; in places where overshoot is unlikely, x_m can be closer to $(x - x_b)/2$ for accuracy. Also, using this method with x_m set close to x , poor guesses for the initial profiles $f_o'(\eta)$ and $g_o'(\eta)$ will still result in acceptable profiles several x positions downstream.

Another device was found to be convenient in connection with initial profiles. In many boundary layer calculations initial velocity and enthalpy profiles are not known. Even when comparing calculations with established data, as in Section IV , initial profiles are not completely specified. This is true, for instance, in the sensitive region near the wall. What is known are the conditions of pressure gradient and heat transfer under which the layer developed and the Reynolds number and displacement thickness at the x position where the calculation is to begin. The initial profiles were therefore produced by recalculating the input profile with several simplifying assumptions. It was assumed that the pressure gradient was produced by a velocity distribution of the form

$$\frac{U}{U_o} = \left(\frac{x}{L}\right)^B \quad , \qquad U(L) = U_o \tag{35}$$

and that the growth of δ^* was linear

$$\frac{\delta^*}{L} = A\left(\frac{x}{L}\right) \quad , \tag{36}$$

which gives the result that

$$\frac{U_x \delta^*}{U} = A\,B \qquad \text{and} \qquad Q = \frac{\left(\rho_e U \delta^*\right)_x}{\rho_e U} = A\left[1 + B(1 - M_e^2)\right] \tag{37}$$

are independent of x . Finally the profiles f' and g' are assumed to be unchanging with x . The momentum and energy equations then become simple ordinary differential equations in η to be solved for f' and g'. The resulting profiles were satisfactory even though the Reynolds number was not allowed to change from profile to profile and therefore the skin friction coefficient and Stanton number are not exact. Then, since there was a slight

discontinuity in values like C_f and δ^* between the reset profile and the first profile moving forward, it was found best to allow space to calculate profiles at two or three stations before the initial station.

The solution of the ordinary differential equations (31a) and (31b) was carried out iteratively. The succession of calculations in a single iteration was as follows. The momentum equation (31a) was solved for f_m', f_m'' and δ_m^*. Then the parameters Q and V were recalculated based on the new δ_m^*. The energy equation was solved next for h_m' and h_m'' and then θ_m was determined from equation (31c). Finally the effective viscosity and conductivity were calculated from (27a) and (27b) using the variables at x_m. This method proved very satisfactory. The solution of the energy equation followed the iterations of the momentum very well. Therefore it was unnecessary to have an internal iteration loop for the energy equation to assure its convergence as did Smith and Clutter [13]. Speed of convergence for the whole loop varied, but no cases required more than seven iterations and in simple cases two iterations were sufficient.

A fourth degree Runge-Kutta method was used to solve equations (31a) and (31b). In order to use this method the f' and g' equations were written in pseudo-linear form

$$\left\{ C_6(\eta) \left[f'' + C_5(\eta) \right] \right\}' = C_3(\eta)\, f'' + C_2(\eta)\, f' + C_1(\eta)\, f + C_4 \qquad (38)$$

where the coefficients are the quantities in brackets in equations (31a,b) These coefficients were evaluated from the solution obtained from the previous iteration. The Runge-Kutta equations for the solution of (38) are given in Appendix C.

The calculation of each equation was begun from the wall with the specification of two boundary conditions as given by (28). The outer boundary conditions on (31a) and (31b) were met with the use of an asymptotic solution for large η which assured the correct exponential behavior as shown in equation (22a). The derivation of the asymptotic solution is performed with the additional simplifying assumption that the turbulent Prandtl number is unity (see Appendix D). For compressible flow with heat transfer the asymptotic forms of f' and g' can be expressed in terms of f' and g' at point η_1, far out in the layer,

$$f'(\eta,x) = f'(\eta_1,x) \exp \frac{(\eta_1 - 1)^2 - (\eta - 1)^2}{2r(x)} \quad , \tag{39a}$$

$$g'(\eta,x) = g'(\eta_1,x) \exp \frac{(\eta_1 - 1)^2 - (\eta - 1)^2}{2r(x)} \quad , \tag{39b}$$

$$r(x) = \left(\frac{\rho_{e_o} U_o \delta_o^*}{\rho_e U \delta^*}\right)^2 r(x_o) + \frac{2K}{(\rho_e U \delta^*)^2} \int_{x_o}^{x} \frac{\delta_k^*}{\delta^*} (\rho_e U)^2 \delta^* dx \tag{40}$$

The numerical solutions were matched to the asymptotic solution by exploiting the effective linearity of equations (31a) and (31b) . Both homogeneous and particular solutions were obtained for each equation. The solution of the homogeneous equation was added to the particular solution in the proportion to make the numerical solution join the analytical solution at η_1 . In this manner the third inner boundary condition which had been guessed to perform the integration was reset to the proper value afterwards. This was done according to the equations

$$f' = f_p' + A_f f_h' \quad , \tag{41a}$$

$$g' = g_p' + A_g g_h' \quad , \text{ etc.} \tag{41b}$$

The constants A_f and A_h are obtained using the derivatives of equations (39a) and (39b) , evaluated at the matching point η_1 ,

$$f''(\eta_1) = - \frac{(\eta_1 - 1)}{r} f'(\eta_1) \quad , \tag{42a}$$

$$g''(\eta_1) = -\frac{\left(\eta_1 - 1\right)}{r}\, g'(\eta_1) \quad . \tag{42b}$$

Therefore A_f and A_g are given by

$$A_f = -\frac{f_p''(\eta_1) + \dfrac{\left(\eta_1 - 1\right)}{r} f_p'(\eta_1)}{f_h''(\eta_1) + \dfrac{\left(\eta_1 - 1\right)}{r} f_h'(\eta_1)} \quad , \tag{43a}$$

$$A_g = -\frac{g_p''(\eta_1) + \dfrac{\left(\eta_1 - 1\right)}{r} g_p'(\eta_1)}{g_h''(\eta_1) + \dfrac{\left(\eta_1 - 1\right)}{r} g_p'(\eta_1)} \tag{43b}$$

The method of calculation from an operational viewpoint is as follows. First, profiles of f' and g' are read in to the program as functions of η. These profiles correspond to the first x position, $x = x_1$, say. If these profiles are complete and satisfactory as they stand, they are used unaltered. If, on the other hand, they are not the desired initial profiles, approximate initial profiles are calculated for the required initial Mach number, Reynolds number, displacement thickness, lateral wall curvature, and heat transfer rate or wall temperature. If the f' and g' profiles are to be recalculated, the input profiles are used as initial guesses.

Next the values of the mainstream Mach number and wall heat flux or temperature are read in corresponding to the discrete values of x at which profiles are to be calculated. Also read in for each x is a number between 0.5 and 1.0 which indicates the position in the interval between x values where the actual calculation of the profile is to take place. Then the profiles and parameters for each succeeding x position are calculated and reported until the last x position has been reached.

IV. COMPARISON WITH EXPERIMENTAL DATA

Zero Pressure Gradient

A wide variety of experimental velocity profiles measured in constant pressure adiabatic flows are available. Calculations were performed for a few of these profiles representing a range of Mach number from 2 up to 4.5. No data at lower Mach numbers are compared because there are few experiments in the transonic region. This is the result of experimental difficulties not related to the development of the boundary layer itself. Furthermore, the boundary layer in the subsonic and transonic range differs only slightly from the incompressible boundary layer, as is evident from Figure 10.

Calculations, for the flows considered, were begun by generating an initial constant pressure profile internally as described in Section III. Then, starting at a Reynolds number somewhat below that of the data profile, the calculation proceeded until the data Reynolds number was reached. These profiles were calculated two ways, once with the assumption $h^{o}(y) = h_e^{o}$ (or $g'(\eta) = 0$), and once using the full energy equation with $Pr = .78$ and $Pr_t = 1.0$. The results were identical within the accuracy of the graphs. Experimental profiles were chosen which had values of $U\delta_k^*/\bar{\nu}_s$ above 2500, where δ_k^* is the kinematic displacement thickness and $\bar{\nu}_s$ is the local molecular viscosity at the edge of the laminar sublayer. As explained in Section II this criterion assures that the hypothesis is well within its range of validity. The calculations and experiments are compared in Figures 4 through 9. It is clear from the figures that the prediction of the velocity profiles and skin friction coefficients is remarkably good.

Further comparison with established results was provided by calculating the skin friction coefficient for constant pressure adiabatic flows over a range of Mach number. The calculations were carried out as described for the profiles above. Initial profiles were generated and then allowed to develop until a high enough R_θ had been reached. Then, for R_θ of 2000 and 7000, the skin friction was normalized by the corresponding, incompressible skin friction. Above $M_e \approx 1$, in the $R_\theta = 2000$ case, the Reynolds number $R_s (= U\delta_k^*/\bar{\nu}_s)$ was below 2500; therefore that curve was not continued. Above $R_\theta = 7000$, there was no discernable change of the calculated values of C_f/C_f with R_θ. The results of these calculations are compared with experimental skin friction coefficients from Kuethe [20] in Figure 10.

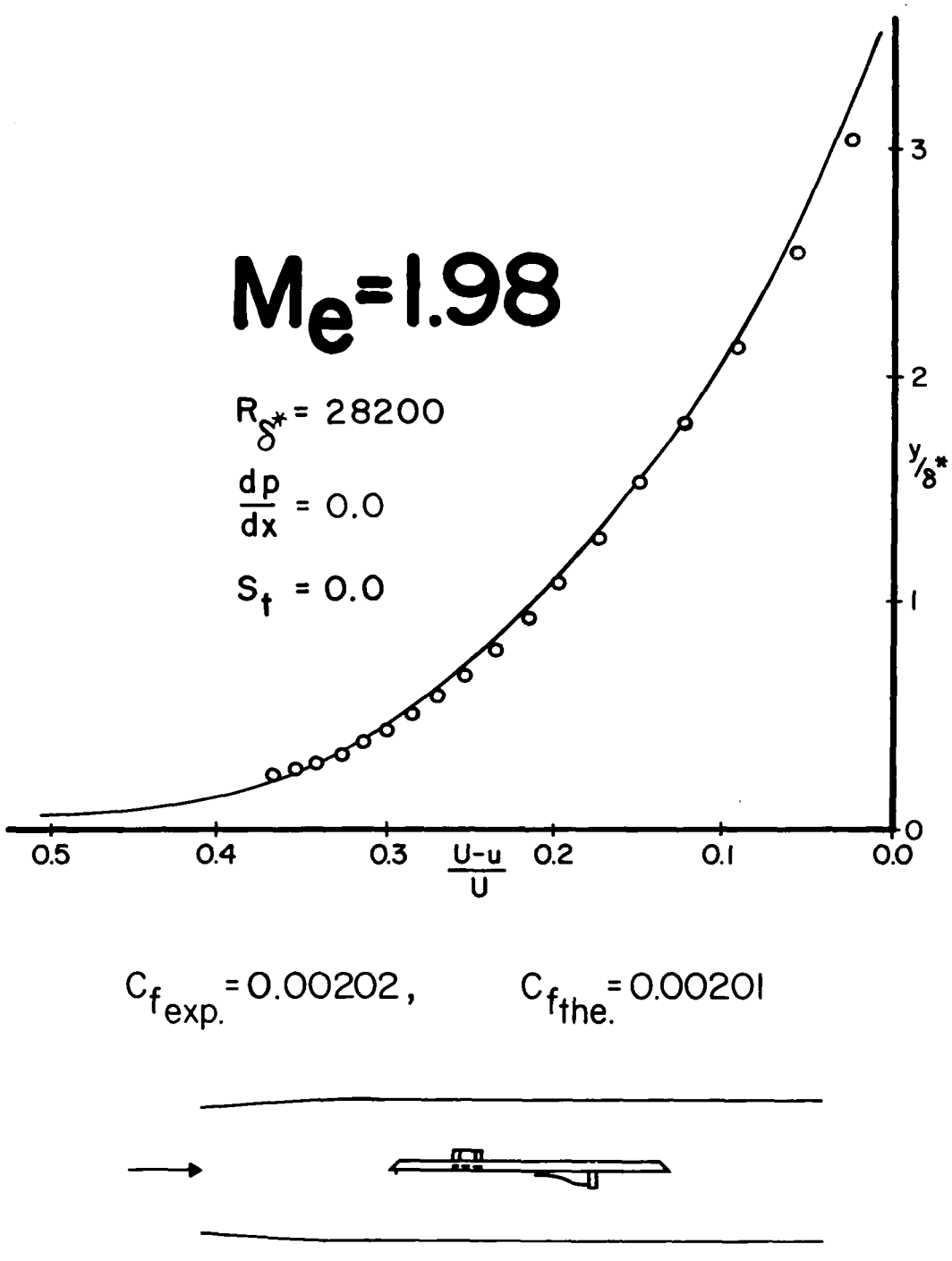

FIGURE 4. Comparison between a velocity profile measured by Coles [14] on a flat plate at M_e = 1.98, and the calculated profile shown with an unbroken line. The experimental skin friction, which was measured with a floating surface element, is also compared with the calculated value.

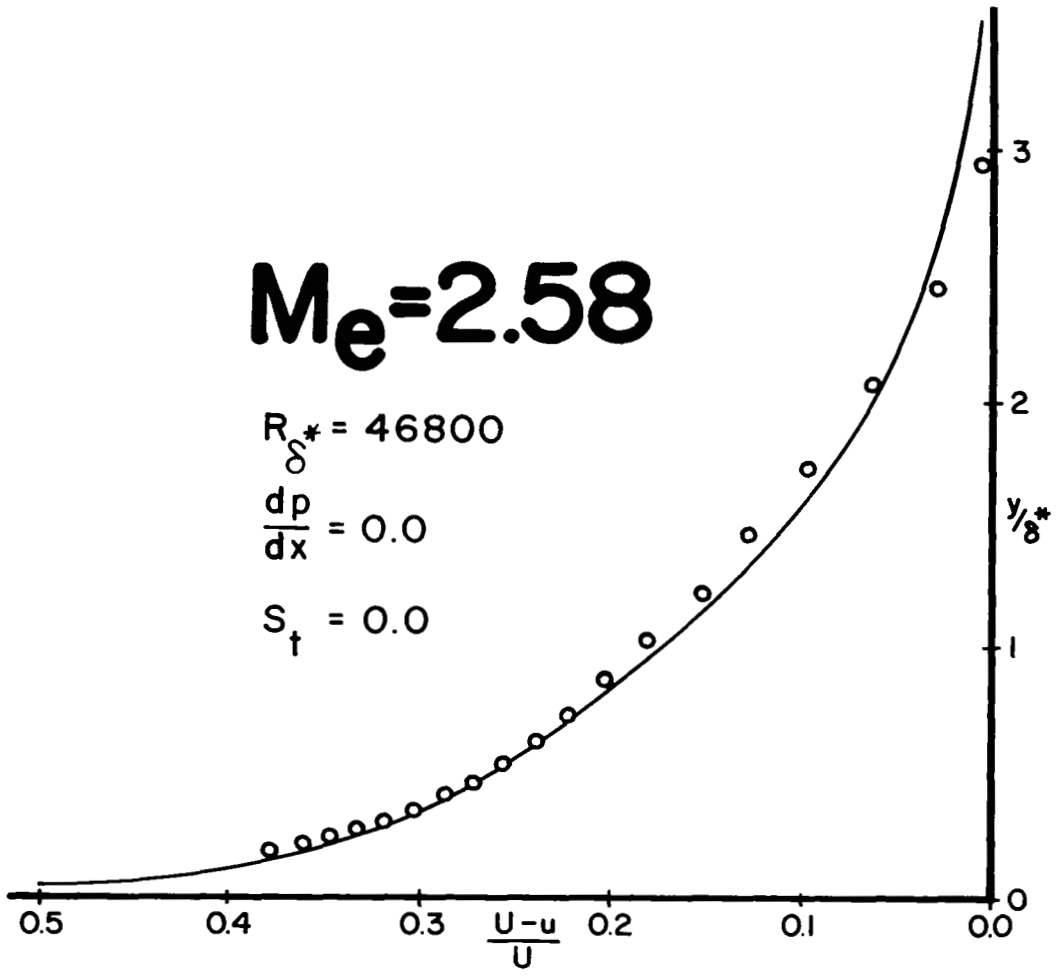

FIGURE 5. Comparison between a velocity profile measured by Coles [14] on a flat plate at M_e = 2.58, and the calculated profile shown with an unbroken line. The experimental skin friction, which was measured with a floating surface element, is also compared with the calculated value.

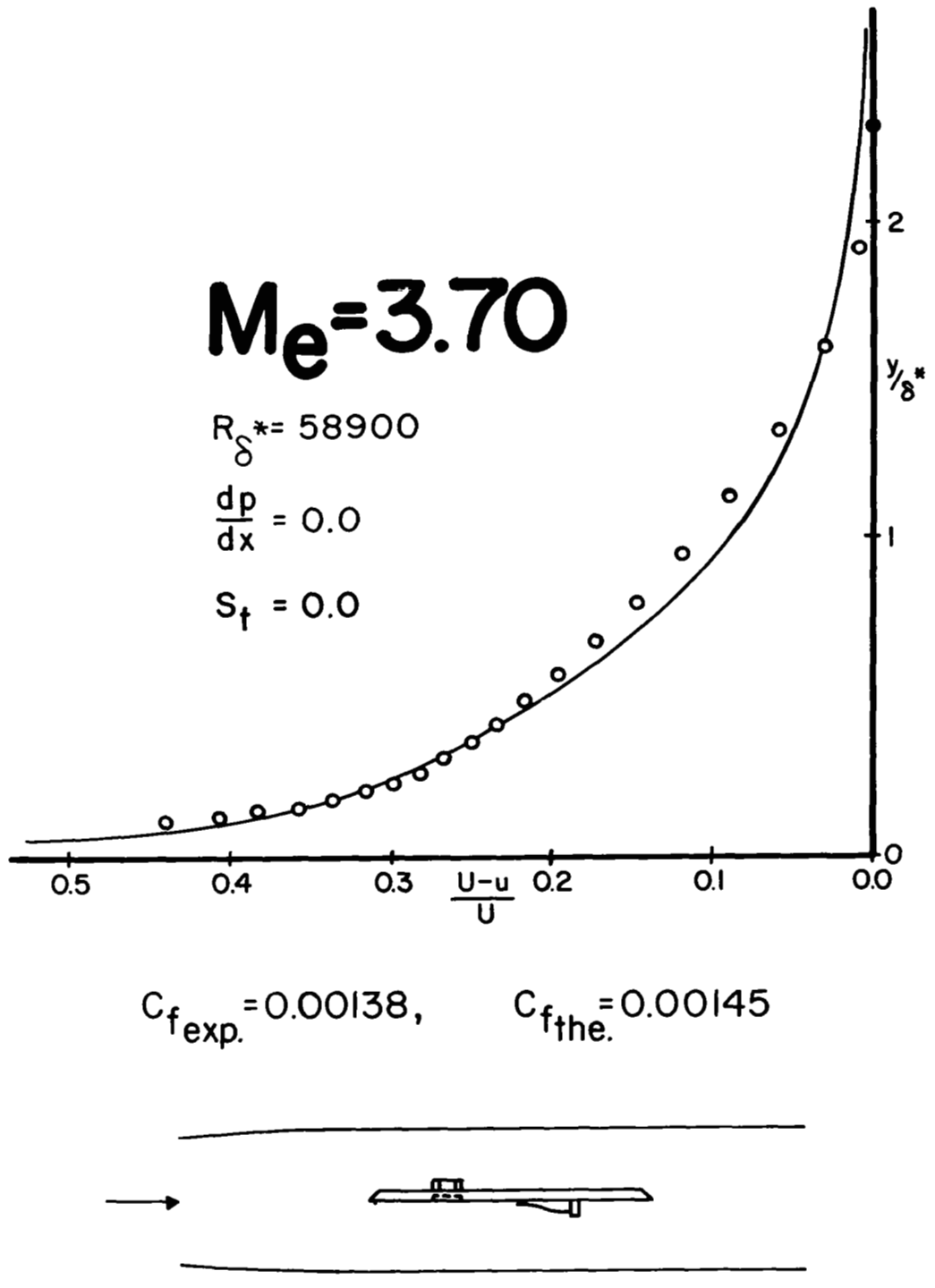

FIGURE 6. Comparison between a velocity profile measured by Coles [14] on a flat plate at M_e = 3.70, and the calculated profile shown with an unbroken line. The experimental skin friction, which was measured with a floating surface element, is also compared with the calculated value.

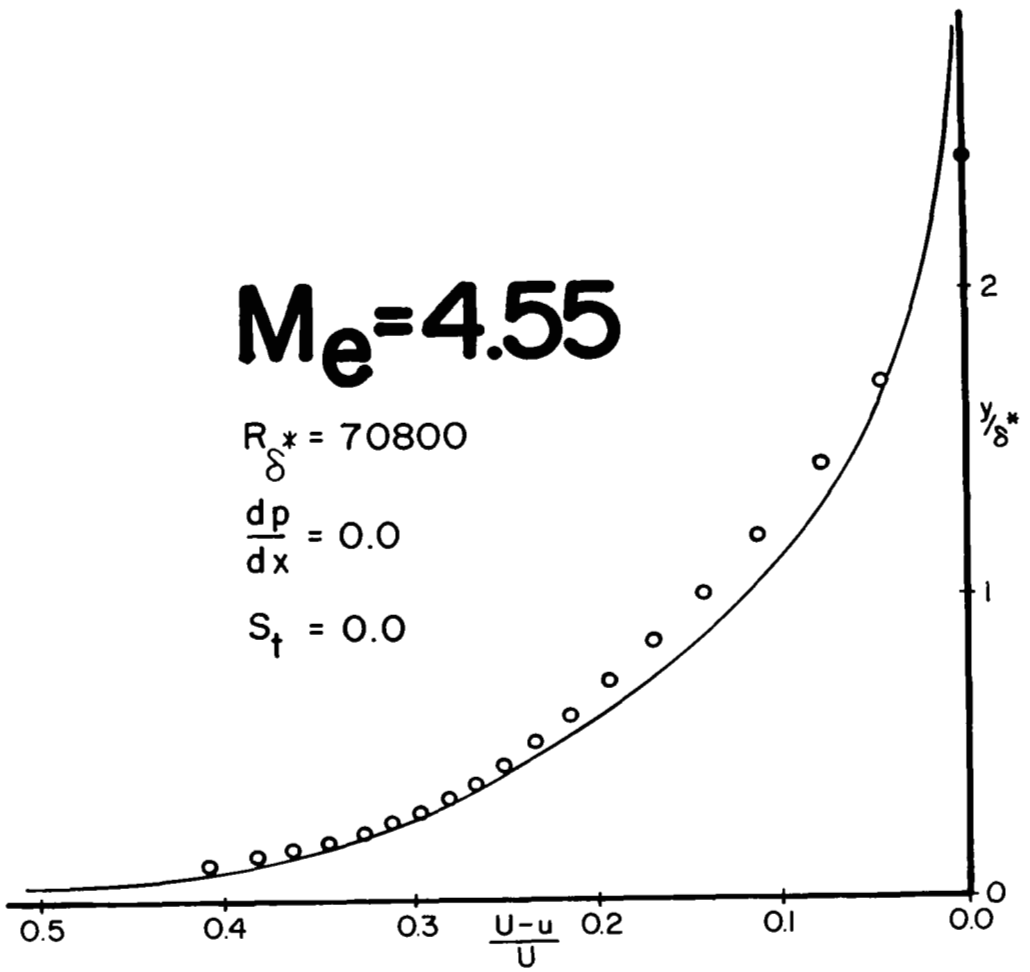

$C_{f_{exp.}} = 0.00122$, $C_{f_{the.}} = 0.00126$

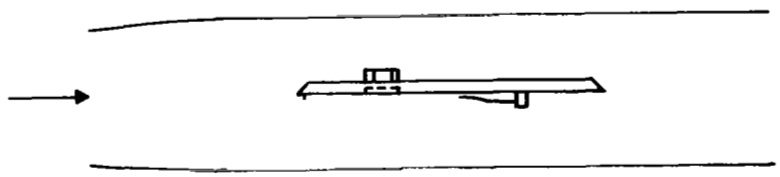

FIGURE 7. Comparison between a velocity profile measured by Coles [14] on a flat plate at M_e = 4.55, and the calculated profile shown with an unbroken line. The experimental skin friction, which was measured with a floating surface element, is also compared with the calculated value.

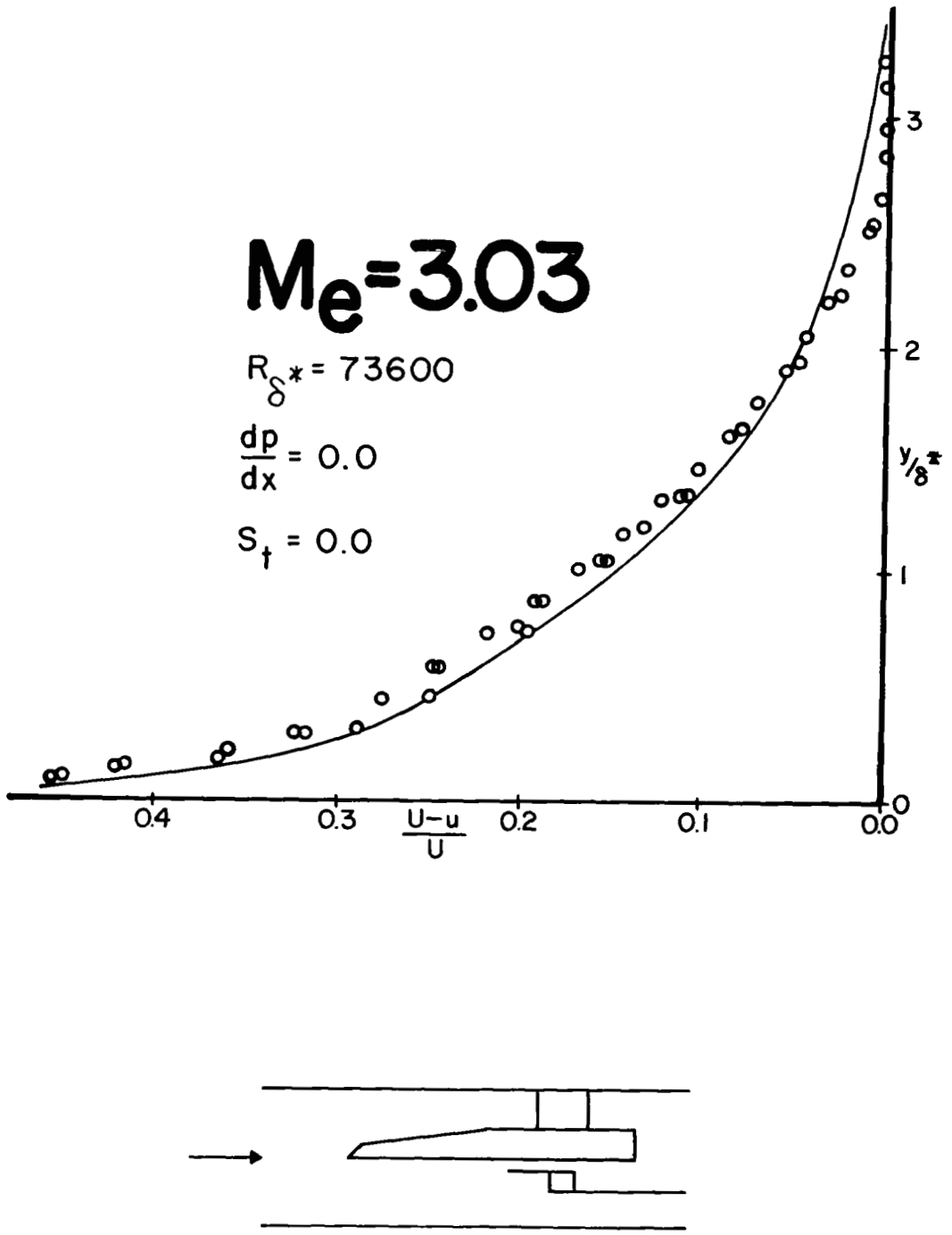

FIGURE 8. Comparison between a velocity profile measured by Nothwang [15] with a pitot tube on a flat plate at M_e = 3.03, and the calculated profile shown with an unbroken line.

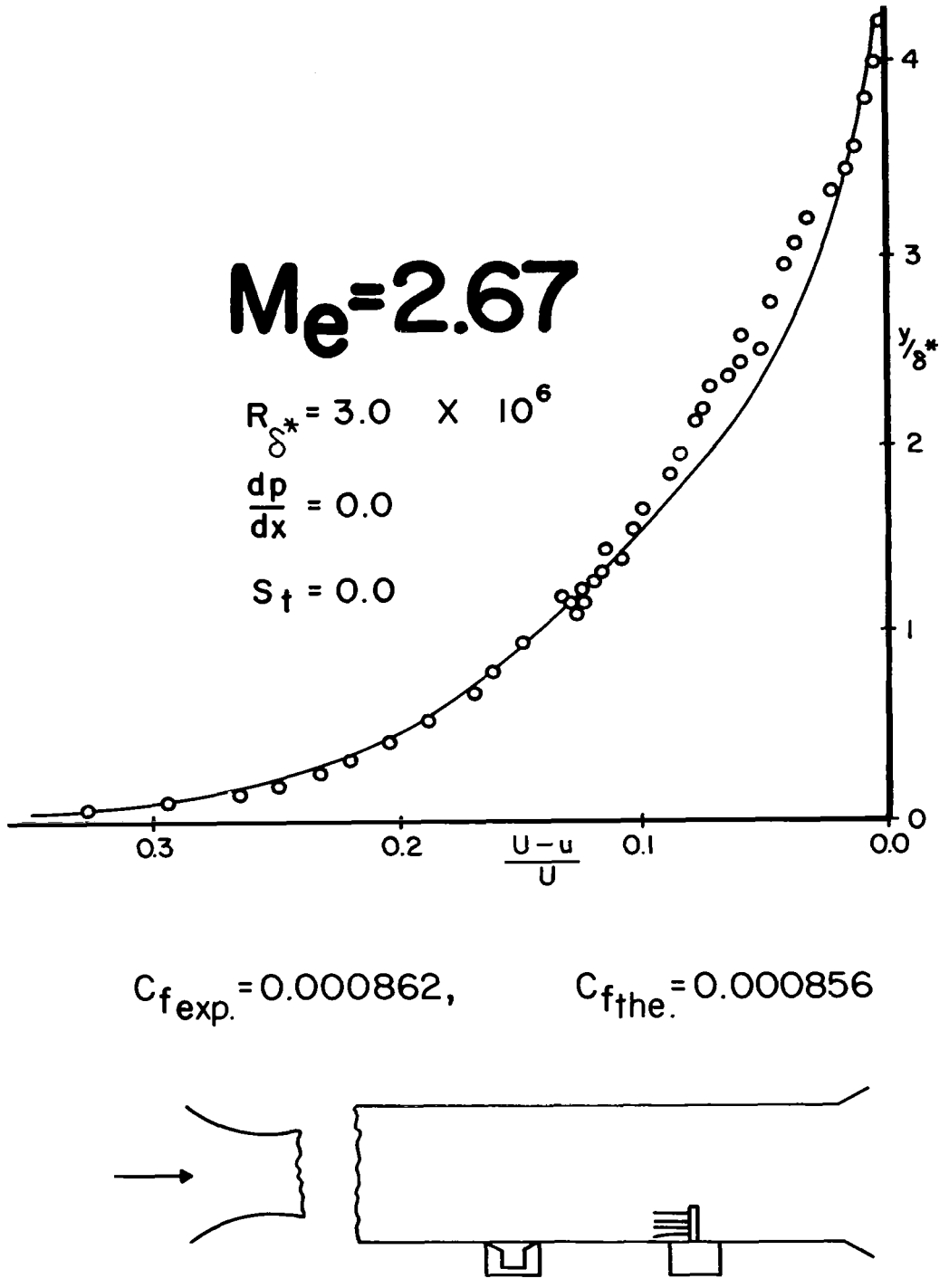

FIGURE 9. Comparison between a very high Reynolds number velocity profile measured by Moore and Harkness [16] on a tunnel wall at M_e = 2.67, and the calculated profile shown with an unbroken line.

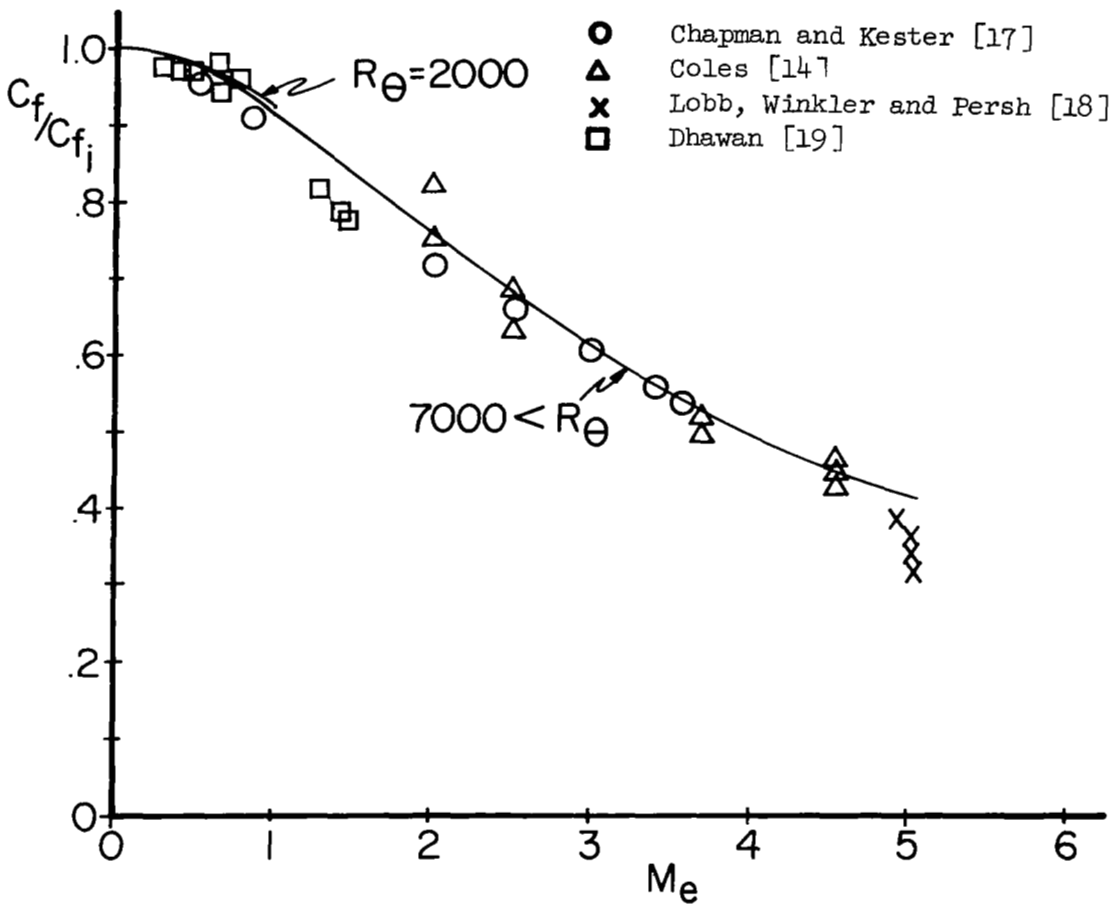

FIGURE 10. Comparison between experimental skin friction measurements obtained by a number of investigators (after Kuethe [20]), and the calculated skin friction. C_f/C_{f_i} is the ratio of compressible skin friction coefficient to incompressible skin friction coefficient at the same value of $R_\theta = 2000$, and one for R_θ greater than 7000. The calculation for $R_\theta = 2000$ does not extend beyond $M_e = 1$ because of the Reynolds number limitation on the effective viscosity hypothesis.

Again the comparison with the data is favorable.

Having seen the degree of success achieved by the effective viscosity assumption in cases where $\underset{\sim}{R}_s$ is high enough, it is valuable to study the nature of the error incurred for small values. Some examples of this are shown in Figures 11 through 16 . Figure 11 illustrates this especially well. Beginning with the first profile, for which the calculated value of $\underset{\sim}{R}_s$ is 1,260, a progressive improvement in the theoretical prediction is evident up to the last profile for which $\underset{\sim}{R}_s$ is 2,440. However, although the shape of the profile is not too good for low $\underset{\sim}{R}_s$ the growth of δ^* is quite accurate as is also shown in Figure 11 . The calculation of this series was begun by generating a constant pressure profile internally at the appropriate Mach number. Because of the slight discontinuity in skin friction and other parameters after the generated profile, which was mentioned in Section III, this profile was calculated for approximate values of δ^* and $R_{\delta}{}^*$ at x_o somewhat upstream of the first profile measurement at $x = 5.95$. Trial calculations were made from x_o up to $x = 5.95$ so that δ^* and $R_{\delta}{}^*$ matched the experimental values at $x = 5.95$.

The importance of considering $\underset{\sim}{R}_s (= U\delta_k^*/\bar{\nu}_s)$ rather than the external Reynolds number $R_{\delta}{}^* (= U\delta^*/\nu_\infty)$ is brought out in Figure 12 , where $R_{\delta}{}^*$ would be sufficiently high if the Mach number were low. However, the Mach number is high, making $\underset{\sim}{R}_s$ too low and therefore the theoretical prediction is poor. Figures 13 through 16 also exhibit the same effect for a range of Mach numbers. At the beginning of each series the prediction is poor and, although it improves slightly as the layers develop and $\underset{\sim}{R}_s$ increases, the Reynolds number is still not high enough at the end of each series, especially in the higher Mach number cases. In spite of this, it is interesting to note that the growth of θ is predicted accurately. For the calculation of the sets of profiles shown in Figures 13 through 16, as in Figure 11 , both δ^* and $R_{\delta}{}^*$ matched the experimental values at the initial x station according to the procedure described above.

Because of the variation of $\bar{\nu}$ across the layer, boundary layers with low values of $\underset{\sim}{R}_s$ occur in practice much more frequently in compressible flows than in incompressible flows. It would be useful to modify the

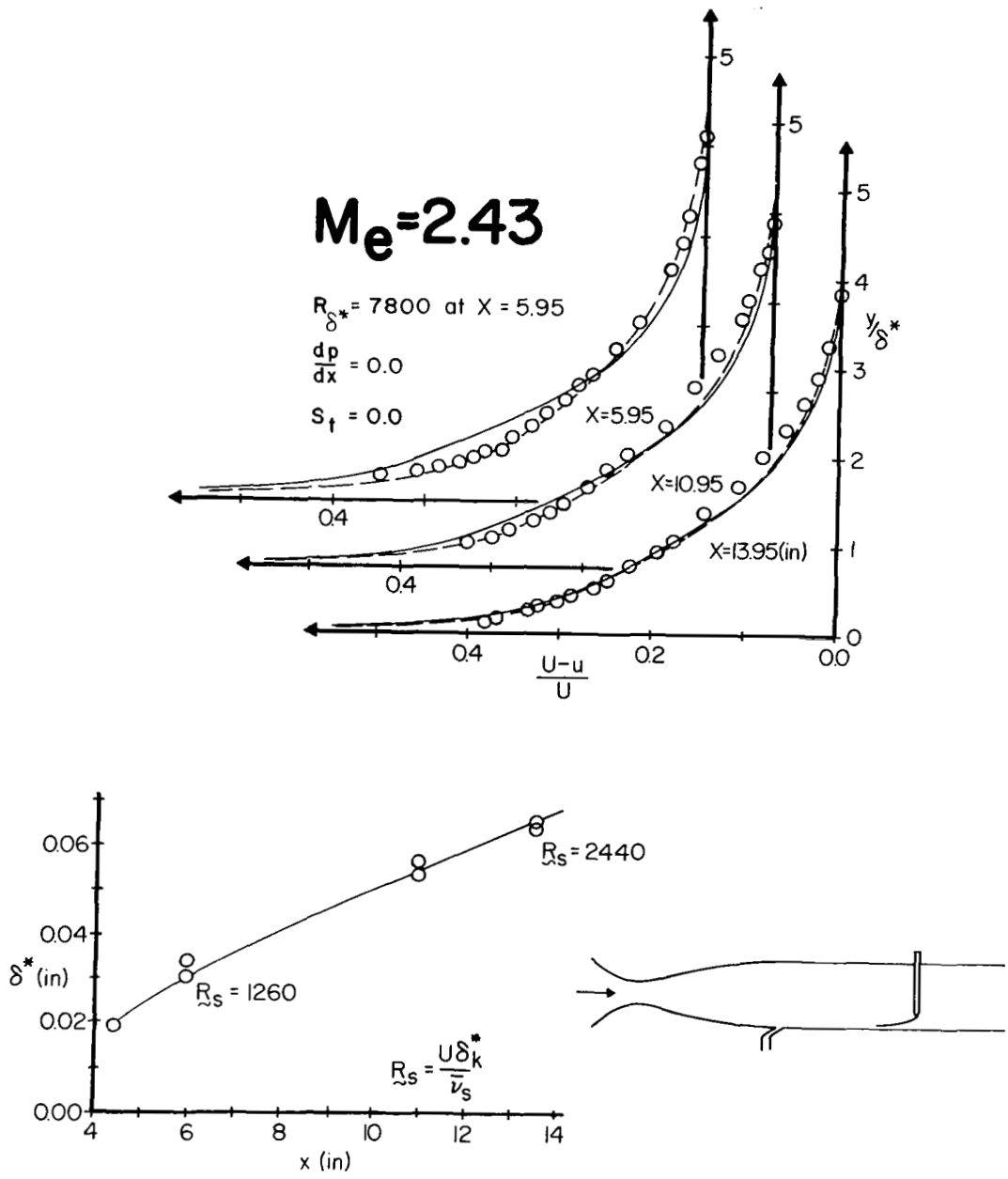

FIGURE 11. Comparison between a series of velocity profiles measured by Monaghan and Johnson [21] on the flat wall of a tunnel, and the calculated profiles. Profiles calculated using K = 0.016 in the effective viscosity function are shown with unbroken lines, and profiles calculated using $K = 0.016\ [1 + (1100/R_s)^2]$ are shown with dashed lines. The measured growth of δ^* with x is compared with the calculated growth illustrated with an unbroken line. The calculated growth of δ^* for both values of K are indistinguishable. The initial and final values of R_s are also given.

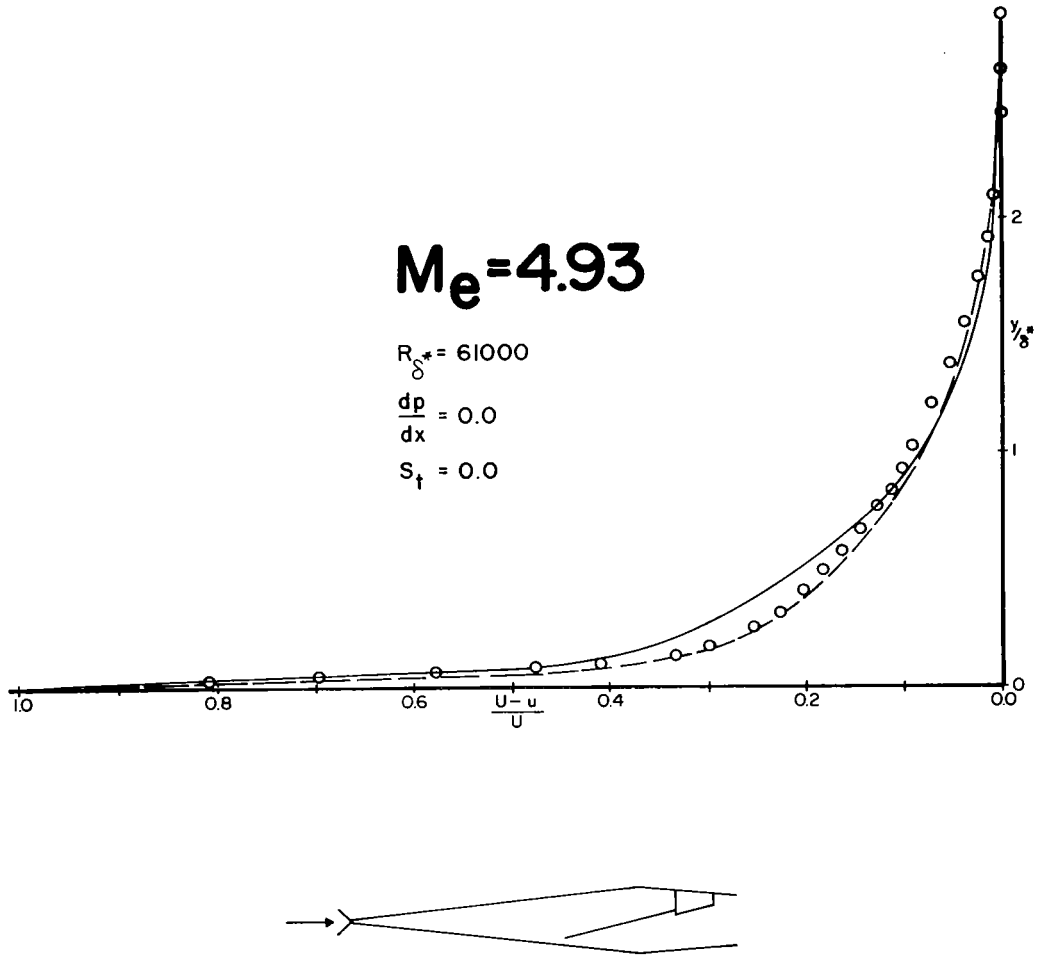

FIGURE 12. Comparison between a velocity profile measured by Lobb, Winkler and Persh [18] on a flat tunnel wall, and calculated profiles. The profile calculated using K = 0.016 in the effective viscosity function is shown with an unbroken line and the profile calculated using K = 0.016 $[1 + (1100/\underset{\sim}{R}_s)^2]$ is shown with a dashed line. The value of $\underset{\sim}{R}_s (=U\delta_k^*/\bar{\nu}_s)$ for this profile is 1050.

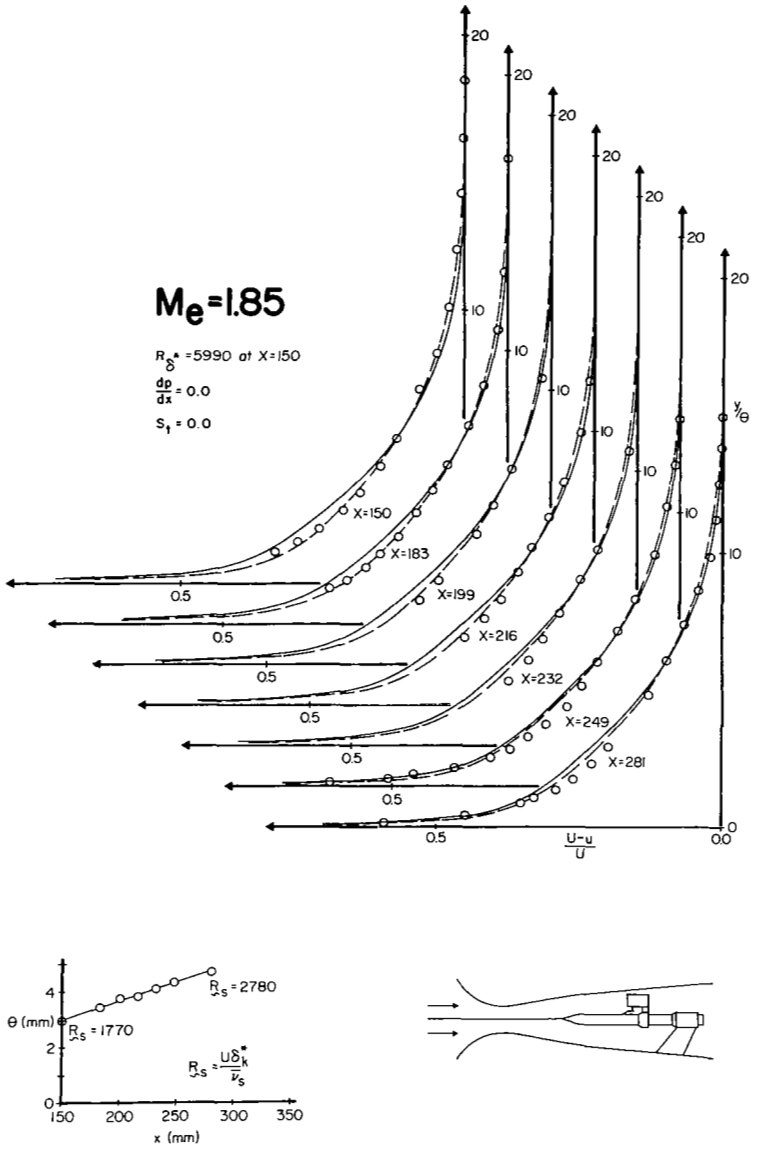

FIGURE 13. Comparison between a series of velocity profiles, measured by Michel [22] on a cylindrical model whose radius was large with respect to the boundary layer thickness, and the calculated profiles. Profiles calculated using K = 0.016 in the effective viscosity function are shown with unbroken lines and profiles calculated using $K = 0.016X [1 + (1100/\underset{\sim}{R}_s)^2]$ are shown with dashed lines.

The measured growth of θ with x is compared with the calculated growth illustrated with an unbroken line. The calculated growth of θ for both values of K are indistinguishable. The initial and final values of $\underset{\sim}{R}_s$ are also given.

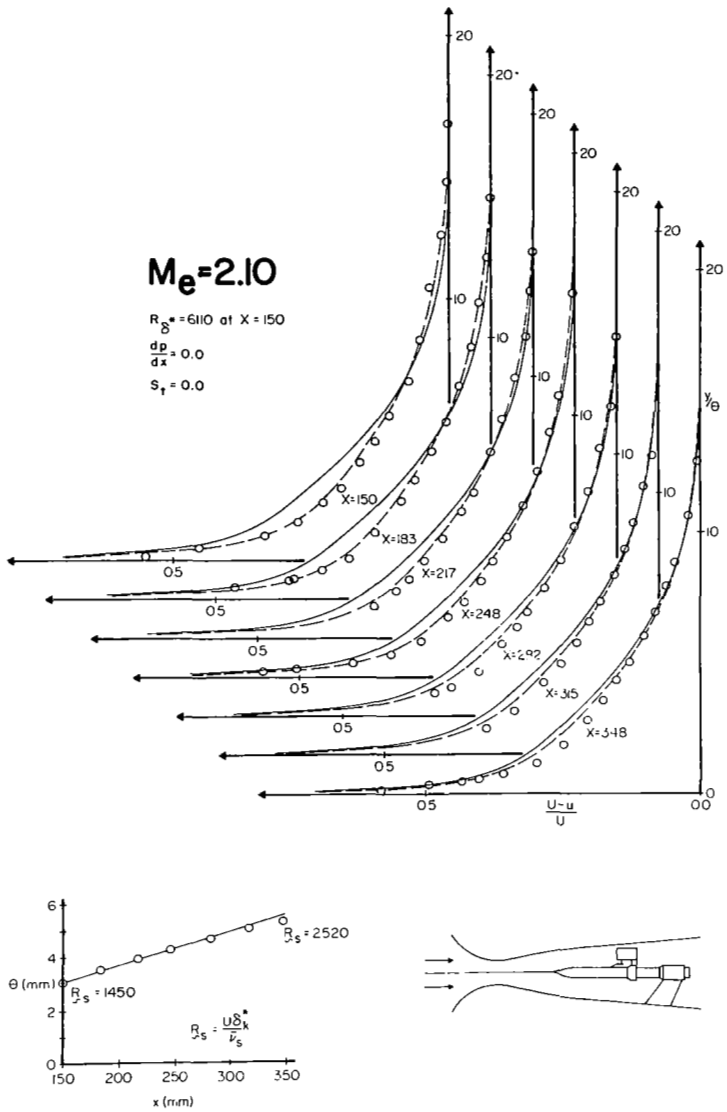

FIGURE 14. Comparison between a series of velocity profiles, measured by Michel [22] on a cylindrical model whose radius was large with respect to the boundary layer thickness, and the calculated profiles. Profiles calculated using K = 0.016 in the effective viscosity function are shown with unbroken lines and profiles calculated using $K = 0.016 X [1 + (1100/R_{\tilde{s}})^2]$ are shown with dashed lines.

The measured growth of θ with x is compared with the calculated growth illustrated with an unbroken line. The calculated growth of θ for both values of K are indistinguishable. The initial and final values of $R_{\tilde{s}}$ are also given.

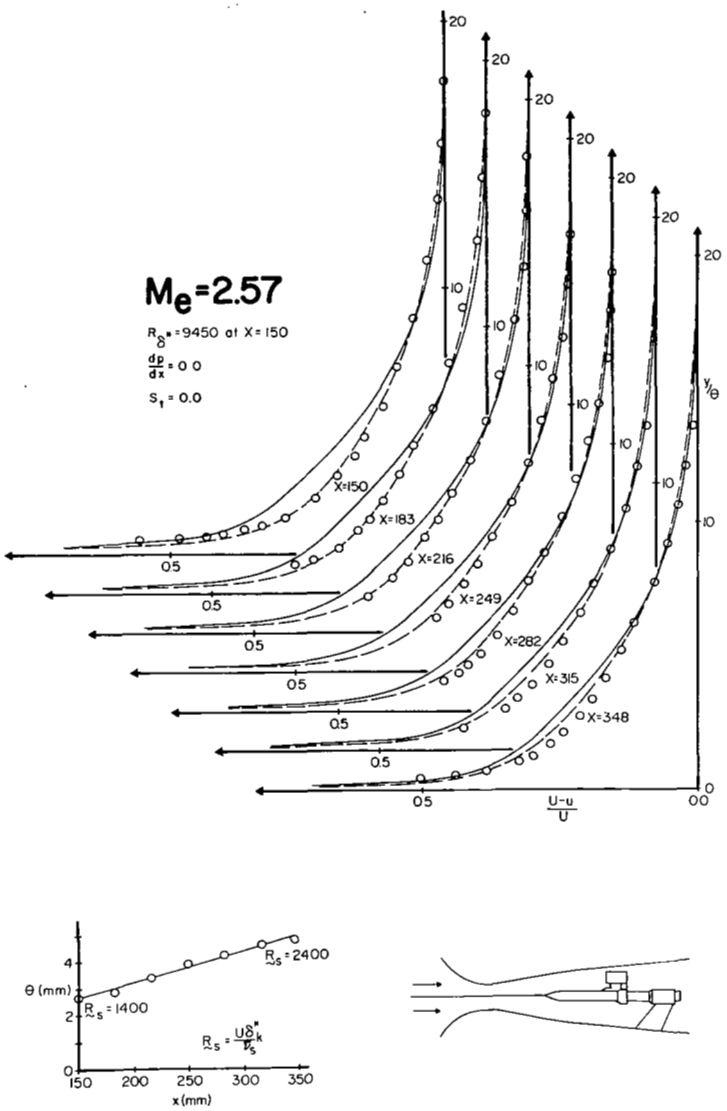

FIGURE 15. Comparison between a series of velocity profiles, measured by Michel [22] on a cylindrical model whose radius was large with respect to the boundary layer thickness, and the calculated profiles. Profiles calculated using K = 0.016 in the effective viscosity function are shown with unbroken lines and profiles calculated using $K = 0.016X[1 + (1100/R_s)^2]$ are shown with dashed lines.

The measured growth of θ with x is compared with the calculated growth illustrated with an unbroken line. The calculated growth of θ for both values of K are indistinguishable. The initial and final values of R_s are also given.

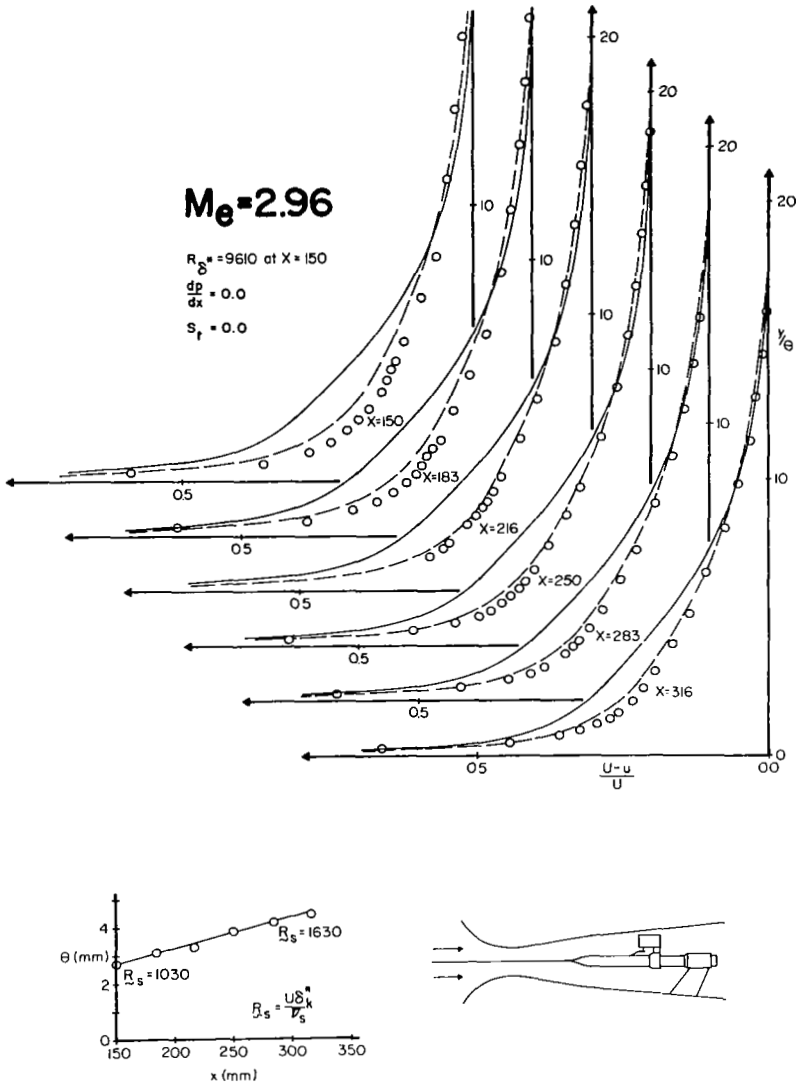

FIGURE 16. Comparison between a series of velocity profiles, measured by Michel [22] on a cylindrical model whose radius was large with respect to the boundary layer thickness, and the calculated profiles. Profiles calculated using K = 0.016 in the effective viscosity function are shown with unbroken lines and profiles calculated using $K = 0.016X[1 + (1100/\underset{\sim}{R}_s)^2]$ are shown with dashed lines.

The measured growth of θ with is compared with the calculated growth illustrated with an unbroken line. The calculated growth of θ for both values of K are indistinguishable. The initial and final values of $\underset{\sim}{R}_s$ are also given.

behavior of the effective viscosity to account for this. Accordingly, some numerical experiments were performed with trial amendments to the effective viscosity function for low Reynolds numbers. The most successful method seemed to be to vary K according to the following rule

$$K = .016\left[1 + \left(\frac{1100}{R}\right)^2\right] \quad . \tag{44}$$

Then the overlap layer, which ordinarily would have disappeared as the outer region met the sublayer, is maintained. Although this procedure maintains the essential overlap layer specified in the third assumption of the hypothesis, the device used is somewhat artificial. The results of this correction are shown as dashed lines on the velocity profiles where the Reynolds numbers were too low for the usual effective viscosity. The profiles in all cases are considerably improved. Of course, this approach is merely exploratory and the principle conclusion seems to be that it works. Furthermore, it does not seem to represent a truly systematic extension of the first order hypothesis represented by equation (12).

Axisymetric Flow with a Pressure Gradient

Variable pressure gradient data are also rare, due to the greatly increased difficulty of carrying out boundary layer investigations in flow with Mach waves. The pressure gradient experiments performed by Winter, Smith and Rotta [23] were chosen for comparison here. These data are complete and carefully taken, but the results include other effects besides pressure gradients since measurements were taken on a surface of revolution. The effects, which must be accounted for, include lateral and longitudinal curvature as well as freestream Mach number variation. Although the Mach number variation is not excessive, the change in lateral curvature causes strong convergence and divergence of the stream lines. Furthermore, in some places the approximation that $\delta/R_{LAT.} \ll 1$ was no longer valid and the equations of motion had to be written in axisymmetric form (see Appendix E). The approximation that the boundary layer was perpendicular to the axis of symmetry was still valid, however, since $\delta/R_{LONG.} \ll 1$.

Boundary layer development was calculated for four series of profiles. The approximate Mach number range represented is from 0.5 to 3.3 and the approximate Reynolds number range is from $U\delta^*/\nu_\infty = 5000$ to 45000. The lowest Mach number flow had only small changes in Mach number, whereas the Mach number variation in the other flows was more substantial. Calculations

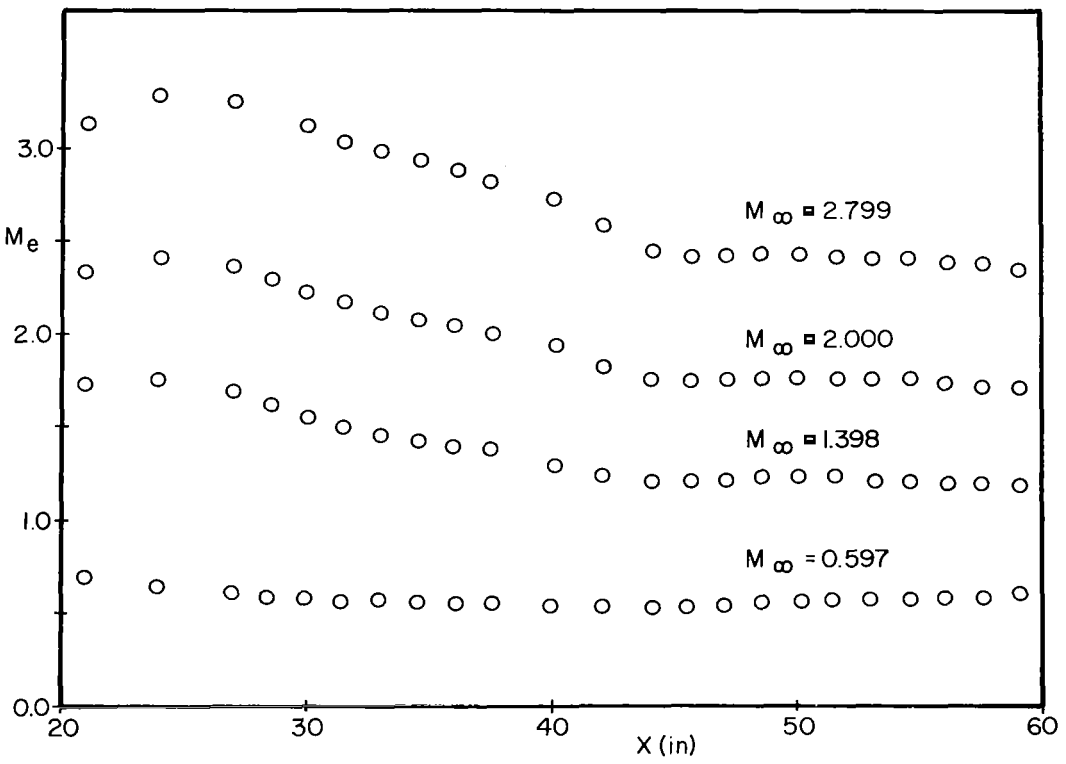

FIGURE 17. Free stream Mach number distribution measured by Winter, Smith and Rotta [23] which was used in the calculations.

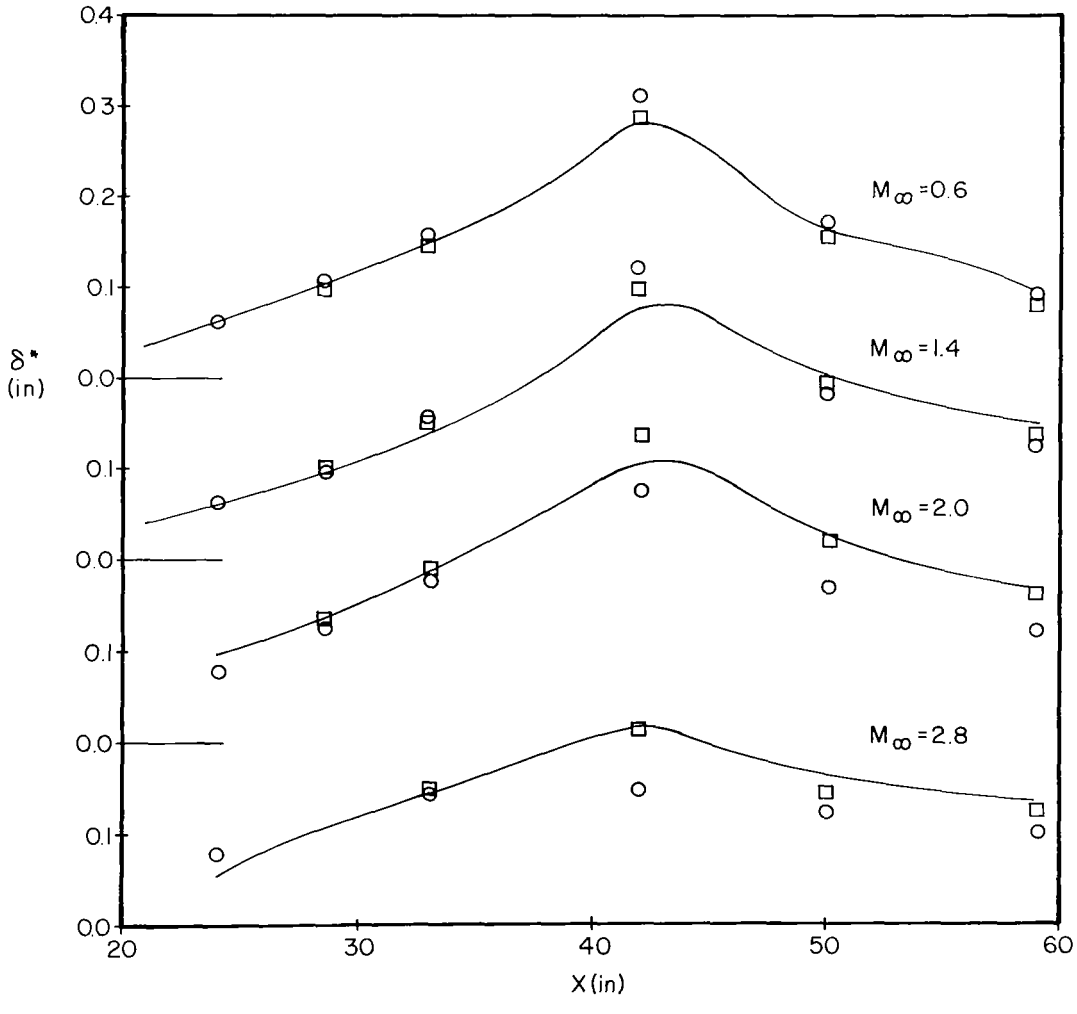

FIGURE 18. Comparison between displacement thickness variation measured by Winter, Smith and Rotta [23], and the calculated variation, shown with an unbroken line. The circles indicate the experimental values obtained directly from the profiles and the squares indicate the values calculated with the Von Karman integral momentum equation beginning with the initial experimental θ and the experimental values of C_f and δ^*/θ.

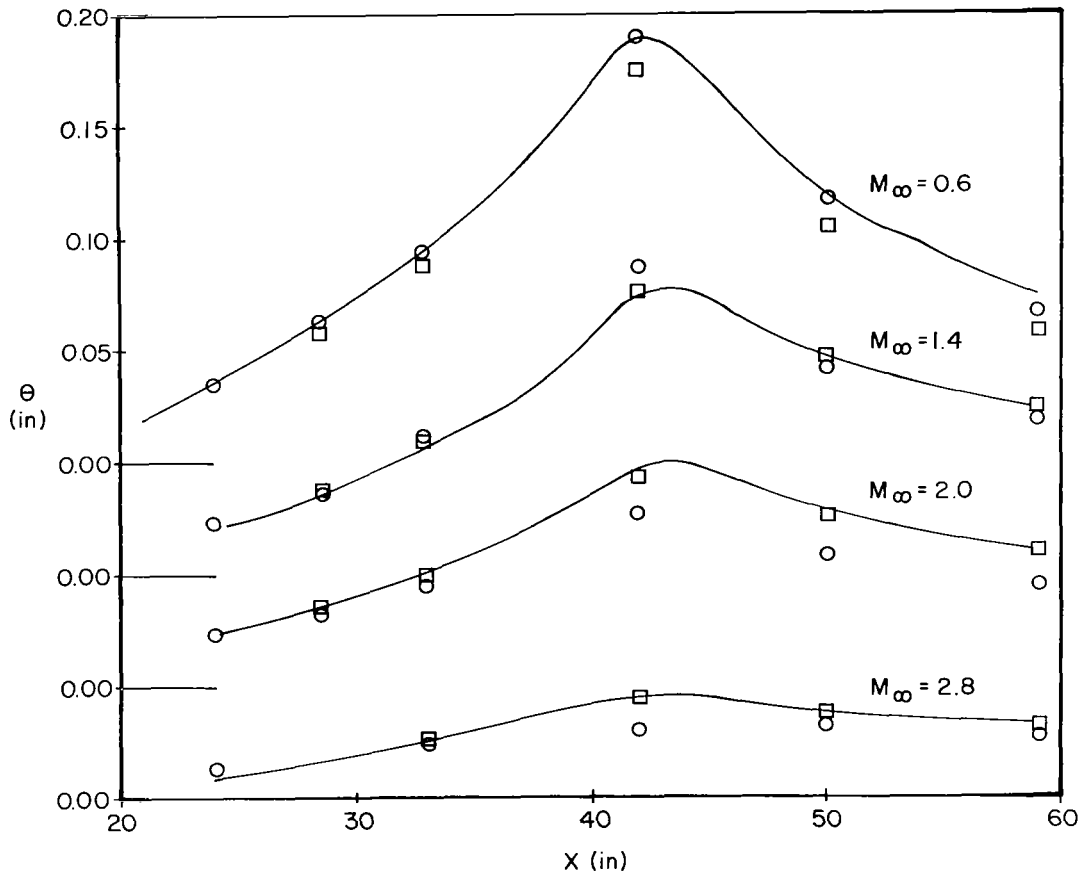

FIGURE 19. Comparison between momentum thickness variation measured by Winter, Smith and Rotta [23], and the calculated variation, shown with an unbroken line. The circles indicate the experimental values obtained directly from the profiles, and the squares indicate the values calculated with the Von Karman integral momentum equation beginning with the initial experimental θ and the experimental values of C_f and δ^*/θ.

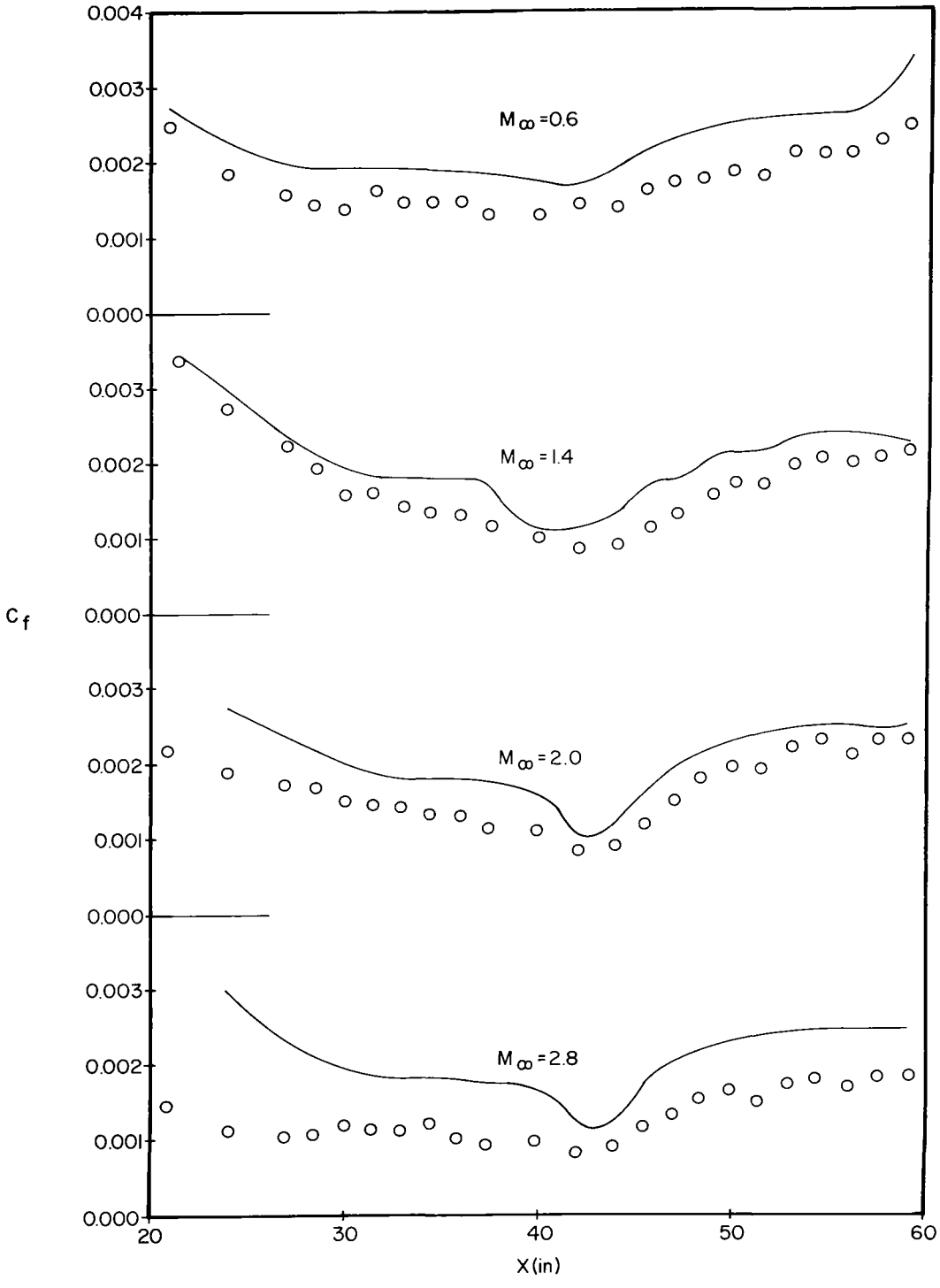

FIGURE 20. Comparison bewteen the distribution of skin friction coefficient measured by Winter, Smith and Rotta [23] with surface pitot tubes, and the calculated distribution, shown with an unbroken line.

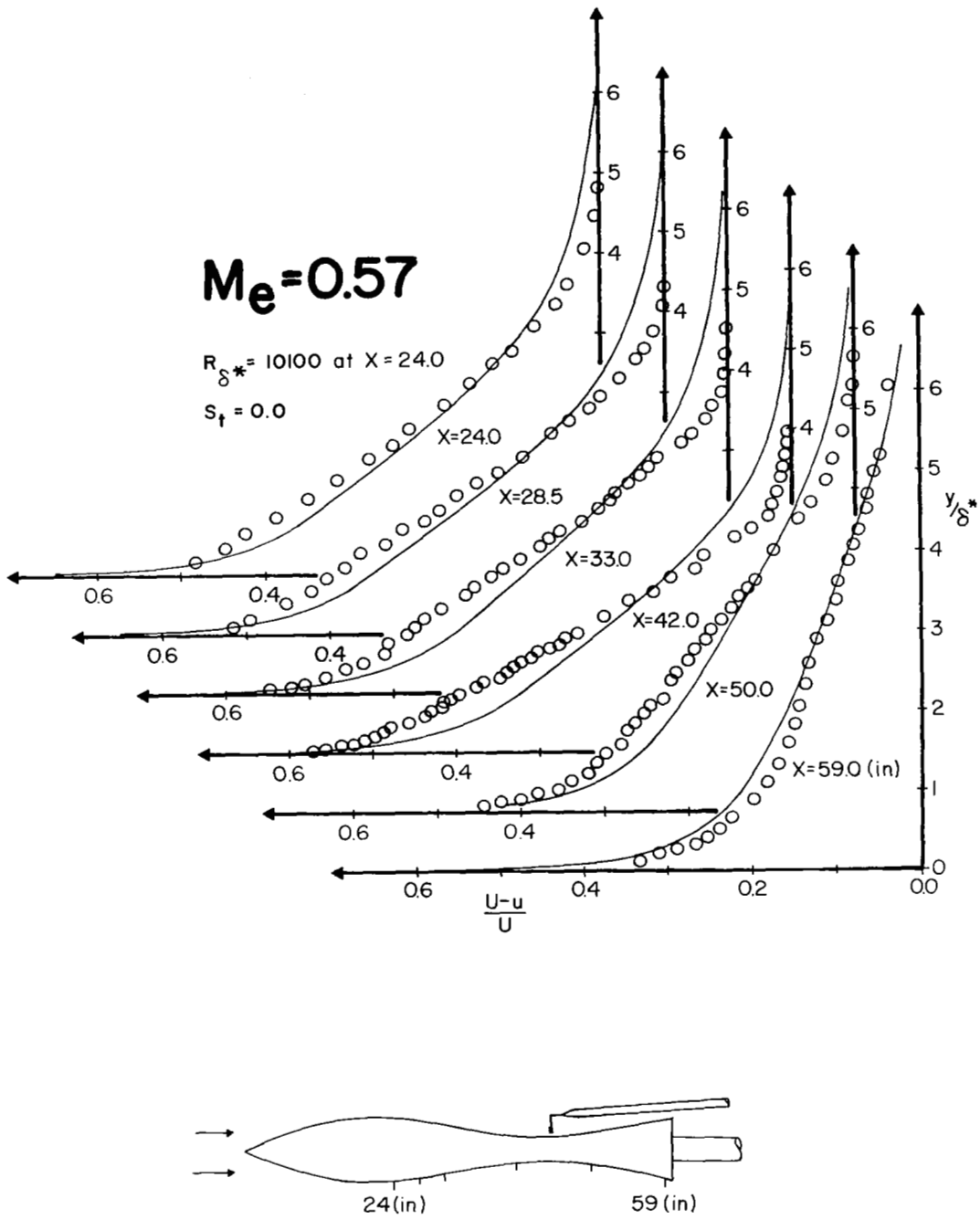

FIGURE 21. Comparison between a series of velocity profiles measured by Winter, Smith and Rotta [23] on a waisted body of revolution, and the calculated profiles, shown with an unbroken line.

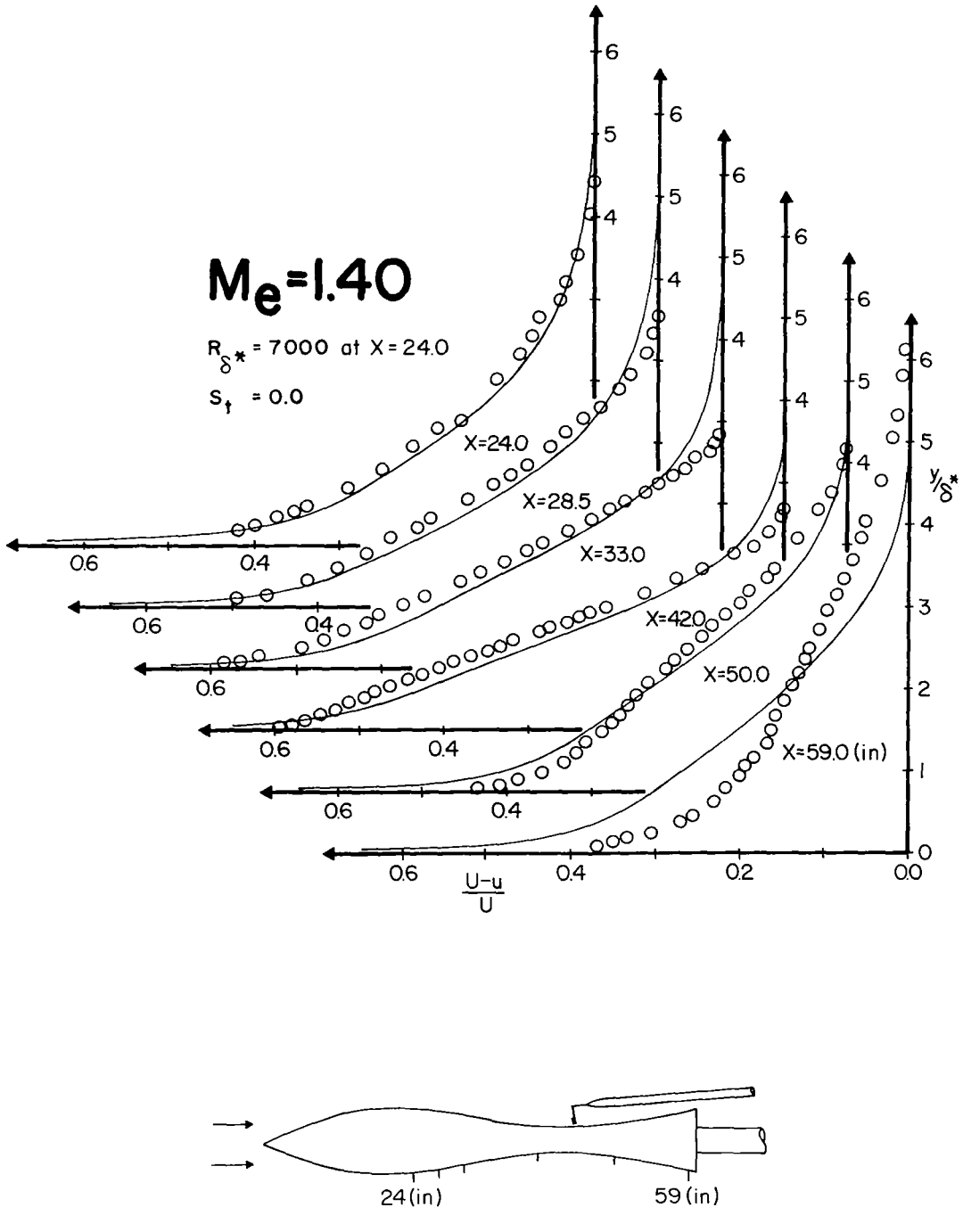

FIGURE 22. Comparison between a series of velocity profiles measured by Winter, Smith and Rotta [23] on a waisted body of revolution, and the calculated profiles, shown with an unbroken line.

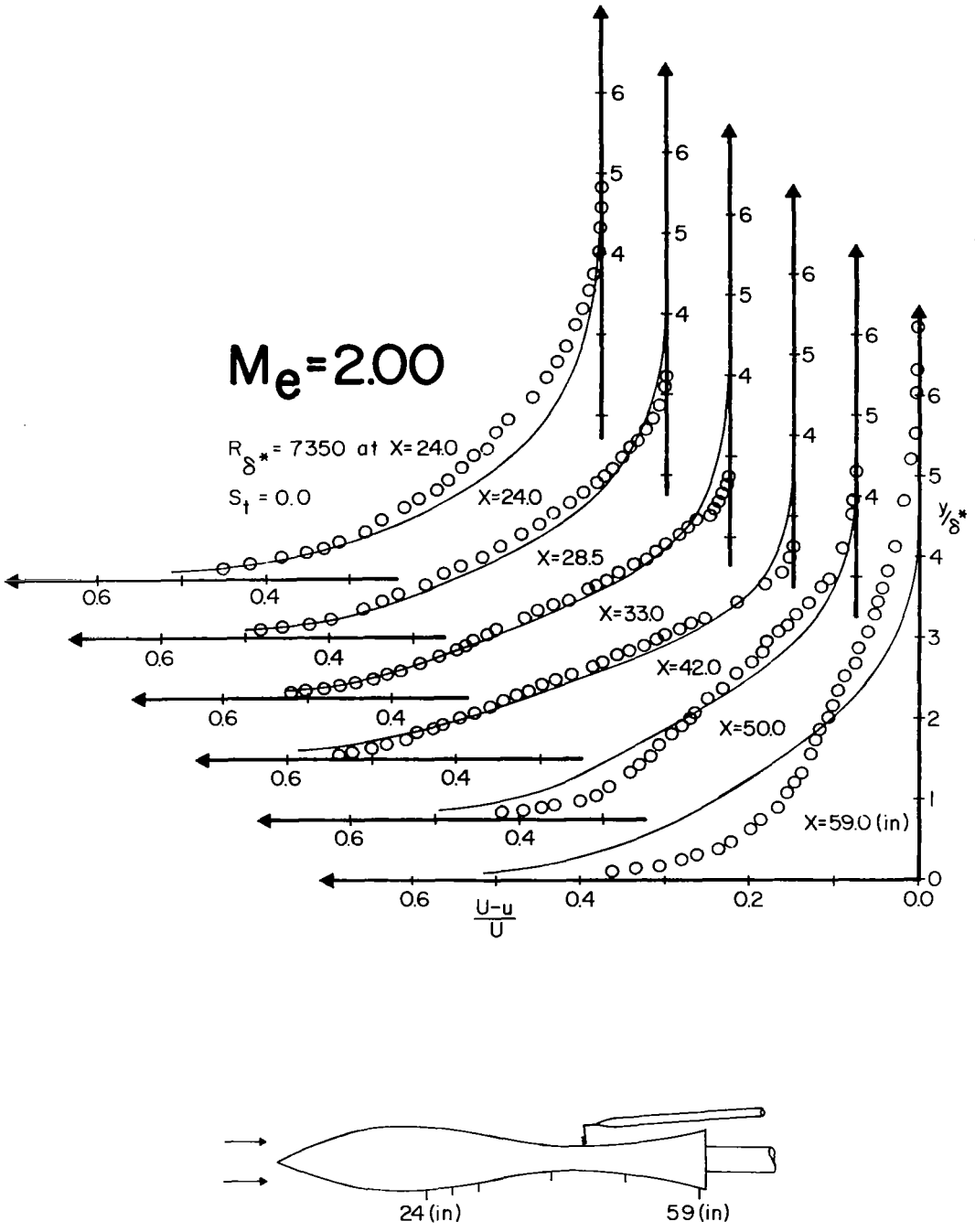

FIGURE 23. Comparison between a series of velocity profiles measured by Winter, Smith and Rotta [23] on a waisted body of revolution, and the calculated profiles, shown with an unbroken line.

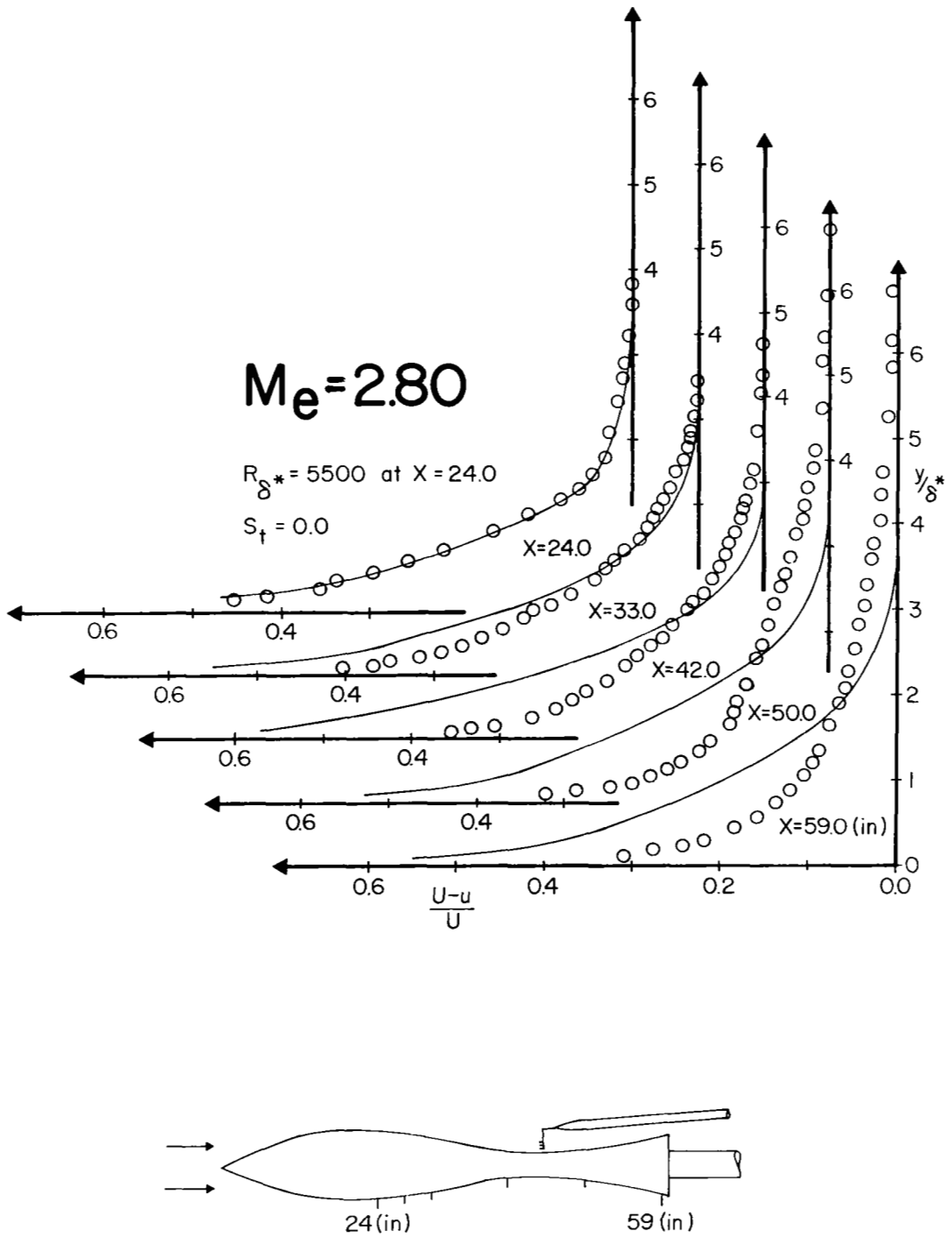

FIGURE 24. Comparison between a series of velocity profiles measured by Winter, Smith and Rotta [23] on a waisted body of revolution, and the calculated profiles, shown with an unbroken line.

were begun by generating profiles internally under the proper conditions of pressure gradient and lateral radius gradient for a station upstream of the first measured profile. Then trial calculations were carried out to find the Reynolds number and displacement thickness at the upstream station that would result in the experimental conditions at the first experimental profile. The final calculations were initialized with these values. The Mach number distributions in Figure 17, and the assumption of an adiabatic wall were used as boundary conditions. Calculations were performed twice, first with the assumption of constant total enthalpy, ($g' = 0$) and again using the energy equation with $Pr = 0.78$ and $Pr_t = 1.0$. As in the case of the constant pressure profiles the difference was small.

Figures 18 and 19 show the experimental and theoretical variation of δ^* and θ . In both cases the calculated values compare very well showing that the convergence and divergence has been properly accounted for. The points marked with squares were calculated using the von Karman integral momentum equation with the experimental values of C_f and δ^*/θ . This verifies that the symmetry of the flow was good. The results of the skin friction calculation are shown in Figure 20. Although the tendency of the calculated C_f is correct in all cases, the prediction is generally somewhat high. At present the reason for this is not known.

The profiles are shown in Figures 21 to 24 . The first few profiles compare well in most cases, which shows that the method of initializing the calculation is adequate. However, near the region of the waist of the body the calculated profiles begin to diverge from the experimental profiles. Beyond the region of the waist the Mach number distribution outside the boundary layer reported by Winter, Smith and Rotta is almost constant in each case. On the other hand, the experimental profiles change very much beyond this point. Therefore, either the external Mach number variation is not indicative of the Mach number variation inside the layer, due perhaps to the presence of Mach waves, or there is an effect other than that of pressure gradient which has not been taken into account. One possibility is the effect of longitudinal curvature on the structure of the turbulence itself. Experiments such as those of Eskinazi and Yeh [24] in constant property flow have shown that the mechanism of the turbulent motion is affected by longitudinal curvature. Mellor also pointed out [5] that this was probably a significant effect in some incompressible boundary layer flows. It is proposed that faster moving fluid farther from the wall would be inhibited from mixing with fluid close to the wall by a centrifugal force acting away from the wall on a convex wall, and encouraged to mix by a centrifugal force on a concave wall. Thus in the more stable case on a convex wall, the effective viscosity would be reduced, and on a concave wall the effective viscosity would be increased. This is the defect which is apparent in the theoretical calculations. In the region before the waist, where logitudinal curvature is small, the cal-

culations compare well. Beyond the waist, where longitudinal curvature is large, the calculated profiles are not as full as the experimental ones, indicating that the effective viscosity used in the calculations was not large enough. This effect was also apparent in calculations of data measured by McLafferty and Barber [25] on a concave surface. Here, although the experimental boundary layer did not separate, the calculated boundary layer separated after a short distance in the adverse pressure gradient. Again it is likely that this separation resulted from a lower value of effective viscosity in the calculations than in the experimental flow. Recently Rotta [26] has re-examined the Winter, Smith and Rotta [23] data. He points out that in compressible flow on an adiabatic wall the curvature effect is amplified by the density stratification. This would explain the observation that the theory predicts the profiles after the waist better for the lower Mach number cases than in the higher ones.

Heat Transfer

Although a considerable amount of work has been done on heat transfer in turbulent boundary layers, very few temperature profiles have been measured compared to the number of velocity profiles measured. Furthermore, few heat transfer measurements have been at moderate Mach numbers. Most of the data is either from constant property or hypersonic flow. Unfortunately, the hypersonic experiments, such as Lobb, Winkler and Persh [18] and Danberg [27] were at Reynolds numbers which were too low for the hypothesis. A series of temperature profiles for an incompressible, constant density flow was calculated for comparison with some profiles measured by Reynolds, Kays and Kline [28]. Following the boundary conditions reported for the data, calculations were made at constant pressure and constant wall temperature. The profiles were calculated with $Pr = 0.78$ and $Pr_t = 1.0$. A turbulent Prandtl number of one gave the best results although small variations in Pr_t had little effect. However, the data available are not sufficient to make a definitive judgement on the best value. The calculations of the series of temperature profiles are compared with the data in Figure 25 . The prediction is quite good.

Another comparison is afforded by a group of Stanton number distributions measured by Moretti and Kays [29]. These again are incompressible constant density flows but they include a wide variety of longitudinal wall temperature distributions and pressure distributions. The calculations were performed with the experimental velocity and temperature boundary conditions shown in the bottom two graphs of Figures 26 to 37 . The experimental Reynolds number and momentum thickness were only reported at one point in the flows. These are noted on the graphs of mainstream velocity distribution and the position of the measurement is indicated with an arrow. In order

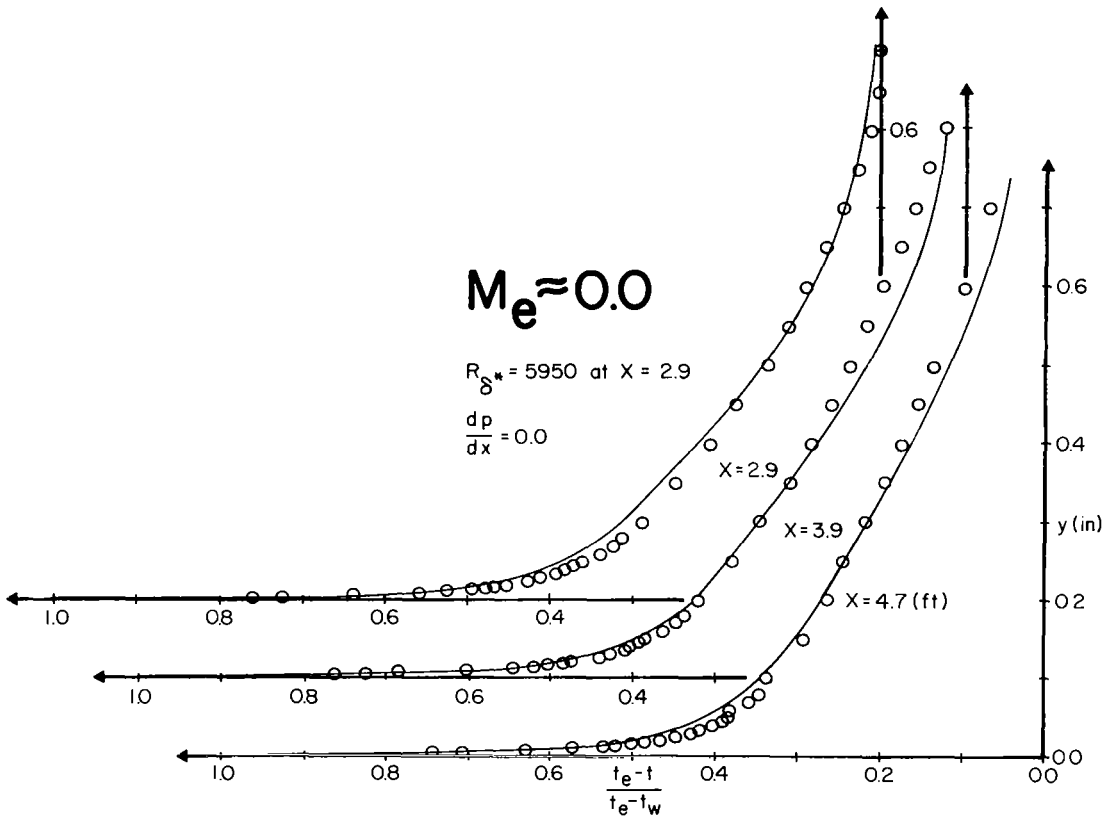

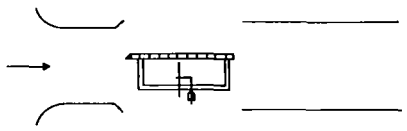

FIGURE 25. Comparison between a series of low Mach number, constant-property temperature profiles, measured by Reynolds, Kays and Kline [28] on a heated flat plate in a free jet tunnel, and the calculated temperature profiles, shown with unbroken lines.

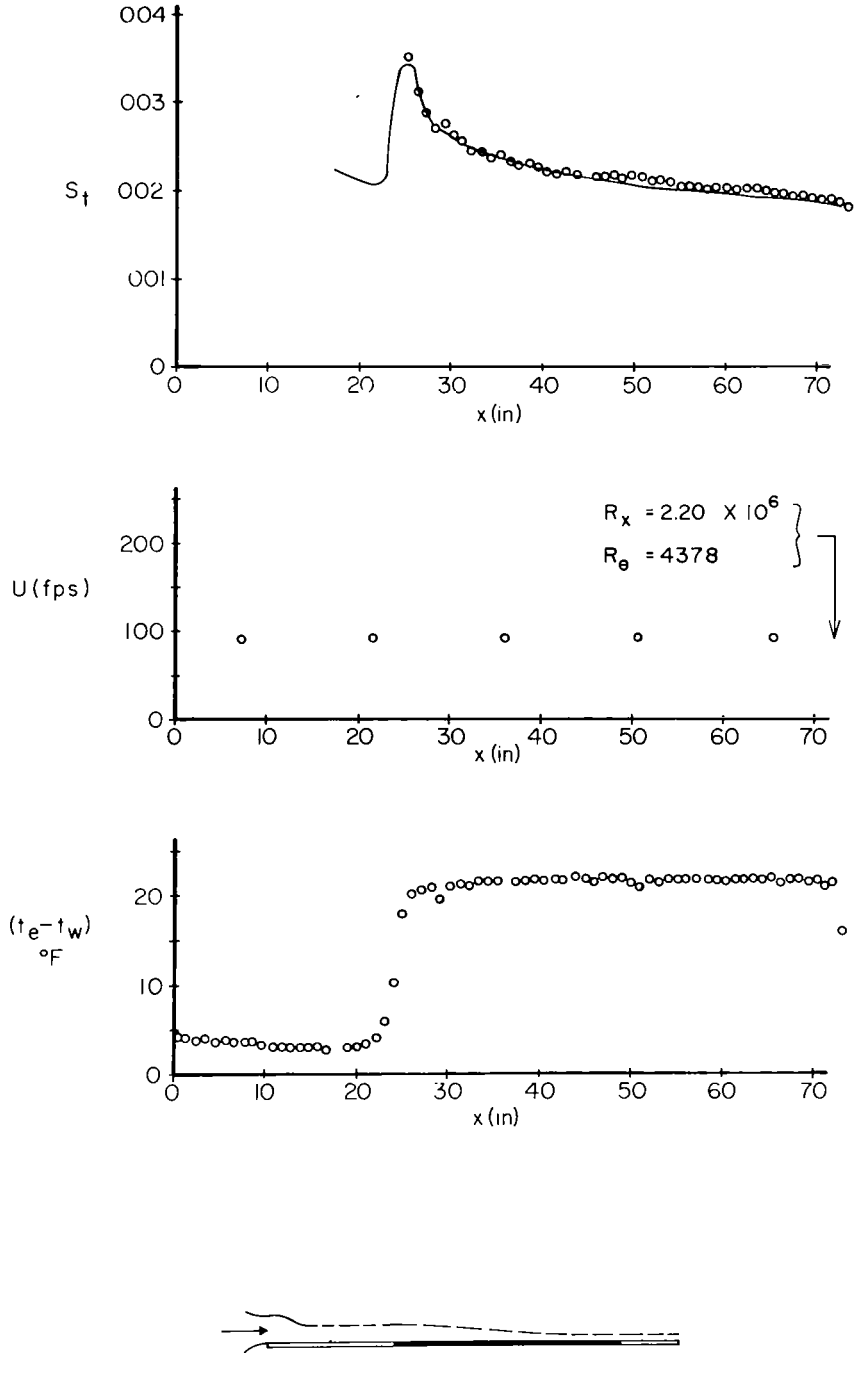

FIGURE 26. Comparison between a Stanton number distribution measured by Moretti and Kays [29] on a cooled flat plate, and the calculated Stanton number distribution shown with an unbroken line. Also shown are the experimental velocity distribution and wall temperature distribution which were used for the calculations.

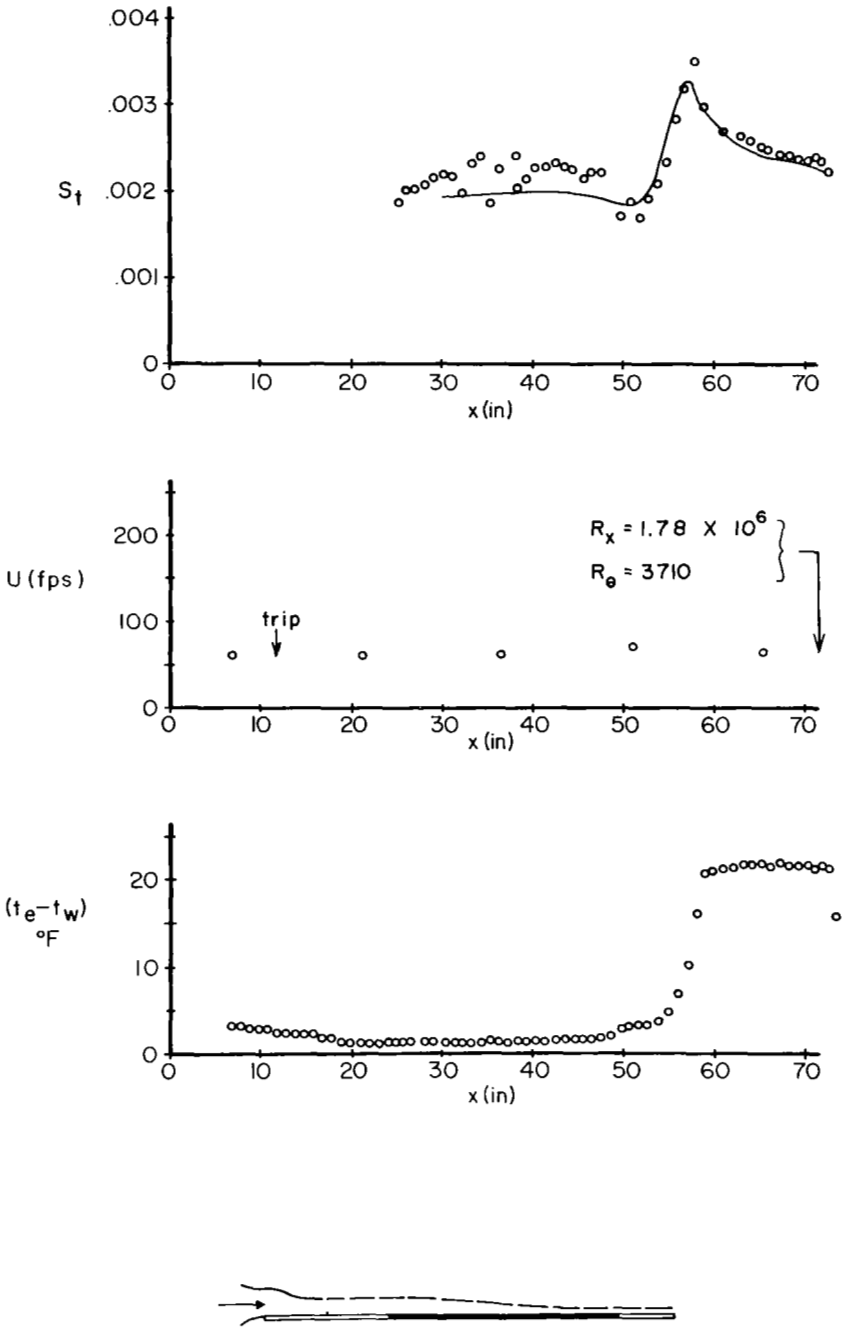

FIGURE 27. Comparison between a Stanton number distribution measured by Moretti and Kays [29] on a cooled flat plate, and the calculated Stanton number distribution shown with an unbroken line. Also shown are the experimental velocity distribution and wall temperature distribution which were used for the calculations.

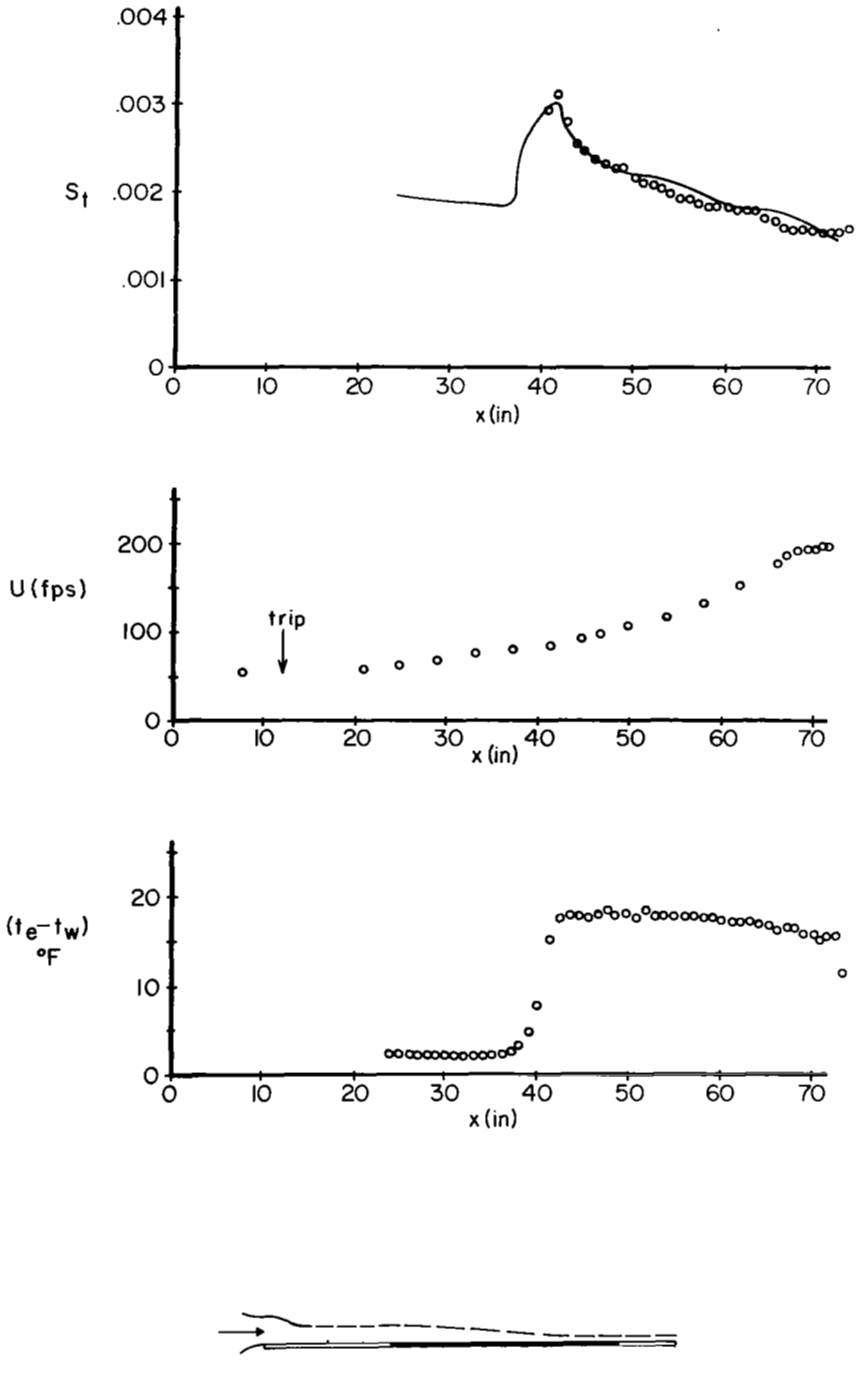

FIGURE 28. Comparison between a Stanton number distribution measured by Moretti and Kays [29] on a cooled flat plate, and the calculated Stanton number distribution shown with an unbroken line. Also shown are the experimental velocity distribution and wall temperature distribution which were used for the calculations.

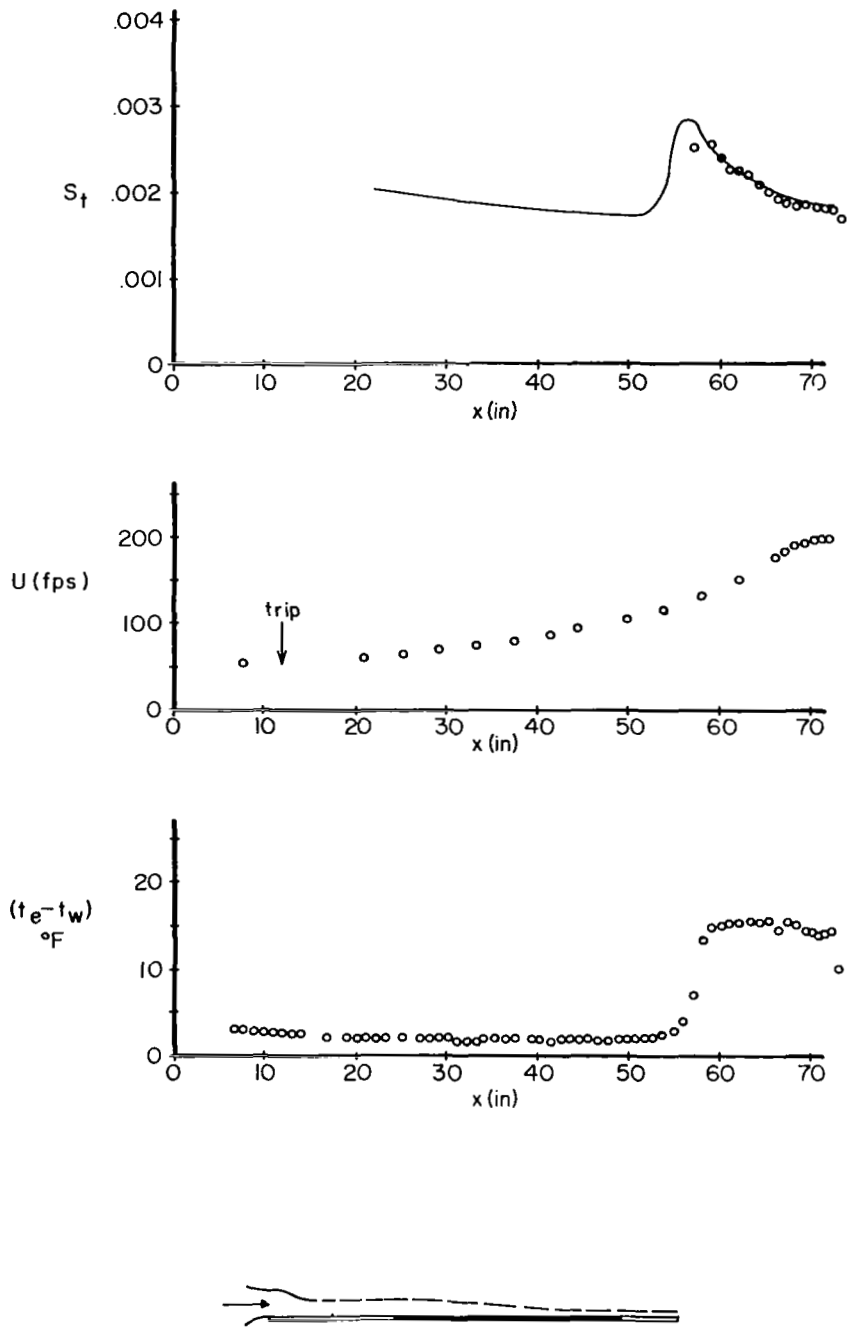

FIGURE 29. Comparison between a Stanton number distribution measured by Moretti and Kays [29] on a cooled flat plate, and the calculated Stanton number distribution shown with an unbroken line. Also shown are the experimental velocity distribution and wall temperature distribution which were used for the calculations.

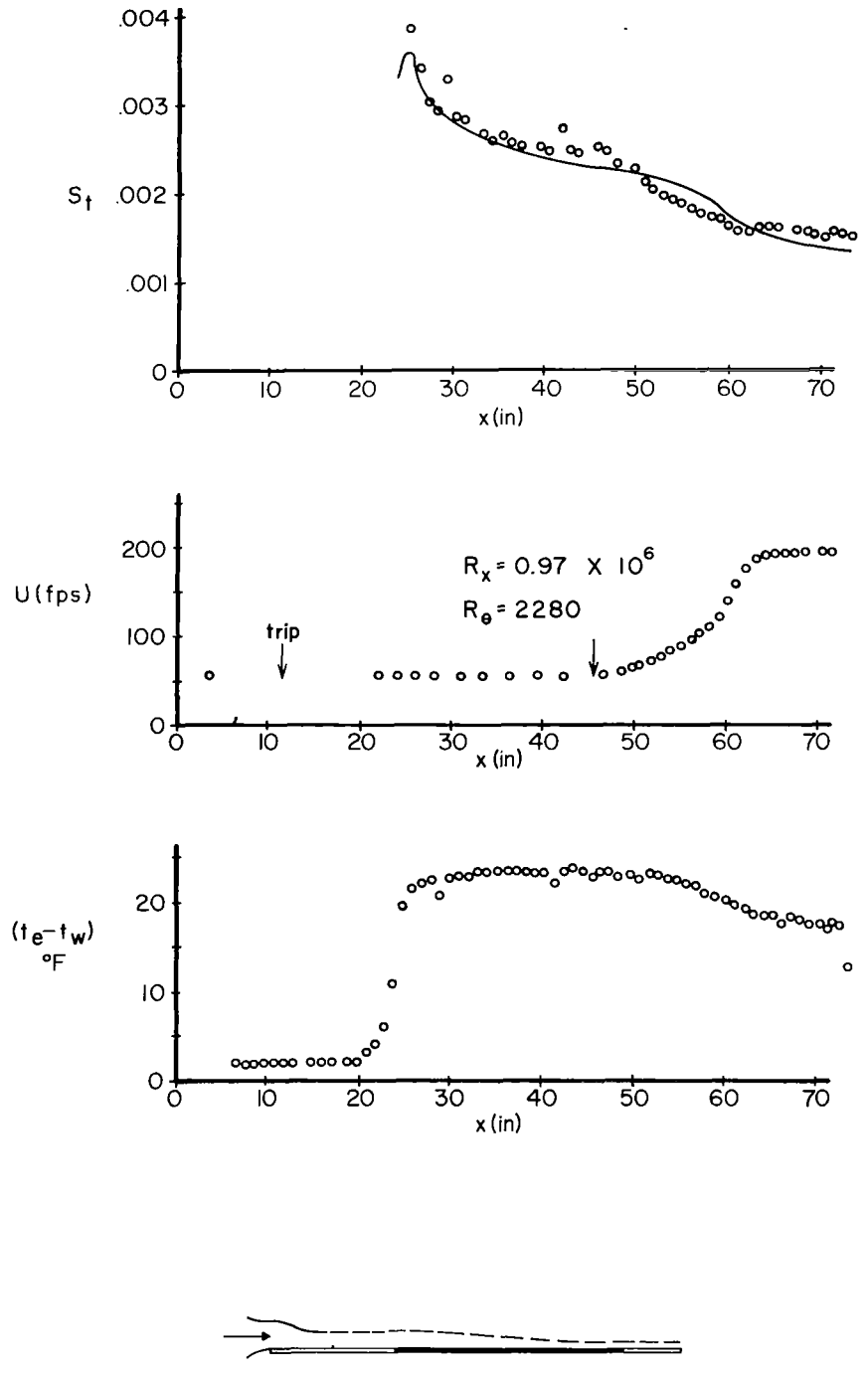

FIGURE 30. Comparison between a Stanton number distribution measured by Moretti and Kays [29] on a cooled flat plate, and the calculated Stanton number distribution shown with an unbroken line. Also shown are the experimental velocity distribution and wall temperature distribution which were used for the calculations.

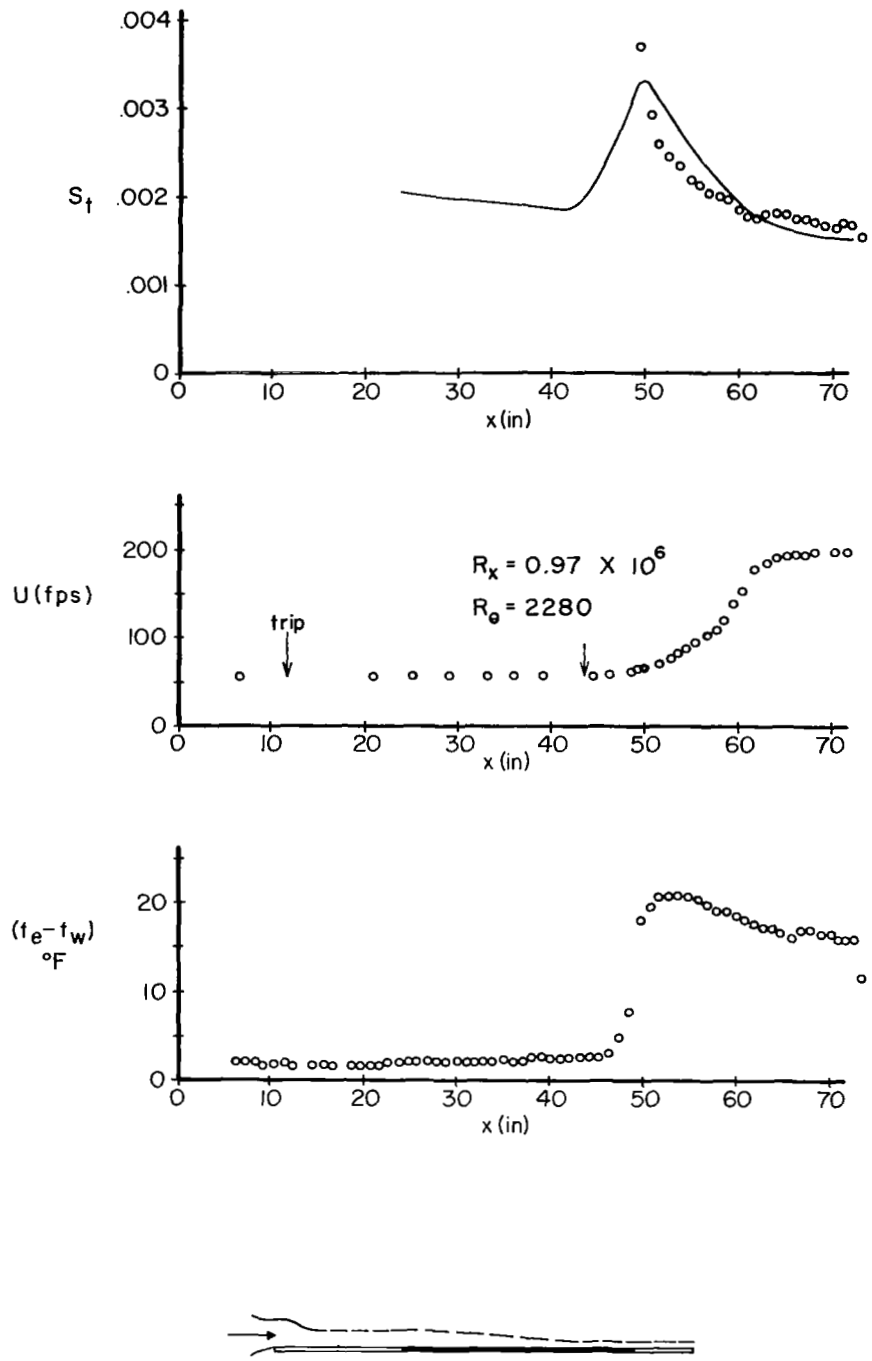

FIGURE 31. Comparison between a Stanton number distribution measured by Moretti and Kays [29] on a cooled flat plate, and the calculated Stanton number distribution shown with an unbroken line. Also shown are the experimental velocity distribution and wall temperature distribution which were used for the calculations.

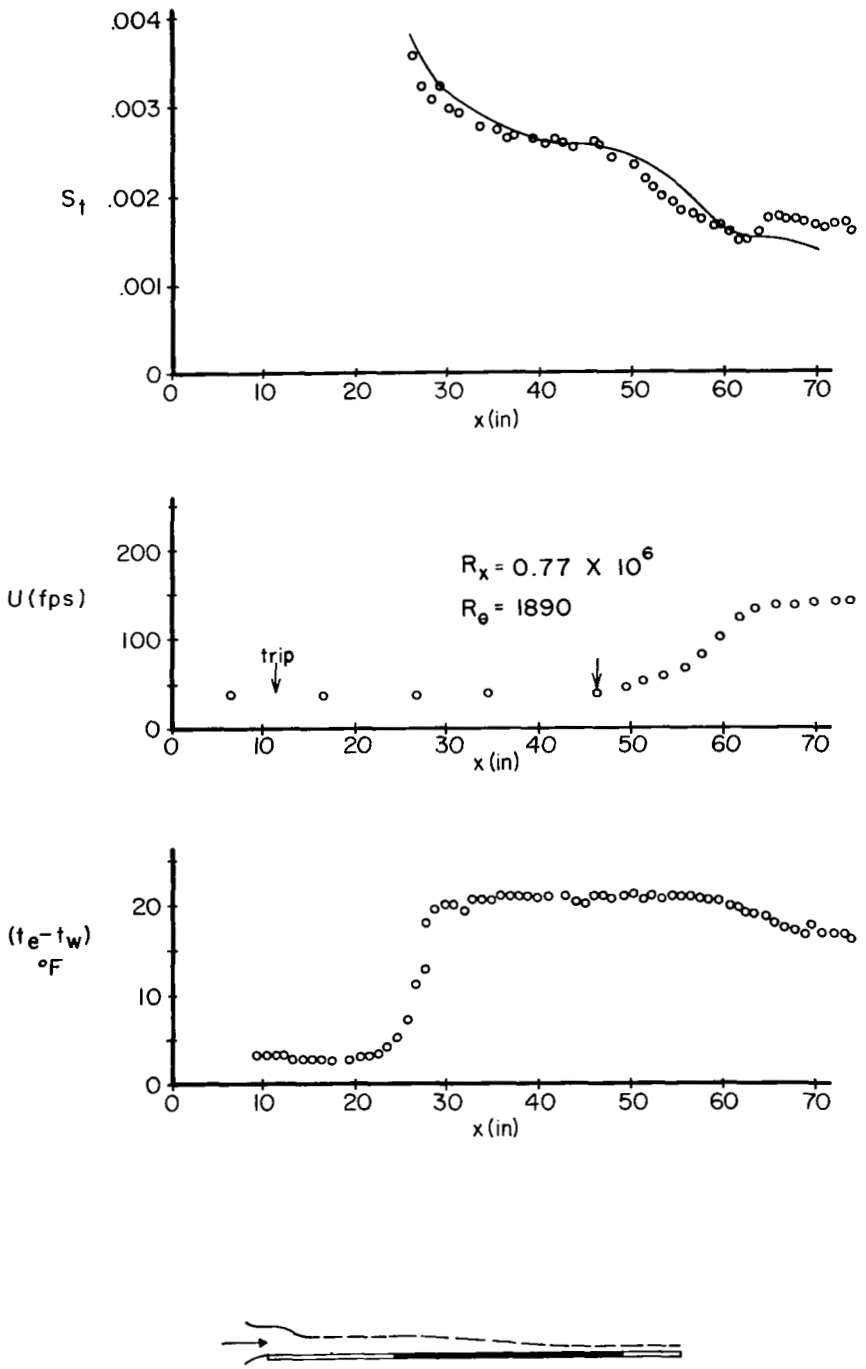

FIGURE 32. Comparison between a Stanton number distribution measured by Moretti and Kays [29] on a cooled flat plate, and the calculated Stanton number distribution shown with an unbroken line. Also shown are the experimental velocity distribution and wall temperature distribution which were used for the calculations.

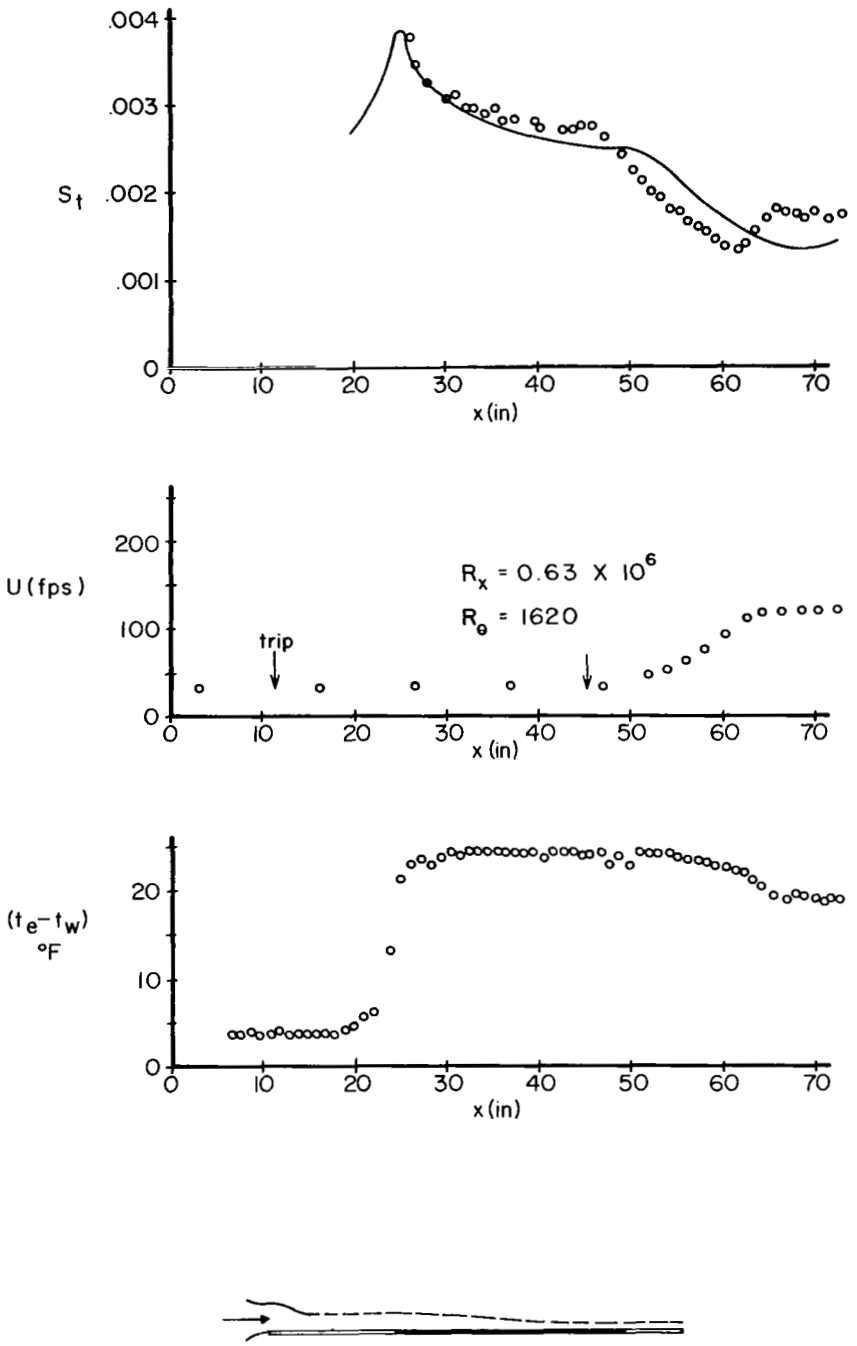

FIGURE 33. Comparison between a Stanton number distribution measured by Moretti and Kays [29] on a cooled flat plate, and the calculated Stanton number distribution shown with an unbroken line. Also shown are the experimental velocity distribution and wall temperature distribution which were used for the calculations.

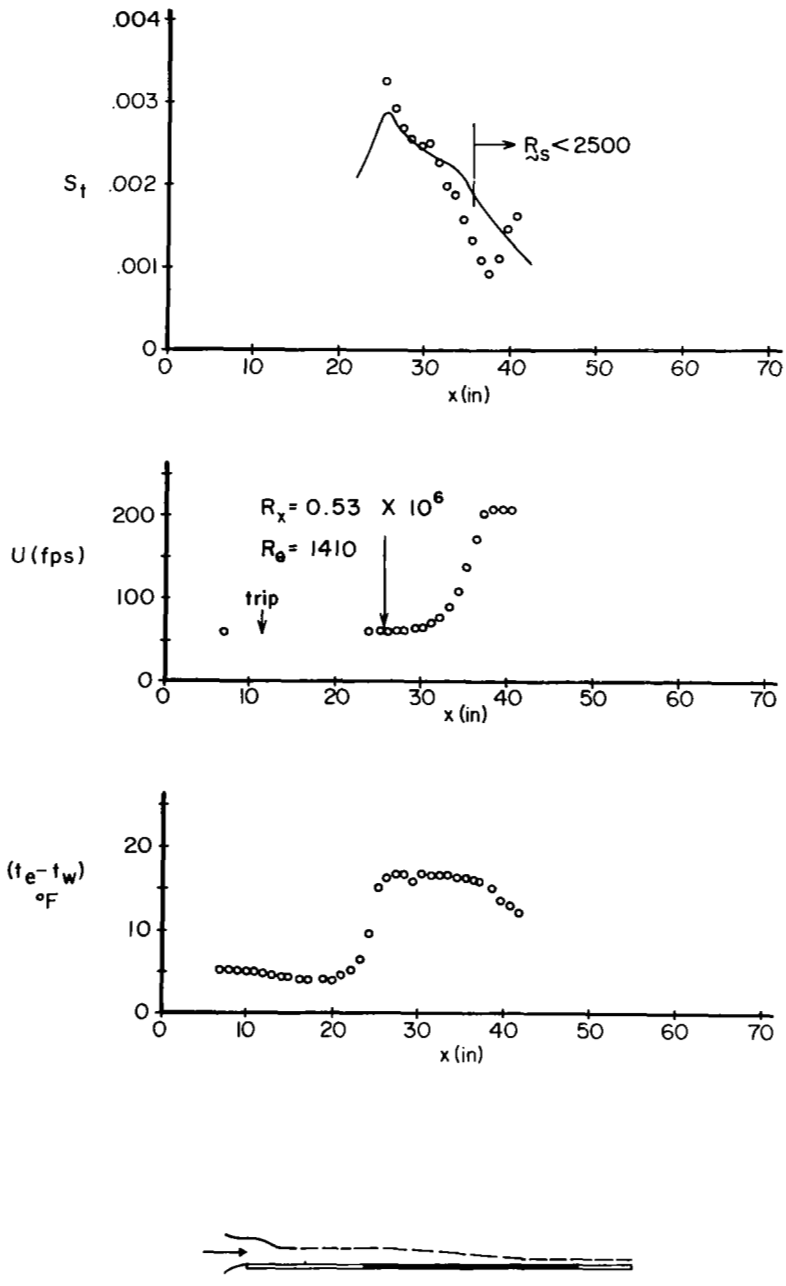

FIGURE 34. Comparison between a Stanton number distribution measured by Moretti and Kays [29] on a cooled flat plate, and the calculated Stanton number distribution shown with an unbroken line. Also shown are the experimental velocity distribution and wall temperature distribution which were used for the calculations. The x position marked with a vertical line on the Stanton number curve shows the position that $\underset{\sim}{R}_s (= U\delta_k^*/\bar{\nu}_s)$ becomes less than 2500.

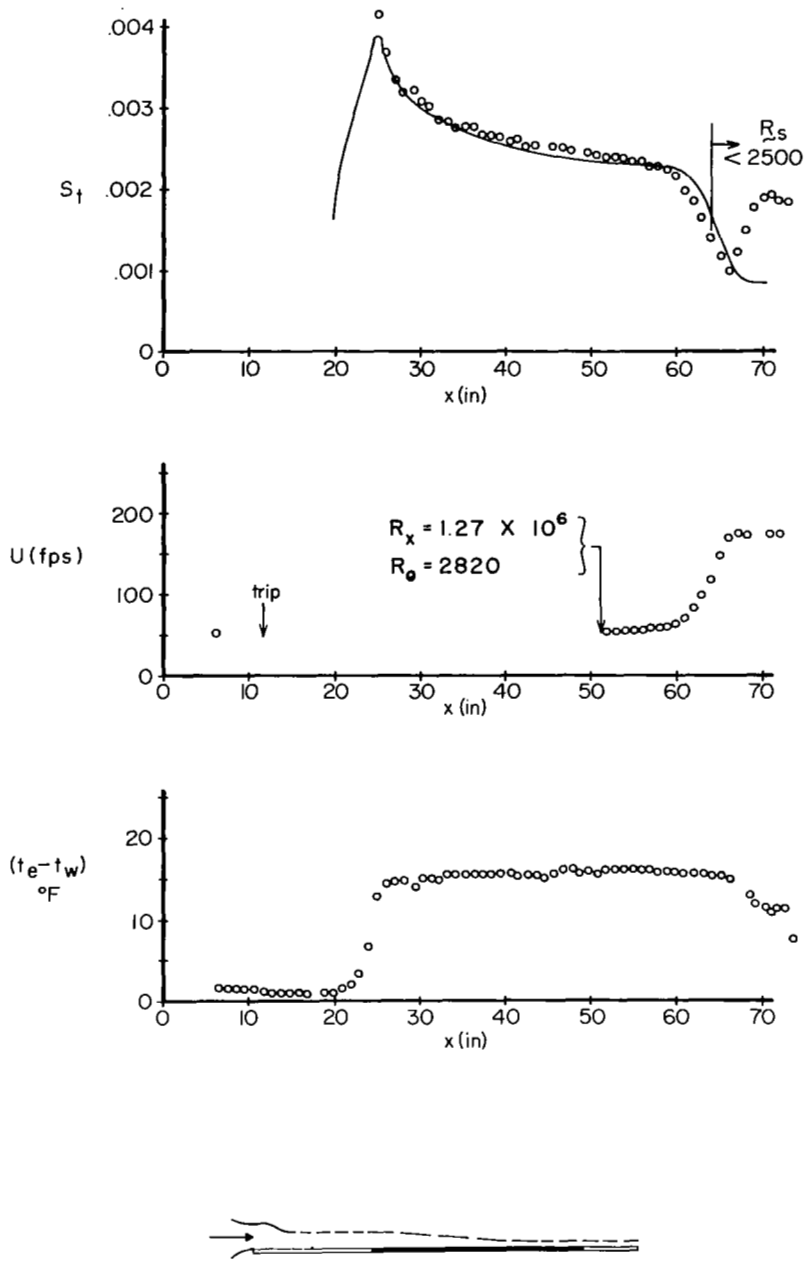

FIGURE 35. Comparison between a Stanton number distribution measured by Moretti and Kays [29] on a cooled flat plate, and the calculated Stanton number distribution shown with an unbroken line. Also shown are the experimental velocity distribution and wall temperature distribution which were used for the calculations. The x position marked with a vertical line on the Stanton number curve shows the position that $\underset{\sim}{R}_s (= U\delta_k^*/\bar{\nu}_s)$ becomes less than 2500.

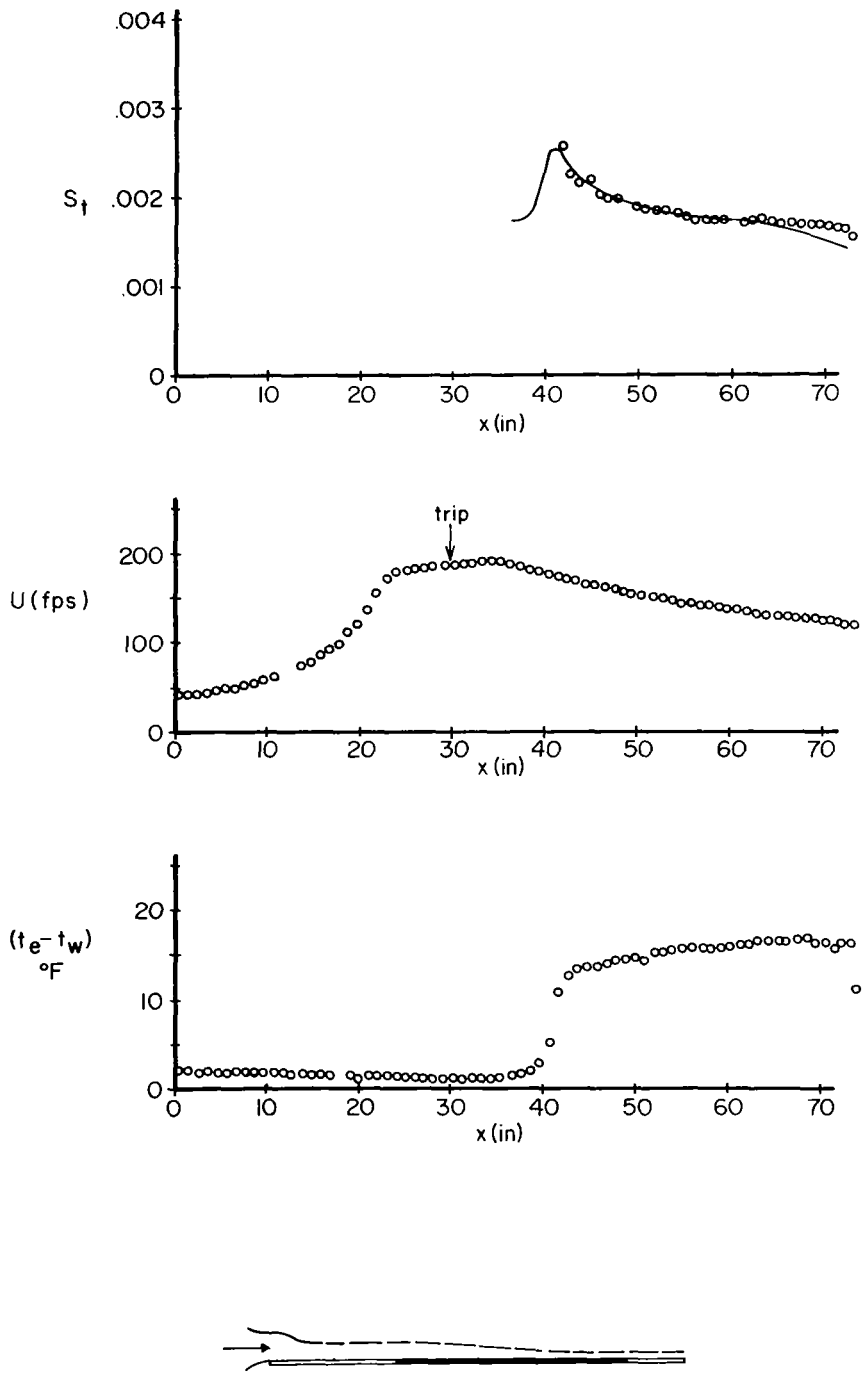

FIGURE 36. Comparison between a Stanton number distribution measured by Moretti and Kays [29] on a cooled flat plate, and the calculated Stanton number distribution shown with an unbroken line. Also shown are the experimental velocity distribution and wall temperature distribution which were used for the calculations.

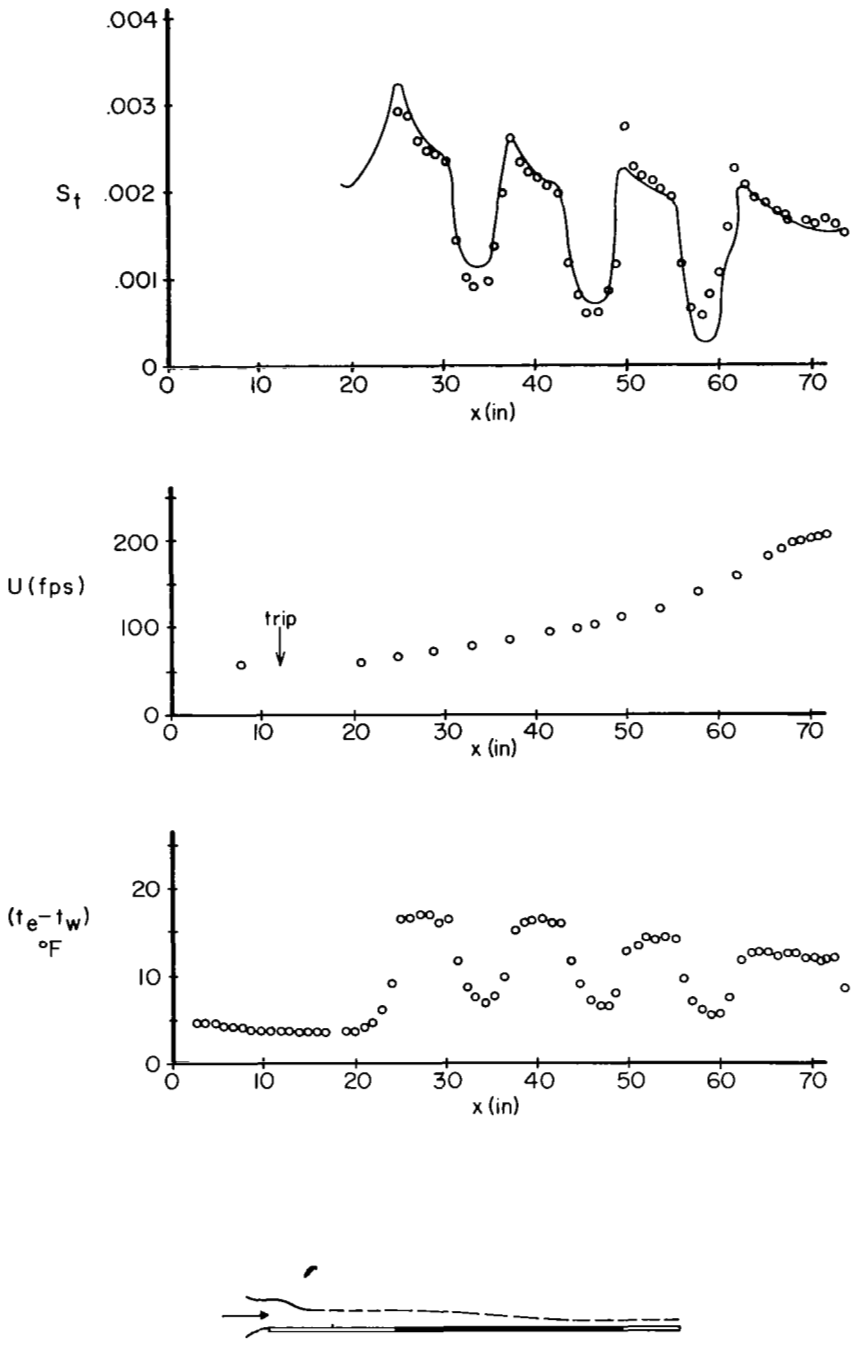

FIGURE 37. Comparison between a Stanton number distribution measured by Moretti and Kays [29] on a cooled flat plate, and the calculated Stanton number distribution shown with an unbroken line. Also shown are the experimental velocity distribution and wall temperature distribution which were used for the calculations.

to match these values, preliminary calculations were made and the initial conditions reset to match the experimental momentum thickness at the reported point. Unfortunately the values of $\underset{\sim}{R}_s$ for all of these flows were rather low. Although in many cases $\underset{\sim}{R}_s$ stayed above 2500, the strong mainstream accelerations in other cases caused δ^* to decrease and therefore $\underset{\sim}{R}_s$ to drop below 2500. Because of this the hypothesis is in error at some of the most interesting places. Those cases in which this happens are marked with a vertical line on the Stanton number plot at the x position where it occurs.

The measured and calculated values of the Stanton number distribution are plotted together at the top of Figures 26 through 37 . The rapid changes in Stanton number are predicted well in the decelerating case, Figure 36, and the cases with lower accelerating pressure gradients. Even the last case, where the temperature distribution is a series of alternate temperature steps is predicted well. The calculated Stanton numbers continue to compare well in the flows with strong pressure gradients (Figures 30 to 33) as long as $\underset{\sim}{R}_s$ is above 2500. Furthermore, when $\underset{\sim}{R}_s$ does go too low, the calculations still have the correct tendency for a short distance. Therefore, this is a favorable beginning for the effective diffusivity . Still more data are necessary in compressible flow at higher Reynolds numbers to test fully the validity of the effective diffusivity.

V. CONCLUDING REMARKS

The results cited demonstrate that the effects of compressibility have been correctly incorporated into the effective viscosity hypothesis for constant Mach number flows. The effect of Mach number on the skin friction coefficient, on the profile shape, and on the growth of δ^* are predicted quite well. It is unfortunate that more data in compressible flow with pressure gradients are not available. The only flows for which calculations were made were flows with positive pressure gradients. In these cases the results were quite good, although to complete the verification of the hypothesis data taken in flows with favorable pressure gradients and data in flows with separation are required. In the positive pressure gradient data that was examined there were regions of almost constant pressure flow but with strong longitudinal curvature which were not predicted well. This and other circumstantial evidence seems to indicate that there is an effect of longitudinal curvature on the turbulent structure which has not as yet been included in the hypothesis. (An experimental study of wall curvature effect is in progress at Princeton University.)

Based on the limited amount of data, the results obtained using

the effective diffusivity in incompressible flow with heat transfer are also favoralbe. Again, it would be useful if more temperature profiles were available, expecially from compressible flow, to establish further confidence in the theoretical predictions.

Princeton University
Princeton, N.J., April 11, 1968

APPENDIX A. ORDER OF MAGNITUDE ANALYSIS

FOR EQUATIONS OF MOTION

An order of magnitude analysis is most conveniently performed with the equations in non-dimensional form. Accordingly, the dependent variables will be referred to their values at some point, r, in the undisturbed stream, and x and y will be referred to a representative dimension of the body, ℓ, such that $\partial u^+/\partial x^+$ is of order unity. The new variables are

$$u^+ = \frac{u}{U_r} \quad , \quad v^+ = \frac{v}{U_r} \quad , \quad w^+ = \frac{w}{U_r} \quad , \quad \rho^+ = \frac{\rho}{\rho_{e_r}} \quad , \quad p^+ = \frac{p - p_{e_r}}{\rho_{e_r} U_r^2}$$

$$h^{o^+} = \frac{h^o}{h^o_{e_r}} \quad , \quad h^+ = \frac{h}{h_{e_r}} \quad , \quad x^+ = \frac{x}{\ell} \quad , \quad y^+ = \frac{y}{\ell} \quad . \qquad (A1)$$

If these variables are introduced into equations (2a) through (2f), the results are

$$\frac{\partial \overline{\rho^+}\,\overline{u^+}}{\partial x^+} + \frac{\partial \overline{\rho^{+\prime} u^{+\prime}}}{\partial x^+} + \frac{\partial \overline{\rho^+}\,\overline{v^+}}{\partial y^+} + \frac{\partial \overline{\rho^{+\prime} v^{+\prime}}}{\partial y^+} = 0 \qquad (A2a)$$

$$(1+\Delta\overline{\rho^+}) \qquad \varepsilon\overline{\Delta\rho^+} \qquad \frac{(\varepsilon+\varepsilon\overline{\Delta\rho^+})}{\varepsilon} \qquad \frac{\varepsilon\overline{\Delta\rho^+}}{\varepsilon}$$

$$\overline{\rho^+}\,\overline{u^+}\frac{\partial \overline{u^+}}{\partial x^+} + \frac{\partial \overline{\rho^+ u^{+\prime 2}}}{\partial x^+} + \overline{\rho^{+\prime} u^{+\prime}}\frac{\partial \overline{u^+}}{\partial x^+} + \frac{\partial \overline{u^+}\,\overline{\rho^{+\prime} u^{+\prime}}}{\partial x^+}$$

$$1 \qquad (\varepsilon+\varepsilon_{\Delta\rho}\overline{{}^+}) \qquad \varepsilon_{\Delta\rho}\overline{{}^+} \qquad \varepsilon_{\Delta\rho}\overline{{}^+}$$

$$+ \overline{\rho^+}\,\overline{v^+}\frac{\partial \overline{u^+}}{\partial y^+} + \overline{\rho^{+\prime} v^{+\prime}}\frac{\partial \overline{u^+}}{\partial y^+} + \frac{\partial \overline{\rho^+ u^{+\prime} v^{+\prime}}}{\partial y^+} + \frac{\partial \overline{v^+}\,\overline{\rho^{+\prime} u^{+\prime}}}{\partial y^+} = -\frac{\partial \overline{p^+}}{\partial x^+} \qquad \text{(A2b)}$$

$$\varepsilon\,\frac{1}{\varepsilon} \qquad \varepsilon_{\Delta\rho}\overline{{}^+}\,\frac{1}{\varepsilon} \qquad \frac{(\varepsilon+\varepsilon_{\Delta\rho}\overline{{}^+})}{\varepsilon} \qquad \frac{\varepsilon\,\varepsilon_{\Delta\rho}\overline{{}^+}}{\varepsilon} \qquad 1$$

$$\overline{\rho^+}\,\overline{v^+}\frac{\partial \overline{u^+}}{\partial x^+} + \overline{\rho^{+\prime} v^{+\prime}}\frac{\partial \overline{u^+}}{\partial x^+} + \frac{\partial \overline{\rho^+ u^{+\prime} v^{+\prime}}}{\partial x^+} + \frac{\partial \overline{v^+}\,\overline{\rho^{+\prime} u^{+\prime}}}{\partial x^+}$$

$$\varepsilon \qquad \varepsilon_{\Delta\rho}\overline{{}^+} \qquad (\varepsilon_{\Delta\rho}\overline{{}^+}+\varepsilon) \qquad \varepsilon\,\varepsilon_{\Delta\rho}\overline{{}^+}$$

$$+ \overline{\rho^+}\,\overline{v^+}\frac{\partial \overline{v^+}}{\partial y^+} + \overline{\rho^{+\prime} v^{+\prime}}\frac{\partial \overline{v^+}}{\partial y^+} + \frac{\partial \overline{v^+}\,\overline{\rho^{+\prime} v^{+\prime}}}{\partial y^+} + \frac{\partial \overline{\rho^+ v^{+\prime 2}}}{\partial y^+} = -\frac{\partial \overline{p^+}}{\partial y^+} \qquad \text{(A2c)}$$

$$\varepsilon\,\frac{\varepsilon}{\varepsilon} \qquad \varepsilon_{\Delta\rho}\overline{{}^+}\,\frac{\varepsilon}{\varepsilon} \qquad \frac{\varepsilon\,\varepsilon_{\Delta\rho}\overline{{}^+}}{\varepsilon} \qquad \frac{\varepsilon+\varepsilon_{\Delta\rho}\overline{{}^+}}{\varepsilon} \qquad \frac{(\varepsilon+\varepsilon_{\Delta\rho}\overline{{}^+})}{\varepsilon}$$

$$\underset{\overline{\Delta h^{o+}}}{\overline{\rho^+ u^+ \frac{\partial h^{o+}}{\partial x^+}}} + \underset{\overline{\varepsilon \Delta\rho^+ \Delta h^{o+}}}{\overline{\rho^{+\prime} u^{+\prime} \frac{\partial h^{o+}}{\partial x^+}}} + \underset{\overline{(\varepsilon \Delta h^{o+} + \varepsilon \Delta h^{o+} \Delta\rho^+)}}{\overline{\frac{\partial \rho^+ u^{+\prime} h^{o+\prime}}{\partial x^+}}} + \underset{\overline{(\varepsilon \Delta\rho^+ \Delta h^{o+})}}{\overline{\frac{\partial u^+ \rho^{+\prime} h^{o\prime +}}{\partial x^+}}}$$

$$\underset{\varepsilon \overline{\frac{\Delta h^{o+}}{\varepsilon}}}{\overline{\rho^+ v^+ \frac{\partial h^{o+}}{\partial y^+}}} + \underset{\varepsilon \Delta\rho^+ \overline{\frac{\Delta h^{o+}}{\varepsilon}}}{\overline{\rho^{+\prime} v^{+\prime} \frac{\partial h^{o+}}{\partial y^+}}} + \underset{\overline{\frac{(\varepsilon \Delta h^{o+} + \varepsilon \Delta h^{o+} \Delta\rho^+)}{\varepsilon}}}{\overline{\frac{\partial \rho^+ v^{+\prime} h^{o+\prime}}{\partial y^+}}} + \underset{\overline{\frac{\Delta\rho^+ \Delta h^{o+} \varepsilon\, \varepsilon}{\varepsilon}}}{\overline{\frac{\partial v^+ \rho^{+\prime} h^{o+\prime}}{\partial y^+}}} = 0 \qquad \text{(A2d)}$$

$$\underset{1}{\left(1 + \frac{\gamma-1}{2} M_e^2\right)\overline{h^{o+}}} = \underset{1}{\overline{h^+}} + \underset{1}{\frac{\gamma-1}{2} M_e^2 \left(\overline{u^{+2}} + \underset{\varepsilon}{\overline{u^{+\prime 2}}} + \underset{\varepsilon}{\overline{v^{+\prime 2}}} + \underset{\varepsilon}{\overline{w^{+\prime 2}}}\right)} \qquad \text{(A2e)}$$

$$\underset{1}{1 + \gamma M_e^2 \overline{p^+}} = \underset{1}{\overline{\rho^+}\,\overline{h^+}} + \underset{\varepsilon \overline{\Delta\rho^+} \overline{\Delta h^+}}{\overline{\rho^{+\prime} h^{+\prime}}} \qquad \text{(A2f)}$$

Below each term is a notation of its' magnitude in accordance with the discussion which follows.

To begin with, the thickness of the boundary layer, δ , is assumed to be considerably smaller than ℓ , so that $\partial(\ )/\partial y^+$ is of order $1/\varepsilon$, $(\varepsilon = \delta/\ell \ll 1)$. Then, on the basis of experimental evidence, (Laufer [7], Kistler [30]) some assumptions are made about the turbulent correlation terms,

$$\overline{u^{+\prime} v^{+\prime}} = O(C_f) \quad , \tag{A3a}$$

$$\overline{u^{+\prime 2}} = O(\overline{u^{+\prime} v^{+\prime}}) \quad , \tag{A3b}$$

$$\overline{v^{+\prime 2}} = O(\overline{u^{+\prime} v^{+\prime}}) \quad , \tag{A3c}$$

$$\overline{\rho^{+\prime} u^{+\prime}} = O(\overline{\rho^{+\prime} v^{+\prime}}) \quad . \tag{A3d}$$

Now, since the change of y^+ across the layer is of order ε , it is clear from (A2a) that $\overline{v^+}$ must also be of order ε . Furthermore, if the equations are to describe a boundary layer flow, the turbulent shear stress term, $\partial(\rho' u^{+\prime} v^{+\prime})/\partial y^+$, must be of the same order as the inertia terms in the x momentum equation. Therefore C_f must be of order ε , which is in agreement with experimental results. Finally, changes of $\overline{\rho^+}$ and $\overline{h^+}$ in the x^+ direction are assumed to be of the same order as the changes across the layer, $\Delta\overline{\rho^+}$ and $\Delta\overline{h^+}$ respectively. This is in keeping with the method used for $\overline{u^+}$, where $\Delta\overline{u^+}$ in the x^+ direction is taken as order 1.

To make statements about terms containing $\overline{\rho^{+\prime} u^{+\prime}}$ and $\overline{\rho^{+\prime} v^{+\prime}}$ it is necessary to put an upper bound on $\rho^{+\prime}$. For an order of magnitude analysis it is sufficient to say that $\rho^{+\prime}$ could result from several causes: a) turbulent bulk transport of fluid from regions of different density, velocity and enthalpy; b) turbulent pressure fluctuations; c) molecular viscous dissipation caused by the fluctuating velocity; and d) molecular heat transfer driven by the fluctuating enthalpy.

Except in the regions very near the wall, molecular transport is generally assumed to exert negligible effect on the mean equations of motion. The role of viscosity, or conductivity, is to establish the smallest possible scale of turbulence. But for sufficiently large Reynolds number this smallest scale is far removed from the scales of turbulence that play a role in the turbulent transport processes.

The possible effect of pressure fluctuations is not as clear. Kovasznay [31] has measured the pressure fluctuation (expressed as the mass flow fluctuation) just outside the boundary layer, which he feels to be indicative of the pressure fluctuation inside the boundary layer. He found the mass flow fluctuation to be of the order of 0.1 per cent at a Mach number of 1.75, whereas he found the velocity fluctuation in the boundary layer to be 2 to 3 per cent. Therefore, until more data is available, the assumption that the pressure fluctuations are negligible seems to be justified.

If the bulk transport is the major cause of density and enthalpy fluctuations, then the fluctuations should be correlated with the velocity fluctuations, since it is the latter which carry fluid with one density and enthalpy into regions with other average values. Furthermore, density and enthalpy should be correlated if pressure fluctuations are negligible. Both Kovasznay [31] and Kistler [30] have found a strong negative correlation between the temperature and the velocity. This should be expected since the region near the wall has a relatively lower velocity and higher temperature than the region far from the wall. Furthermore, studying a wide variety of Mach numbers and, therefore, static temperature differences across the layer, Kistler found that the distribution of static temperature fluctuations was very nearly proportional to the static temperature difference across the layer. This is also to be expected if the dominant effect is bulk transport, since more extreme fluctuations can only occur if there are wider variations of the transport property available within the layer. Although these observations are far from a proof that bulk transport is the dominant cause of density and enthalpy fluctuations, they make an assumption to that effect seem reasonable.

The conventional representation of this assumption is the Reynolds analogy. The Reynolds analogy is that the fluctuation of the transported property is proportional to the product of the gradient of the transported property and the velocity fluctuation. In the case of $\overline{\rho^{+\prime}v^{+\prime}}$, this is

$$\overline{\rho^{+\prime}v^{+\prime}} \approx \overline{u^{+\prime}v^{+\prime}} \frac{\partial \overline{\rho^{+}}}{\partial y^{+}} \Big/ \frac{\partial \overline{u^{+}}}{\partial y^{+}} \quad . \tag{A4}$$

Of course equation (A4) is consistant with equations (7) and (13) which are discussed in Section II. For an order of magnitude analysis it is adequate to approximate $\partial\overline{\rho^{+}}/\partial y^{+}$ as the average density gradient across the layer, $\Delta\overline{\rho^{+}}/\varepsilon$, and $\partial\overline{u^{+}}/\partial y^{+}$ as the average velocity gradient, $\Delta\overline{u^{+}}/\varepsilon$ $(\sim 1/\varepsilon)$. Therefore

$$\overline{u^{+\prime}v^{+\prime}}\frac{\partial\overline{\rho^{+}}}{\partial y^{+}}\Bigg/\frac{\partial\overline{u^{+}}}{\partial y^{+}}\approx\overline{u^{+\prime}v^{+\prime}}\,\Delta\overline{\rho^{+}} \quad ,$$

or

$$\overline{\rho^{+\prime}v^{+\prime}} = O(\varepsilon\Delta\overline{\rho^{+}}) \quad . \tag{A5}$$

The remaining term in the x momentum equation is the pressure gradient, $\partial\overline{p^{+}}/\partial x^{+}$, which must be of the same order as the inertia terms so long as the velocity in the external flow does not approach zero. However, the only term on the left hand side of the y momentum equation that is of importance is $\partial(\overline{\rho^{+}}\,\overline{v^{+\prime 2}})/\partial y^{+}$. If the magnitude of the pressure gradient across the layer, $\partial\overline{p^{+}}/\partial y^{+}$, is represented by $\Delta\overline{p^{+}}/\varepsilon$, it is clear that $\Delta\overline{p^{+}} = O(\varepsilon + \varepsilon\Delta\overline{\rho^{+}})$.

By following the same approach that yielded (A5), the following relations may be shown:

$$\overline{u^{+\prime}h^{+\prime}} \quad , \quad \overline{v^{+\prime}h^{+\prime}} = O(\varepsilon\Delta\overline{h^{+}}) \quad , \tag{A6}$$

and

$$\overline{\rho^{+\prime}h^{+\prime}} = O(\varepsilon\Delta\overline{\rho^{+}}\,\Delta\overline{h^{+}}) \quad . \tag{A7}$$

For correlations involving the total enthalpy fluctuation, $h^{o+\prime}$, this quantity can be obtained by subtracting equation (A2e) from the same equation before Reynolds averaging has been performed. The result is

$$\left(1 + \frac{\gamma-1}{2}M_e^2\right)h^{o+\prime} = h^{+\prime} + \frac{(\gamma-1)}{2}M_e^2\left[2\overline{u^{+}}u^{+\prime} + u^{+\prime 2} - \overline{u^{+\prime 2}} + v^{+\prime 2} - \overline{v^{+\prime 2}} + w^{+\prime 2} - \overline{w^{+\prime 2}}\right] \tag{A8}$$

Then, after multiplying (A8) by $v^{+\prime}$, for example, and Reynolds averaging, the result is

$$\overline{v^{+\prime} h^{o+\prime}} = \frac{1}{1 + \frac{\gamma-1}{2} M_e^2} \left[\underbrace{\overline{v^{+\prime} h^{+\prime}}}_{\varepsilon \overline{\Delta h^{+}}} + (\gamma-1) M_e^2 \underbrace{\overline{u^{+}}}_{\varepsilon} \overline{u^{+\prime} v^{+\prime}} \right] \quad , \tag{A9}$$

Therefore

$$\overline{v^{+\prime} h^{o+\prime}} = O(\varepsilon \overline{\Delta h^{+o}}) \quad . \tag{A10a}$$

Similiarly it can be shown that

$$\overline{u^{+\prime} h^{o+\prime}} = O(\varepsilon \overline{\Delta h^{o+}}) \quad , \tag{A10b}$$

and

$$\overline{\rho^{+\prime} h^{o+\prime}} = O(\varepsilon \overline{\Delta \rho^{+}}\ \overline{\Delta h^{o+}}) \quad . \tag{A10c}$$

Having estimated the magnitudes of the terms as noted on equations (2), the significance of these terms may be assessed under various conditions. Evidently the magnitude of $\overline{\Delta \rho^{+}}$,

$$\overline{\Delta \rho^{+}} = 1 - \frac{h_e^o / h_w}{1 + \frac{\gamma-1}{2} M_e^2} \quad , \tag{A11}$$

is of prime importance in the ordering of the terms. For very small Mach number and heat transfer, $\overline{\Delta \rho^{+}}$ is small. In this case equations (2) would simply reduce to the familiar constant property equations of motion. However, if the heat transfer is substantial or the Mach number is large, $\overline{\Delta \rho^{+}}$ will be of order unity. Apparently several more terms in equations (2) become important and the resulting equations can be written

$$\frac{\partial}{\partial x^+}\left(\overline{\rho^+}\,\overline{u^+}\right) + \frac{\partial}{\partial y^+}\left(\overline{\rho^+}\,\overline{v^+} + \overline{\rho^{+\prime} v^{+\prime}}\right) = 0 \quad , \tag{A12a}$$

$$\overline{\rho^+}\,\overline{u^+}\frac{\partial \overline{u^+}}{\partial x} + \left(\overline{\rho^+}\,\overline{v^+} + \overline{\rho^{+\prime} v^{+\prime}}\right)\frac{\partial \overline{u^+}}{\partial y^+} + \frac{\partial}{\partial y^+}\left(\overline{\rho^+}\,\overline{u^{+\prime} v^{+\prime}}\right) = -\frac{d\overline{p^+}}{dx} \quad , \tag{A12b}$$

$$\overline{\rho^+}\,\overline{u^+}\frac{\partial \overline{h^{o+}}}{\partial x^+} + \left(\overline{\rho^+}\,\overline{v^+} + \overline{\rho^{+\prime} v^{+\prime}}\right)\frac{\partial \overline{h^{o+}}}{\partial y^+} + \frac{\partial}{\partial y^+}\left(\overline{\rho^+}\,\overline{v^{+\prime} h^{o+\prime}}\right) = 0 \quad , \tag{A12c}$$

$$\left(1 + \frac{\gamma-1}{2} M_e^2\right)\overline{h^{o+}} = \overline{h^+} + \frac{\gamma-1}{2} M_e^2 \overline{u^{+2}} \quad , \tag{A12d}$$

$$1 + \gamma M_e^2 \overline{p^+} = \overline{\rho^+}\,\overline{h^+} \quad . \tag{A12e}$$

The y momentum equation is not included since its only contribution is to show that $\Delta\overline{p^+} = O(\varepsilon + \varepsilon\Delta\overline{\rho^+})$ and therefore, the variation of $\partial\overline{p^+}/\partial x^+$ across the layer is negligible in the x momentum equation.

It is interesting to note that the size of $\Delta\overline{h^{o+}}$ does not serve to distinguish between the relative importance of the terms in the energy equation, but simply whether or not the equation as a whole has significance in a particular situation. In the energy equation, as in the x momentum equation, it is the magnitude of $\Delta\overline{\rho^+}$ which selects the meaningful terms.

In equations (A12b) and (A12c) it is possible to rewrite the shear stress and heat flux terms. The turbulent shear stress may be written as

$$\overline{\tau_t^+} = -\overline{\rho^+}\,\overline{u^{+\prime} v^{+\prime}} \quad . \tag{A13}$$

Then with the aid of equation (A8) the third term in equation (A12c) may be

written

$$-\overline{\rho^+ v^+{}' h^{o+}{}'} = -\overline{\rho^+ v^+{}' h^+{}'} + \overline{u^+}\left(-\overline{\rho^+ u^+{}' v^+{}'}\right) \quad . \tag{A14}$$

If the turbulent heat flux is defined as

$$\overline{q_t^+} = -\overline{\rho^+ v^+{}' h^+{}'} \quad , \tag{A15}$$

equation (A14) becomes

$$-\overline{\rho^+ v^+{}' h^{o+}{}'} = \overline{q_t^+} + \overline{u^+}\,\overline{\tau_t^+} \quad . \tag{A16}$$

When written in terms of the original variables, the boundary layer equations (2) are

$$\frac{\partial}{\partial x}\left(\bar{\rho}\,\bar{u}\right) + \frac{\partial}{\partial y}\left(\bar{\rho}\,\bar{v} + \overline{\rho' v'}\right) = 0 \tag{A17a}$$

$$\bar{\rho}\,\bar{u}\frac{\partial \bar{u}}{\partial x} + \left(\bar{\rho}\,\bar{v} + \overline{\rho' v'}\right)\frac{\partial \bar{u}}{\partial y} = -\frac{d\bar{p}}{dx} + \frac{\partial \bar{\tau}_t}{\partial y} \quad , \tag{A17b}$$

$$\bar{\rho}\,\bar{u}\frac{\partial \overline{h^o}}{\partial x} + \left(\bar{\rho}\,\bar{v} + \overline{\rho' v'}\right)\frac{\partial \overline{h^o}}{\partial y} = \frac{\partial}{\partial y}\left(\bar{q}_t + \bar{u}\,\bar{\tau}_t\right) \quad , \tag{A17c}$$

$$\overline{h^o} = \bar{h} + \tfrac{1}{2}\bar{u}^2 \quad , \tag{A17d}$$

$$p_e = \frac{\gamma - 1}{\gamma}\,\bar{\rho}\,\bar{h} \quad , \tag{A17e}$$

where

$$\bar{\tau}_t = - \bar{\rho}\, \overline{u'v'} \quad , \tag{A17f}$$

and

$$\bar{q}_t = - \bar{\rho}\, \overline{v'h'} \quad . \tag{A17g}$$

APPENDIX B. COMPARISON OF EFFECTIVE VISCOSITY HYPOTHESIS WITH ALTERNATE FORMS

It is interesting to compare the functional relationship for ν_e used in other hypotheses with (8) . This comparison is complicated by the fact that apparently there are no effective viscosity hypotheses in the literature (see Rotta, [32], for instance) besides the present one (Mellor, [57]) that have used two scales. Some simply restrict their range of applicability to the wall layer or the defect layer. Many others, however, stipulate a wall layer relation and then assume the validity of the scaleless overlap layer formulation to the edge of the boundary layer. Since these are all essentially single layer models they will be treated as such and a comparison will be made on that basis. Furthermore most effective viscosity hypotheses were originally intended for use in incompressible flow. Many of them could be extended to include the effects of compressibility and a few have (Lin and Chen, [33]). However, if they are untenable, their weaknesses are usually evident even in incompressible flow.

The first class of hypotheses in Table I is based on the assumption

$$\nu_e = \nu_e(u_\tau , y , \bar{\nu}) \quad , \tag{B1}$$

in the wall layer. Although, for small pressure gradients, the results of these hypotheses may not differ greatly from the present hypothesis, they will, near separation. As $u_\tau = \sqrt{\frac{\tau_w}{\rho_e}} \to 0$ these hypotheses all yield $\nu_e \to \bar{\nu}$ for the entire wall layer, which is clearly an unacceptable result. For the same reason, Clauser's [2] assumption for the defect layer,

$$\nu_e = \nu_e(u_\tau , y , \delta_k^* U) \quad , \tag{B2}$$

is also invalid. Besides these hypotheses in which ν_e is explicitly assumed to be a function of u_τ , most of the other hypotheses in Table I use u_τ as

a parameter in the condition for matching the viscous sublayer to the overlap layer. Again, near separation these conditions would cease to be meaningful. However, on the assumption that the matching conditions could be redefined, the effective viscosity functions themselves will be considered.

The next class of hypotheses are those which use a von Karman [41] similarity hypothesis for the overlap layer, and which supply some other function for the viscous sublayer. When the pressure gradient is zero, the von Karman similarity hypothesis does give the correct logarithmic velocity profile in the overlap region (where $\overline{\tau} = \tau_w$) . It also yields the correct functional dependence, $\bar{u} \sim \sqrt{y}$, when $\tau_w = 0$ at separation. However, if the constant of proportionality is adjusted to fit the zero pressure gradient case, the result for the separating flow is a factor of two too high to agree with Stratford's [42] data. Stratford's data appear to favor a variation in the overlap layer which goes as

$$\bar{u} = \frac{1}{2K} \sqrt{\frac{d\bar{p}}{dx} \frac{y}{\bar{\rho}}} + \text{constant.} \qquad \text{(B3)}$$

This is the result predicted by the Prandtl mixing length form used in the present hypothesis. Furthermore, both of the examples of this type of hypothesis might more legitimately be called three layer models since the forms of the effective viscosity in the laminar sublayer are not the same as they are in the overlap layer. In the laminar sublayer, Bjorgum [37] assumes

$$\nu_e = \nu_e \left(\bar{u} , \frac{\partial \bar{u}}{\partial y} , \bar{\nu} \right) \quad , \qquad \text{(B4a)}$$

and Deissler [38] assumes

$$\nu_e = \nu_e (y , \bar{u} , \bar{\nu}) \quad , \qquad \text{(B4b)}$$

whereas they both use

$$\nu_e = \nu_e \left(\frac{\partial \bar{u}}{\partial y} , \frac{\partial^2 \bar{u}}{\partial y^2} , \bar{\nu} \right) \quad , \tag{B5}$$

in the overlap layer. It would seem that, until the need for a three layer model is evident, a two layer model represents a more concise and simple description of the data.

Table I gives two more hypotheses which do not differ greatly from the present one. The first one (Loitsianskii [39]) applies to the wall layer. Until more data is available in the laminar sublayer, a meaningful comparison with this essentially similar empirical function is not possible. The only reservation about this hypothesis is that the parameter which defines the range of the functions depends on u_τ , as discussed above.

The last hypothesis in the table (Maise and McDonald, [40]) pertains only to the defect layer. It also appears to be the only one originally proposed for compressible flow. It was presented not as an equation but in the form of a plot demonstrating the near Mach number independence of the mixing length function for constant pressure boundary layers. For this reason the equation given in the table is only an approximation. The functional relationship for ν_e is

$$\nu_e = \nu_e \left(\delta , y , \frac{\partial \bar{u}}{\partial y} \right) \quad , \tag{B6}$$

or

$$\frac{\nu_e}{\delta^2 \frac{\partial \bar{u}}{\partial y}} = \Phi^+ \left(\delta^2 \frac{\partial \bar{u}}{\partial y} , y , \frac{\partial \bar{u}}{\partial y} \right) \tag{B7}$$

when written in the form of an effective viscosity rather than a mixing length. The strong similarity between these apparently dissimilar hypotheses, (8a) and (B7) , can be established by considering an approximate relation between $U\delta_k^*$ and $\delta^2 \frac{\partial \bar{u}}{\partial y}$ with the aid of Figure 38 which shows that,

TABLE I:* SUMMARY OF HYPOTHESES FOR ν_e

ASSUMED DIMENSIONAL ARGUMENTS	AUTHOR	SPECIFIC FUNCTIONS	RANGE
$\nu_e(u_\tau, y, \nu)$	Squire [34]	$\nu_e = \nu$	$(0 \le y \le y_1^+ \nu/u_\tau)$
		$\nu_e = \kappa(u_\tau y - y_1^+ \nu) + \nu$	$(y_1^+ \nu/u_\tau \le y)$
	Reichardt [35]	$\nu_e = \kappa[u_\tau y - y_1^+ \nu \tanh(y u_\tau/y_1^+ \nu)] + \nu$	$(0 \le y)$
$\nu_e(u_\tau, y, \delta_k^* U)$	Clauser [2]	$\nu_e = \kappa u_\tau y$	$(y \le \delta_k^* \frac{U}{u_\tau} \frac{K}{\kappa})$
		$\nu_e = \delta_k^* UK$	$(\delta_k^* \frac{U}{u_\tau} \frac{K}{\kappa} \le y)$
$\nu_e(u_\tau, y, \frac{\partial \bar{u}}{\partial y}, \nu)$	Hama [36]	$\nu_e = (-0.1\, y)^4 (u_\tau/\nu)^2 \lvert\partial\bar{u}/\partial y\rvert + \nu$	$(0 \le y \le y_1^+ \nu/u_\tau$
		$\nu_e = \kappa^2 \bar{v}^2 \lvert\partial\bar{u}/\partial y\rvert + \nu$	$(y_1^+ \nu/u_\tau \le y)$
	van Driest [10]	$\nu_e = \kappa^2 y^2 [1 - \exp(y u_\tau/\nu A^+)]^2 \lvert\partial\bar{u}/\partial y\rvert + \nu$	$(0 \le y)$

*Largely from Rotta [32].

TABLE I: (continued)

ASSUMED DIMENSIONAL ARGUMENTS	AUTHOR	SPECIFIC FUNCTIONS	RANGE
$\nu_e(\frac{\partial \bar{u}}{\partial y}, \frac{\partial^2 \bar{u}}{\partial y^2}, \nu)$ and $\nu_e(\bar{u}, \frac{\partial \bar{u}}{\partial y}, \nu)$ or $\nu_e(\bar{u}, y, \nu)$	Bjorgum [37]	$\nu_e = \kappa^2 \bar{u}^2 / \lvert\partial \bar{u}/\partial y\rvert + \nu$	$(0 \leq y \leq y_1^+ \nu/u_\tau)$
		$\nu_e = \kappa_2^2 (\lvert\partial \bar{u}/\partial y\rvert)^3 / (\partial^2 u/\partial y^2)^2 + \nu$	$(y_1^+ \nu/u_\tau \leq y)$
	Deissler [38]	$\nu_e = n^2 \bar{u}\, y[1 - \exp(-n^2 \bar{u}\, y/\nu)] + \nu$	$(0 \leq y \leq y_1^+ \nu/u_\tau)$
		$\nu_e = \kappa^2 (\lvert\partial \bar{u}/\partial y\rvert)^3 / (\partial^2 \bar{u}/\partial y^2)^2 + \nu$	$(y_1^+ \nu/u_\tau \leq y)$
$\nu_e(\frac{\partial \bar{u}}{\partial y}, y, \nu)$	Loitsianskii [39]	$\nu_e = \nu$	$(0 \leq y \leq y_1^+ \nu/u_\tau)$
		$\nu_e = \sqrt{\kappa^4 y^4 (\partial \bar{u}/\partial y)^2 - \kappa^4 y_1^{+4} \nu^2 + \nu^2}$	$(y_1^+ \nu/u_\tau \leq y)$
$\nu_e(\delta, y, \frac{\partial \bar{u}}{\partial y})$	Maise and McDonald [40]	$\nu_e = \kappa^2 y^2 \lvert\partial \bar{u}/\partial y\rvert$	$(y \leq \delta \sqrt{K^+}/\kappa)$
		$\nu_e = K^+ \delta^2 \lvert\partial \bar{u}/\partial y\rvert$	$(\delta \sqrt{K^+}/\kappa \leq y)$

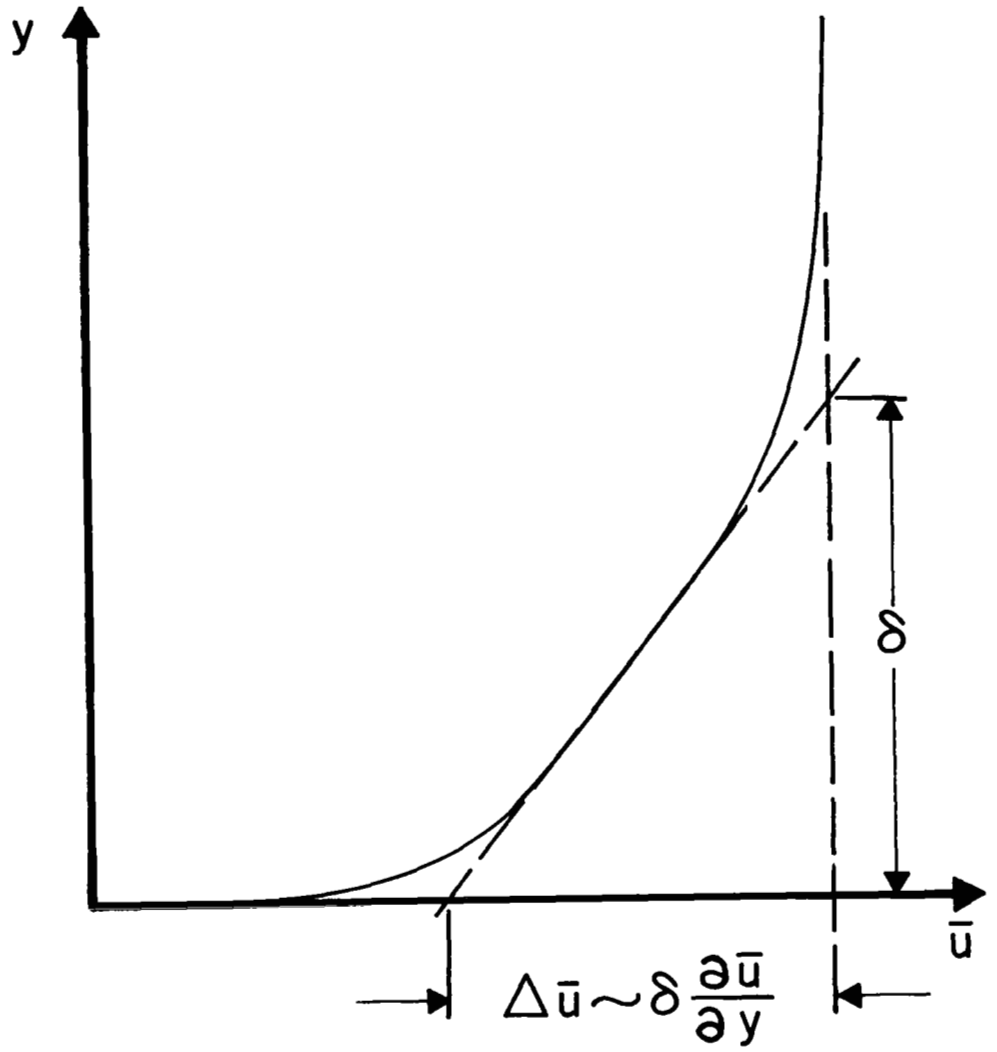

FIGURE 38. Illustration of the relationship between the effective viscosity scales $\delta_k^* U$ and $\delta^2(\partial\bar{u}/\partial y)$ for the defect layer,

$$U\delta_k^* = \int_0^\infty \left(U - \bar{u}\right) dy \approx \tfrac{1}{2}\,\delta\left(\Delta\bar{u}\right) \approx \tfrac{1}{2}\,\delta^2\left(\overline{\frac{\partial \bar{u}}{\partial y}}\right) \quad .$$

$$U\delta_k^* = \int_o^\infty \left(U - \bar{u}\right) dy \approx \tfrac{1}{2}\,\delta\left(\Delta\bar{u}\right) \approx \tfrac{1}{2}\,\delta^2\left(\frac{\partial \bar{u}}{\partial y}\right) \quad . \qquad (B8)$$

In light of equation (B8) there is probably little basis for making a choice between the two. A well defined scale such as δ_k^* is perhaps a slight advantage over the use of the less well defined δ. This is why (8a) was used in the present calculations.

The relationship shown in (B8) brings out the important point that $U\delta_k^*$ is a measure of the average velocity gradient in the boundary layer. A self-consistent effective viscosity hypothesis for compressible flow could also be formulated using the average mass flow gradient, $\rho_e U\delta^* = \int_o^\infty (\rho_e U - \bar{\rho}\,\bar{u})dy$. Several hypotheses of this type actually have been proposed for compressible turbulent wakes (Zakkay and Fox, [43]). By analogy with the argument preceeding (8), such an hypothesis might be written

$$\bar{\tau} = \mu_e \frac{\partial \bar{u}}{\partial y} \qquad (B9)$$

with

$$\mu_e = \mu_e\left(\bar{\mu}\ ,\ y\ ,\ \frac{\partial \bar{\rho}\,\bar{u}}{\partial y}\right) \quad \text{for the wall layer,} \qquad (B10a)$$

and

$$\mu_e = \mu_e\left(\rho_e U\delta^*\ ,\ y\ ,\ \frac{\partial \bar{\rho}\,\bar{u}}{\partial y}\right) \quad \text{for the defect layer,} \qquad (B10b)$$

so that

$$\frac{\mu_e}{\mu} = \phi^*\left(\frac{\kappa^2 y^2}{\mu}\frac{\partial \bar{\rho}\,\bar{u}}{\partial y}\right) \quad , \qquad (B11a)$$

$$\frac{\mu_e}{\rho_e U\delta^*} = \Phi^*\left(\frac{\kappa^2 y^2}{\rho_e U\delta^*}\frac{\partial \bar{\rho}\,\bar{u}}{\partial y}\right) \quad , \qquad (B11b)$$

and in the overlap region

$$\mu_e = \kappa^2 y^2 \frac{\partial \bar{\rho}\,\bar{u}}{\partial y} \quad . \tag{B12}$$

The correlation $\overline{u'v'} = \bar{\tau}/\bar{\rho}$ must be very nearly invariant under a streamwise Galilean transformation as is the hypothesis of equation (8) . However, that is not the case for the example above or for that matter any hypothesis which uses a function of $(\rho_e U - \bar{\rho}\,\bar{u})$ in the defect layer or $\bar{\rho}\,\bar{u}$ in the wall layer, since both the differential and the integral of these quantities would then depend on the magnitude of the velocity. On the other hand, the differential and integral of $(U - \bar{u})$ and $\bar{u}$ are independent of reference frame as is $\overline{u'v'}$.

APPENDIX C. EQUATIONS FOR THE RUNGE-KUTTA METHOD

The Runge-Kutta method is a procedure for solving first order differential equations. In order to apply this method to a linear equation of the form

$$\left\{ C_6(\eta) \left[f'' + C_5(\eta) \right] \right\} = C_3(\eta)\, f'' + C_2(\eta)\, f' + C_1(\eta)\, f + C_4(\eta) \quad , \tag{C1}$$

the equation must be rewritten as a set of first order equations as follows. Let

$$f^{(1)} = f \quad , \quad f^{(2)} = f' \quad , \quad f^{(3)} = C_6(f'' + C_5) \quad . \tag{C2}$$

Then

$$\frac{\partial f^{(1)}}{\partial \eta} = f^{(2)} \quad , \quad \frac{\partial f^{(2)}}{\partial \eta} = \frac{f^{(3)}}{C_6} - C_5 \quad .$$

$$\frac{\partial f^{(3)}}{\partial \eta} = C_3\left(\frac{f^{(3)}}{C_6} - C_5 \right) + C_2 f^{(2)} + C_1 f^{(1)} + C_4 \quad . \tag{C3}$$

From Hildebrand [44], if the values of $f_n^{(i)}$ at η_n are known, the values at $\eta_{n+1} (= \eta_n + \Delta\eta)$ are given to fourth order accuracy by the relation,

$$f_{n+1}^{(i)} = f_n^{(i)} + \frac{1}{6}\left(a_1^{(i)} + 2a_2^{(i)} + 2a_3^{(i)} + a_4^{(i)} \right) \quad , \tag{C4}$$

where

$$a_1^{(1)} = \Delta\eta\ f^{(2)} \quad , \qquad a_1^{(2)} = \Delta\eta\left(\frac{f^{(3)}}{C6_n} - C5_n\right) \quad ,$$

$$a_2^{(1)} = \Delta\eta\left(f^{(2)} + \tfrac{1}{2}\, a_1^{(2)}\right) \quad , \qquad a_2^{(2)} = \Delta\eta\left(\frac{f^{(3)} + \frac{1}{2}\, a_1^{(3)}}{C6_{n+\frac{1}{2}}} - C5_{n+\frac{1}{2}}\right) \quad ,$$

$$a_3^{(1)} = \Delta\eta\left(f^{(2)} + \tfrac{1}{2}\, a_2^{(2)}\right) \quad , \qquad a_3^{(2)} = \Delta\eta\left(\frac{f^{(3)} + \frac{1}{2}\, a_2^{(3)}}{C6_{n+\frac{1}{2}}} - C5_{n+\frac{1}{2}}\right) \quad ,$$

$$a_4^{(1)} = \Delta\eta\left(f^{(2)} + a_3^{(2)}\right) \quad , \qquad a_4^{(2)} = \Delta\eta\left(\frac{f^{(3)} + a_3^{(3)}}{C6_{n+1}} - C5_{n+1}\right) \quad ,$$

$$a_1^{(3)} = \Delta\eta\left[C3_n\left(\frac{f^{(3)}}{C6_n} - C5_n\right) + C2_n\, f^{(2)} + C1_n\, f^{(1)} + C4_n\right] \quad ,$$

$$a_2^{(3)} = \Delta\eta\left[C3_{n+\frac{1}{2}}\left(\frac{f^{(3)} + \frac{1}{2}\, a_1^{(3)}}{C6_{n+\frac{1}{2}}} - C5_{n+\frac{1}{2}}\right) + C2_{n+\frac{1}{2}}\left(f^{(2)} + \tfrac{1}{2}\, a_1^{(2)}\right)\right.$$

$$\left. + C1_{n+\frac{1}{2}}\left(f^{(1)} + \tfrac{1}{2}\, a_1^{(1)}\right) + C4_{n+\frac{1}{2}}\right]$$

$$a_3^{(3)} = \Delta\eta \left[C_{3_{n+\frac{1}{2}}} \left(\frac{f^{(3)} + \frac{1}{2} a_2^{(3)}}{C_{6_{n+\frac{1}{2}}}} - C_{5_{n+\frac{1}{2}}} \right) + C_{2_{n+\frac{1}{2}}} \left(f^{(2)} + \frac{1}{2} a_2^{(2)} \right) \right.$$

$$\left. + C_{1_{n+\frac{1}{2}}} \left(f^{(1)} + \frac{1}{2} a_2^{(1)} \right) + C_{4_{n+\frac{1}{2}}} \right] ,$$

$$a_4^{(3)} = \Delta\eta \left[C_{3_{n+1}} \left(\frac{f^{(3)} + a_3^{(3)}}{C_{6_{n+1}}} - C_{5_{n+1}} \right) + C_{2_{n+1}} \left(f^{(2)} + a_3^{(2)} \right) \right.$$

$$\left. + C_{1_{n+1}} \left(f^{(1)} + a_3^{(1)} \right) + C_{4_{n+1}} \right] ,$$

$$C_{n+\frac{1}{2}} = \frac{1}{2} \left(C_n + C_{n+1} \right) . \qquad \text{(C6)}$$

APPENDIX D. ASYMPTOTIC SOLUTION FOR LARGE η

The turbulent Prandtl number has been assumed to be equal to 1 in the analysis which follows.

For large η , $f \to 1$, $f' \to 0$, $f'' \to 0$, $g' \to 0$, $g'' \to 0$, $T \to K \frac{\delta_k^*}{\delta^*}$, $T_h \to K \frac{\delta_k^*}{\delta^*}$ and from equation (25),

$$\theta \to 1 + \frac{(\gamma - 1) M_e^2 f' - \left(1 + \frac{\gamma-1}{2} M_e^2\right) Hg'}{1 + (\gamma - 1) M_e^2} \quad , \tag{D1}$$

$$\theta' \to \frac{(\gamma - 1) M_e^2 f'' - \left(1 + \frac{\gamma-1}{2} M_e^2\right) Hg''}{1 + (\gamma - 1) M_e^2} \quad , \tag{D2}$$

$$\delta^* \theta_x \to \frac{(\gamma - 1) M_e^2 \delta^* f_x' - \left(1 + \frac{\gamma-1}{2} M_e^2\right) \delta^* Hg_x'}{1 + (\gamma - 1) M_e^2}$$

$$+ V \frac{\left[1 + (\gamma - 1) M_e^2\right]^2 - 1}{\left[1 + (\gamma - 1) M_e^2\right]^2} \left(f' + \frac{H}{2} g'\right) \quad . \tag{D3}$$

Then the asymptotic forms of equations (24a) and (24b) are

$$\frac{\delta_k^*}{\delta^*} K f''' + Q(\eta - 1) f'' - 2V \frac{1 + \frac{\gamma-1}{2} M_e^2}{1 + (\gamma-1) M_e^2} f' - \delta^* f_x' = V \frac{1 + \frac{\gamma-1}{2} M_e^2}{1 + (\gamma-1) M_e^2} Hg' \quad , \tag{D4a}$$

and

$$\frac{\delta_k^*}{\delta^*} K g''' + Q(\eta - 1) g'' - \delta^* g_x' = 0 \qquad \text{(D4b)}$$

In order to insure the satisfaction of the fourth and seventh boundary conditions (28) , the asymptotic solutions of f' and g' were assumed in exponential form,

$$f'(\eta,x) = R(x) \exp\left\{ - \frac{(\eta - 1)^2}{2r(x)} \right\} , \qquad \text{(D5a)}$$

$$g'(\eta,x) = S(x) \exp\left\{ - \frac{(\eta - 1)^2}{2s(x)} \right\} . \qquad \text{(D5b)}$$

Although strictly speaking R and S are functions of η as well as x , the η dependence is small. Furthermore the outer boundary conditions on f' and g' can be satisfied with knowledge of only $r(x)$ and $s(x)$.

$R(x)$ and $S(x)$ can then be eliminated using $f'(\eta_1,x)$ and $g'(\eta_1,x)$, where η_1 is a point far from the wall. Then

$$f'(\eta,x) = f'(\eta_1,x) \exp\left\{ \frac{(\eta_1 - 1)^2 - (\eta - 1)^2}{2r(x)} \right\} \qquad \text{(D6a)}$$

$$g'(\eta,x) = g'(\eta_1,x) \exp\left\{ \frac{(\eta_1 - 1)^2 - (\eta - 1)^2}{2s(x)} \right\} . \qquad \text{(D6b)}$$

Then $r(x)$ and $s(x)$ may be found by inserting (D5a) and (D5b) into (D4a)

and (D4b) . The coefficients of $(\eta - 1)^2$ are

$$\frac{\delta^*}{2} r_x + Qr = K \frac{\delta_k^*}{\delta^*} \quad , \tag{D7a}$$

and

$$\frac{\delta^*}{2} s_x + Qs = K \frac{\delta_k^*}{\delta^*} \quad . \tag{D7b}$$

The solution of these equations can easily be shown to be

$$r(x) = \left(\frac{\rho_{e_o} U_o \delta_o^*}{\rho_e U \delta^*} \right)^2 r(x_o) + \frac{2K}{(\rho_e U \delta^*)^2} \int_{x_o}^{x} \frac{\delta_k^*}{\delta^*} (\rho_e U)^2 \delta^* \, dx \quad , \tag{D8a}$$

and

$$s(x) = \left(\frac{\rho_{e_o} U_o \delta_o^*}{\rho_e U \delta^*} \right)^2 s(x_o) + \frac{2K}{(\rho_e U \delta^*)^2} \int_{x_o}^{x} \frac{\delta_k^*}{\delta^*} (\rho_e U)^2 \delta^* \, dx \quad . \tag{D8b}$$

APPENDIX E. BOUNDARY LAYER EQUATIONS OF MOTION IN AXISYMMETRIC FLOW

Following an argument similar to that in Section II , the boundary layer equations for a steady flow at moderate Mach number and heat transfer for which $\delta/R_{LAT} = O(1)$, are

$$\frac{\partial r\,\bar{\rho}\,\bar{u}}{\partial x} + \frac{\partial}{\partial y}\left[r\left(\bar{\rho}\,\bar{v} + \overline{\rho' v'}\right)\right] = 0 \quad , \tag{E1a}$$

$$r\,\bar{\rho}\,\bar{u}\frac{\partial \bar{u}}{\partial x} + r\left(\bar{\rho}\,\bar{v} + \overline{\rho' v'}\right)\frac{\partial \bar{u}}{\partial y} = -\frac{dp}{dx} + \frac{\partial r\,\tau}{\partial y} \quad , \tag{E1b}$$

$$r\,\bar{\rho}\,\bar{u}\frac{\partial \overline{h^o}}{\partial x} + r\left(\bar{\rho}\,\bar{v} + \overline{\rho' v'}\right)\frac{\partial \overline{h^o}}{\partial y} = \frac{\partial}{\partial y}\left[r\left(\bar{q} + \bar{u}\,\bar{\tau}\right)\right] \quad . \tag{E1c}$$

The definitions of $\bar{\tau}$ and $\bar{q}$ and the effective viscosity hypothesis are unchanged. The sole difference in the effective viscosity is that in flow with lateral curvature the defect scale becomes

$$U\delta_k^* = \int_o^\infty (U - \bar{u})\,\frac{r}{R_{LAT}}\,dy \quad . \tag{E2}$$

As for the two dimensional equations, new variables are introduced,

$$f'(\eta, x) = \Lambda\left(\frac{\rho_e U - \bar{\rho}\,\bar{u}}{\rho_e U}\right) \tag{E3a}$$

$$\theta(\eta,x) = \frac{\rho_e}{\overline{\rho}} \quad , \tag{E3b}$$

$$g'(\eta,x) = \frac{h_e^o - \overline{h^o}}{h_e^o - h_r} \quad , \tag{E3c}$$

$$\Lambda = \frac{r}{R_{LAT}} = 1 + \lambda\eta \quad , \qquad \lambda = \frac{\delta^*}{R_{LAT}} \quad , \tag{E3d}$$

$$\eta = \frac{y}{\delta^*} \quad , \tag{E3e}$$

$$D = \frac{\left(R_{LAT.}\right)_x \delta^*}{R_{LAT.}} \quad , \tag{E3f}$$

$$P = \frac{\left(\rho_e U\right)_x \delta^*}{\rho_e U} \quad , \tag{E3g}$$

$$Q = \frac{\left(R_{LAT.}\, \rho_e U \delta^*\right)_x}{R_{LAT.}\, \rho_e U} \quad , \tag{E3h}$$

$$V = \frac{U_x \delta^*}{U} \quad . \tag{E3i}$$

When rewritten in terms of these variables, the equations of motion become

$$\left\{ \frac{\delta_k^*}{\delta^*} \frac{\Lambda}{\theta} \left[\theta \left(1 - \frac{f'}{\Lambda} \right) \right]' \right\}' = \left\{ \theta \left[\frac{Q}{\Lambda} (\eta - f) + \frac{\lambda \eta^2}{2\Lambda} \left(P + 2\delta_x^* \right) \right] \right\} f''$$

$$+ \left\{ \left(V\theta + \delta^* \theta_x \right) \left(\frac{f'}{\Lambda} - 2 \right) + \left(\delta_x^* \theta' - \frac{\lambda D}{\Lambda} \theta \right) \left(1 - \frac{f'}{\Lambda} \right) \eta \right.$$

$$\left. + \left(\theta' - \frac{\lambda \theta}{\Lambda} \right) \frac{Q}{\Lambda} (\eta - f) + P \frac{\lambda \eta^2}{2\Lambda} - \eta \frac{\delta_x^*}{\Lambda} (1 - f') \right\} f'$$

$$+ \left\{ Q\theta' \right\} f + \left\{ \Lambda V(\theta - 1) + \Lambda \theta_x \delta^* - \theta' \left[\eta Q + \frac{\lambda}{2} \eta^2 \left(P + 2\delta_x^* \right) \right] \right\}$$

$$+ \delta^* f_x \left[\theta' \left(1 - \frac{f'}{\Lambda} \right) - \theta \frac{f''}{\Lambda} + \frac{\lambda \theta}{\Lambda} \frac{f'}{\Lambda} \right] - \delta^* \theta f_x' \left(1 - \frac{f'}{\Lambda} \right) = 0 \quad , \qquad \text{(E4a)}$$

$$\left[\frac{\Lambda}{\theta} \frac{\delta_k^*}{\delta^*} T_h \left\{ -g'' + \frac{\frac{(\gamma - 1)}{2} M_e^2}{H\left(1 + \frac{\gamma - 1}{2} M_e^2 \right)} \left[\frac{T}{T_h} - 1 \right] \left[\theta^2 \left(1 - \frac{f'}{\Lambda} \right)^2 \right] \right\} \right]$$

$$= \left\{ Q(\eta - f) + \frac{\lambda \eta^2}{2} \left(P + 2\delta_x^* \right) - \delta^* f_x \right\} g'' - (\Lambda - f') \delta^* g_x' = 0 \quad , \qquad \text{(E4b)}$$

$$\theta = \frac{2\left(1 + \frac{\gamma-1}{2} M_e^2\right)(1 - Hg')}{1 + \sqrt{1 + \frac{\gamma-1}{2} M_e^2 (1 - f'/\Lambda)^2 \left(1 + \frac{\gamma-1}{2} M_e^2\right)(1 - Hg')}} \quad , \tag{E4c}$$

where primes indicate differentiation with respect to η .

REFERENCES

[1] Clauser, F., Turbulent boundary layers in adverse pressure gradients, Jour. of Aero. Sci., XXI, 91-108, (1954).

[2] Clauser, F., The turbulent boundary layer, Advances in Applied Mechanics, Vol. IV, Academic Press, New York, (1956).

[3] Mellor, G. L. and Gibson, D. M., Equilibrium turbulent boundary layers, Jour. of Fluid Mech., XXIV, 225-253, (1966).

[4] Mellor, G. L., The effect of pressure gradients on turbulent flow near a smooth wall, Jour. of Fluid Mech., XXIV, 255-274, (1966).

[5] Mellor, G. L., Turbulent boundary layers with arbitrary pressure gradients and divergent or convergent cross flows, AIAA Journal, Vol. 5, 1570-1579, (1967).

[6] Prandtl, L., Uber die ausgebildete Turbulenze, ZAMM 5, 136, (1925) and Proc. Second Int. Congress Appl. Mech., Zurich, (1926).

[7] Laufer, J., The structure of turbulence in fully developed pipe flow, NACA Report 1174, (1954).

[8] Van Dyke, M., Perturbation Methods in Fluid Mechanics, Academic Press, New York, (1964).

[9] Bradshaw, P., Ferriss, D. H. and Atwell, N. P., Calculation of boundary layer development using the turbulent energy equation, National Physical Laboratory, Aerodynamics Division, Report 1182, (1966).

[10] Van Driest, E. R., On turbulent flow near a wall, J. Aero. Sci., XXIII, 1007-1011, (1956)

[11] Townsend, A. A., The Structure of Turbulent Shear Flow, Cambridge University Press, (1956).

[12] Millikan, C. B. A., A critical discussion of turbulent flows in channels and circular tubes, Proc. Fifth Int. Congress Appl. Mech., 386-392, (1938).

[13] Smith, A. M. O. and Clutter, D. W., A general method for solving the compressible laminar boundary layer equations, Douglas Aircraft Division Paper 1699, (1963).

[14] Coles, D. E., Measurements in the boundary layer on a smooth flat plate in supersonic flow, III. Measurements in a flat plate boundary layer at the Jet Propulsion Laboratory, Jet Propulsion Laboratory, California Institute of Technology, Pasadena, Calif., Report 20 - 71, (1953).

[15] Nothwang, G. J., An evaluation of four experimental methods of measuring mean properties of a supersonic turbulent boundary layer, NACA TN 3721, (1956).

[16] Moore, D. R. and Harkness, J., Experimental investigation of the compressible turbulent boundary layer at very high Reynolds numbers, Ling-Temco-Vought, Research Center Report 0-7100/4R-9, (1964).

[17] Chapman, D. R. and Kester, R. H., Measurements of turbulent skin friction on cylinders in axial flow at subsonic and supersonic velocities, J. Aero. Sci., XX, N. 7, 441-448, (1953).

[18] Lobb, R. K., Winkler, E. M. and Persh, J., Experimental investigation of turbulent boundary layers in hypersonic flow, Jour. of the Aero. Sci., XXII, 1-9, (1955).

[19] Dhawan, S., Direct measurements of skin friction, NACA Report 1121, (1953).

[20] Kuethe, A. M., Some features of boundary layers and transition to turbulent flow, Jour. of Aero. Sci., XXIII, 444-452, (1956).

[21] Monaghan, R. J. and Johnson, J. E., The measurement of heat transfer and skin friction at supersonic speeds, Aeronautical Research Council C. P. 64, (1952).

[22] Michel, Roger, Résultants sur la couche limite turbulente aux grandes vitesses, Office National d'Etudes et de Recherches Aéronautiques Mémo Technique 22, (1961).

[23] Winter, K. G., Smith, K. G. and Rotta, J. C., Turbulent boundary layer studies on a waisted body of revolution in subsonic and supersonic flow, AGARDograph 97, 933-962, (1965).

[24] Eskinazi, S. and Yeh, H., An investigation on fully developed turbulent flows in a curved channel, J. Aero. Sci., XXIII, 23-34, Jan. (1956).

[25] McLafferty, G. H. and Barber, R. E., The effect of adverse pressure gradients on the characteristics of turbulent boundary layers in supersonic streams, J. Aero. Sci., XXIX, 1-10, (1962).

[26] Rotta, J. C., On the effects of streamwise wall curvature on compressible turbulent boundary layers, Aerodynamische Versuchsanstalt, Gottingen, Report 66A44, (1966).

[27] Danberg, J. E., Characteristics of the turbulent boundary layer with heat and mass transfer at M=6.7, U. S. Naval Ord. Lab. Rept. 64-69, (1964).

[28] Reynolds, W. C., Kays, W. M. and Kline, S. J., Heat transfer in the turbulent incompressible boundary layer; I - Constant wall temperature, NASA MEMO 12-1-58W, (1958).

[29] Moretti,P. M. and Kays, W. M., Heat transfer to a turbulent boundary layer with varying free-stream velocity and varying surface temperature - an experimental study, Int. J. Heat Mass Transfer, VIII, 1187-1202, (1965).

[30] Kistler, A. L., Fluctuation measurements in a supersonic turbulent boundary layer, The Physics of Fluids, II, 290-296, (1959).

[31] Kovasznay, L. S. G., Turbulence in supersonic flow, Jour. of Aero. Sci., XX, 657-675, (1953).

[32] Rotta, J. C., Turbulent Boundary Layers in Incompressible Flow, Pergamon Press, Oxford. Reprinted from Progress in Aeronautical Sciences, Vol. 2, (1962).

[33] Lin, C. C. and Shen, S. F., A similarity theory for turbulent boundary layer over a flat plate in compressible flow, NACA Tech. Note 2542, (1951).

[34] Squire, H. B., Reconsideration of the theory of free turbulence, Phil. Mag. XXXIX, 1-14, (1948).

[35] Reichardt, H., Vollstandige Darstellung der turbulenten Geschwindigkeitsverteilung in glatten Leitungen, Z. Angew. Math. Mech., XXXI, 208-219, (1951).

[36] Hama, F. R., On the velocity distribution in the laminar sublayer and transition region in turbulent shear flows, J. Aero. Sci., XX, 648-649, (1953).

[37] Bjorgum, O., On the steady turbulent flow along an infinitely long smooth and plane wall, Naturw. rekke, No. 7, Univ. Bergen, Arbok, (1951).

[38] Deissler, R. G., Analysis of turbulent heat transfer, mass transfer, and friction in smooth tubes at high Prandtl and Schmidt numbers, NACA Rept. 1210, 69-82, (1955).

[39] Loitsianskii, L. G., The hypothesis of localness in the turbulent motion of a viscous fluid, Prikl. Mat. Mekh., XXII, 560-611. English translation J. Appl. Math. Mech., (1958).

[40] Maise, G. and McDonald, H., Mixing length and kinematic eddy viscosity in a compressible boundary layer, United Aircraft Research Laboratories Report E211557 - 1, (1966).

[41] von Karman, Th., Mechanische Aehnlichkeit und Turbulenz, Nachr. Ges. Wiss. Gottingen, Math. Phys. Kl., 58-68. NACA TM 611, (1930).

[42] Stratford, B. S., An experimental flow with zero skin friction throughout its region of pressure rise, Jour. of Fluid Mech., V, 17-35, (1959).

[43] Zakkay, V. and Fox, H., An experimental and theoretical investigation of the turbulent far wake, AIAA Journal, V, 568-574, (1967).

[44] Hildebrand, F. B., Advanced Calculus for Engineers, Prentice Hall Inc., New York, (1949).

NATIONAL AERONAUTICS AND SPACE ADMINISTRATION
WASHINGTON, D. C. 20546

OFFICIAL BUSINESS

FIRST CLASS MAIL

POSTAGE AND FEES PAID
NATIONAL AERONAUTICS AND
SPACE ADMINISTRATION

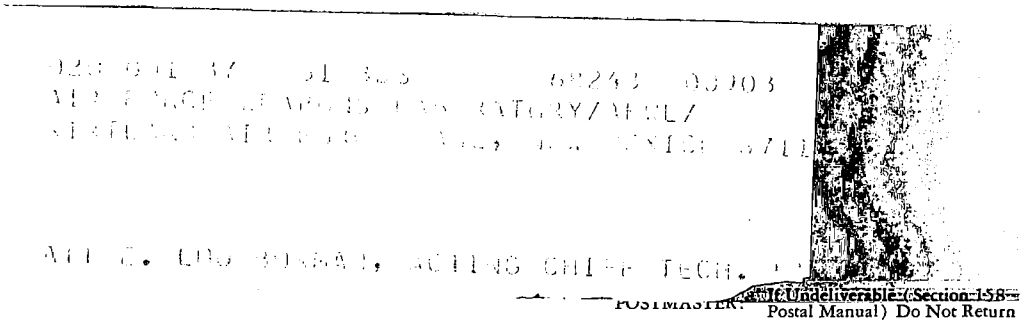

POSTMASTER: If Undeliverable (Section 158
Postal Manual) Do Not Return

"The aeronautical and space activities of the United States shall be conducted so as to contribute . . . to the expansion of human knowledge of phenomena in the atmosphere and space. The Administration shall provide for the widest practicable and appropriate dissemination of information concerning its activities and the results thereof."

—NATIONAL AERONAUTICS AND SPACE ACT OF 1958

NASA SCIENTIFIC AND TECHNICAL PUBLICATIONS

TECHNICAL REPORTS: Scientific and technical information considered important, complete, and a lasting contribution to existing knowledge.

TECHNICAL NOTES: Information less broad in scope but nevertheless of importance as a contribution to existing knowledge.

TECHNICAL MEMORANDUMS: Information receiving limited distribution because of preliminary data, security classification, or other reasons.

CONTRACTOR REPORTS: Scientific and technical information generated under a NASA contract or grant and considered an important contribution to existing knowledge.

TECHNICAL TRANSLATIONS: Information published in a foreign language considered to merit NASA distribution in English.

SPECIAL PUBLICATIONS: Information derived from or of value to NASA activities. Publications include conference proceedings, monographs, data compilations, handbooks, sourcebooks, and special bibliographies.

TECHNOLOGY UTILIZATION PUBLICATIONS: Information on technology used by NASA that may be of particular interest in commercial and other non-aerospace applications. Publications include Tech Briefs, Technology Utilization Reports and Notes, and Technology Surveys.

Details on the availability of these publications may be obtained from:

SCIENTIFIC AND TECHNICAL INFORMATION DIVISION

NATIONAL AERONAUTICS AND SPACE ADMINISTRATION

Washington, D.C. 20546